

Electronic Thesis and Dissertation Repository

11-1-2019 10:15 AM

Rotating Heater Pyrolyzer (RHP): A new pyrolysis technology for biochar production

Ariel Porat, *The University of Western Ontario*

Supervisor: Briens, Cedric, *The University of Western Ontario*

: Briens, Lauren, *The University of Western Ontario*

A thesis submitted in partial fulfillment of the requirements for the Master of Engineering Science degree in Chemical and Biochemical Engineering

© Ariel Porat 2019

Follow this and additional works at: <https://ir.lib.uwo.ca/etd>

 Part of the [Other Chemical Engineering Commons](#)

Recommended Citation

Porat, Ariel, "Rotating Heater Pyrolyzer (RHP): A new pyrolysis technology for biochar production" (2019). *Electronic Thesis and Dissertation Repository*. 6699.
<https://ir.lib.uwo.ca/etd/6699>

This Dissertation/Thesis is brought to you for free and open access by Scholarship@Western. It has been accepted for inclusion in Electronic Thesis and Dissertation Repository by an authorized administrator of Scholarship@Western. For more information, please contact wlsadmin@uwo.ca.

Abstract

Biochar provides an effective and inexpensive carbon sequestration technology to combat climate change. It is formed through a process known as pyrolysis; where biomass is thermally decomposed in the absence of oxygen. In this study, a new pyrolysis reactor called the Rotating Heater Pyrolyzer (RHP) was designed and built for biochar production. RHP derived biochar properties were compared to biochars produced with a standard batch pyrolysis reactor (Pyrolytic Shaker Reactor (PSR)) to determine RHP performance. Using several biochar characterization techniques, the soil amendment potential of two solid anaerobic digestate feedstocks were investigated. Woodchip RHP derived biochar processed between 2-3 hrs exhibited similar biochar yield, electrical conductivity, methylene blue adsorption and colour intensity to woodchip PSR biochars produced at 400 °C. Flower waste digestate biochars were found to have properties beneficial for soil amendment, including lower skeletal density, higher electrical conductivity and methylene blue adsorption compared to food waste digestate biochars.

Keywords

Biochar, pyrolysis, pyrolysis reactor, solid anaerobic digestate, woodchip, leaching, soil amendment

Summary for Lay Audience

Biochar is the solid product of a process known as pyrolysis. During pyrolysis, waste organic material is heated in the absence of oxygen and produces three main products; bio-oil, biochar and permanent gasses. Biochar is the stable solid crystalline form of the carbon that was once present in the original waste material and can take up to centuries to decompose. When incorporated into soils, biochar can effectively create a carbon sink, ultimately delaying greenhouse gas emissions into the atmosphere. In addition to the carbon sequestration abilities of biochar, numerous studies have suggested that biochar can improve soil fertility and agricultural output. Solid anaerobic digestate is one sustainable feedstock that can be used to produce biochar. Anaerobic digestion is the process of producing bio-gas; a renewable source of energy derived from organic waste. It is important to note that biochar properties are highly dependent on pyrolysis parameters and the feedstock used. Therefore, biochar properties must be tailored during production to suit the needs of soil profile it is to be paired with. In this thesis, a new lab scale pyrolysis technology capable of processing relatively large quantities of biomass was designed, built and commissioned. The unit was then used to produce biochar derived from two different solid anaerobic digestate feedstocks, and their soil amendment potential was investigated.

Co-Authorship Statement

Chapters 2, 3 and 4 are research studies that will be submitted for publication in peer reviewed journals. Individual author contributions are listed below with respect to each journal article.

Chapter 2: Rotating Heater Pyrolyzer (RHP) Design and Development

Authors: Ariel Porat, Cedric Briens and Lauren Briens

A. Porat produced all biochars made with the rotating heater pyrolysis reactor. All experiments and biochar characterizations were performed by A.Porat. The data analysis was performed by A. Porat with the assistance of C. Briens and L. Briens. Manuscript was written by A. Porat and revised by C. Briens and L. Briens.

Chapter 3: Comparison of Rotating Heater Pyrolyzer (RHP) Derived Biochar Properties to Standard Batch Pyrolysis Biochar

Authors: Ariel Porat, Francisco Javier Sanchez Careaga, Cedric Briens and Lauren Briens

A. Porat produced all biochars made with the rotating heater pyrolysis reactor and pyrolytic shaker reactor. Pyrolytic shaker was designed and built by F. Careaga. All experiments and biochar characterizations were performed by A. Porat. The data analysis was performed by A. Porat with the assistance of C. Briens and L. Briens. Manuscript was written by A. Porat and revised by C. Briens and L. Briens.

Chapter 4: A Comparison Between Two Anaerobic Digestate Derived Biochars for Soil Amendment Applications

Authors: Ariel Porat, Cedric Briens and Lauren Briens

A. Porat produced all biochars made with the rotating heater pyrolysis reactor and pyrolytic shaker reactor. All experiments and biochar characterizations were performed by A.Porat. The data analysis was performed by A. Porat with the assistance of C. Briens and L. Briens. Manuscript was written by A. Porat and revised by C. Briens and L. Briens.

Acknowledgments

I would like to thank my supervisors; Cedric Briens and Lauren Briens for their continual guidance and support throughout my Masters. The past two years have been an incredible experience that I could not have accomplished without their mentorship.

I would like to thank all my friends and peers at the Institute for Chemicals and Fuels from Alternative Resources (ICFAR), and extend a special thank you to Dr. Francisco J. Sanchez Careaga, Thomas Johnston and Gazelle Chegini for their technical support and training.

I would also like to thank Storm Fisher Environmental and Bayview Flowers for providing the digestate feedstocks processed in this thesis.

Lastly, I would like to thank my family and friends for always providing me with unconditional support throughout the duration of my Masters.

Table of Contents

Abstract.....	ii
Summary for Lay Audience.....	iii
Co-Authorship Statement.....	iv
Acknowledgments.....	v
Table of Contents.....	vi
List of Tables.....	x
List of Figures.....	xi
List of Appendices.....	xvii
Chapter 1.....	1
1 Introduction and Literature Review.....	1
1.1 Pyrolysis and Biochar.....	1
1.2 Pyrolysis Technologies.....	2
1.2.1 Jiggle Bed Reactor.....	3
1.2.2 Fluidized Bed Reactors.....	3
1.2.3 Auger Reactors.....	4
1.2.4 Mechanically Fluidized Reactor (MFR).....	4
1.2.5 Rotary Kiln Reactor.....	5
1.2.6 Laboratory Reactor Needs For the Development of Biochar Products.....	6
1.3 Biochar Applications.....	7
1.3.1 Biochar for Carbon Sequestration.....	7
1.3.2 Biochar as Soil Amendment.....	9
1.3.3 Activated Carbon.....	9
1.3.4 Biocoke for Metallurgical Applications.....	10
1.3.5 Biochar as Bio-coal.....	11

1.3.6	Biochar as a Catalyst	12
1.3.7	Biochar as a Filler for Composite Materials	14
1.4	Biochar for Soil Amendment.....	15
1.4.1	Biochar Formation and Characteristics	15
1.4.2	Biochar Effects on Soil Fertility.....	16
1.4.3	Effects of Aging on Biochar	20
1.4.4	Current Challenges	21
1.5	Granulation	22
1.5.1	Hydrophilic Granulation Mechanism	23
1.5.2	Granulation of Hydrophobic Powders Mechanism	24
1.5.3	Granulation of Biochar	25
1.5.4	Thesis Objectives	27
1.6	References	28
Chapter 2	42
2	Rotating Heater Pyrolysis Reactor (RHP) Design and Development.....	42
2.1	Introduction	42
2.2	Rotating Heater Pyrolyzer (RHP).....	44
2.2.1	Principles of the RHP Design	44
2.2.2	Design and Set-up	45
2.3	Materials and Methods.....	49
2.3.1	Methods to Characterize RHP Performance	49
2.3.2	Feedstock	51
2.3.3	RHP Experimental Procedure	52
2.3.4	Biochar Production Conditions	52
2.3.5	Methods to Characterize Biochar	53
2.4	Results and Discussion.....	58

2.4.1	RHP Characterization and Performance	58
2.4.2	Effect of Process Time on Biochar Properties	63
2.5	Conclusions	69
2.6	References	70
Chapter 3	75
3	Comparison of RHP Derived Biochar Properties to Standard Batch Pyrolysis Biochar	75
3.1	Introduction	75
3.2	Materials and Pyrolysis Methods.....	76
3.2.1	Feedstock	76
3.2.2	Standard Batch Pyrolysis Reactor: Pyrolytic Shaker Reactor (PSR)	77
3.2.3	Rotating Heater Pyrolyzer (RHP)	78
3.2.4	Pyrolysis Procedures	79
3.2.5	Biochar Production Conditions	79
3.3	Feedstock and Biochar Characterization Methods	79
3.4	Results and Discussion.....	87
3.5	Conclusions	96
3.6	References	97
Chapter 4	100
4	A Comparison Between Two Anaerobic Digestate Derived Biochars for Soil Amendment Applications.....	100
4.1	Introduction	100
4.2	Materials and Pyrolysis Methods.....	101
4.2.1	Feedstock	101
4.2.2	Standard batch pyrolysis reactor: Pyrolytic Shaker Reactor (PSR)	102
4.2.3	Rotating Heater Pyrolyzer (RHP)	103
4.2.4	PSR Procedure	103

4.2.5 RHP Procedure.....	104
4.2.6 Biochar Production Conditions	105
4.3 Feedstock and Biochar Characterization Methods	105
4.4 Results and Discussion.....	110
4.5 Conclusions	124
4.6 References	125
5 Conclusions	129
6 Recommendations and Future Work	130
Appendix A: Gast Air Motor Product Specifications.....	131
Appendix B: PSR Mixing Images.....	132
Appendix C: Skeletal Density and Ash Content of WCP Biochars.....	133
Appendix D: Nespresso™ Extraction.....	134
Appendix E: Equivalent PSR Temperatures for PSR Digestate Derived Biochars.....	136
Ciriculum Vitae.....	144

List of Tables

Table 1-1: Summary of operating conditions and heat capacities of different lab scale pyrolysis reactors.....	6
Table 1-2: Recent studies investigating the co-application of biochar and fertilizer a soil amendment. Agronomic responses are based on a comparison of soils amended exclusively with biochar vs. fertilizer biochar mixtures.	18
Table 2-1: Particle Size Distributions of Feedstocks.	51
Table 2-2: Bulk density of feedstocks.	58
Table 2-3: Biomass loadings for different RHP runs.	59
Table 2-4: Current through the induction system with the spiral heater, tube heater and plate heater.....	60
Table 2-5: Energy consumption required to operate the rotating heater.	62
Table 3-1: Equivalent PSR temperatures of RHP derived chars based on individual biochar characterization for all feedstocks.	95
Table 4-1: Average moisture content of SFD and BFD feedstocks.	101
Table 4-2: Biochar properties for PSR chars produced at 250 °C.....	123
Table 4-3: Biochar properties for PSR chars produced at 500 °C.	123
Table 4-4: Biochar properties for average of RHP chars processed between 2 to 3 hrs.	124

List of Figures

Figure 1-1: Carbon Sequestration Processes and Methods (Adapted from Nogia et al. (17))..	8
Figure 2-1: RHP Schematic.	46
Figure 2-2: Reactor Vessel Drawing.	47
Figure 2-3: Reactor lid and rotating heater diagram.....	48
Figure 2-4: (a) Woodchips (b) Storm Fisher Digestate (c) Bayview Flowers Digestate.	51
Figure 2-5: RGB peak intensity.	54
Figure 2-6: Soxhlet extractor (Adapted from Dolinowski (32))	57
Figure 2-7: Rotating heater designs (a) Spiral Heater; (b) Tube Heater; (c) Plate Heater.	59
Figure 2-8: Power supplied to the reaction bed with the plate heater. Empirical curve fit was used.....	62
Figure 2-9: Tar deposits along lid of RHP.....	63
Figure 2-10: Effect of RHP process time (hrs) on biochar yield.	64
Figure 2-11: Effect of process time (hrs) on mode red intensity of woodchip derived biochar. Raw woodchip feedstock mode red intensity is represented at a process time of 0 hrs, Triplicate results are displayed.....	65
Figure 2-12: Effect of RHP process time (hrs) on the red mode intensity coefficient of variation. Triplicate results are displayed.	66
Figure 2-13: Effect of RHP process time (hrs) on the ash content of woodchip derived biochar. Triplicate results are displayed.	66
Figure 2-14: Effect of RHP process time (hrs) on the skeletal density of woodchip derived biochar. Triplicate results are displayed.	67

Figure 2-15: Effect of RHP process time on the electrical conductivity of biochar Soxhlet extract from biochar with respect to the electrical conductivity of raw woodchip Soxhlet extract. Average of duplicate measurements displayed.....	68
Figure 2-16: Effect of RHP processing time (hrs) on methylene blue adsorption of woodchip derived biochar.....	69
Figure 3-1: Schematic drawing of Pyrolytic Shaker Reactor (PSR): (a) Trimetric view (b) Front view.....	77
Figure 3-2: RHP Schematic.....	78
Figure 3-3: RGB peak intensity.....	81
Figure 3-4: Soxhlet extractor (Adapted from Dolinowski(16)).....	85
Figure 3-5: Correlation between electrical conductivity (EC) of Soxhlet extracted and Nespresso extracted liquids. BC: Biochar, BM: Biomass.....	86
Figure 3-6: Effect of RHP process times on biochar yield.....	88
Figure 3-7: Effect of temperature on PSR biochar yield. Dotted line represents an empirical curve fit. Dashed line represents the corresponding PSR pyrolysis temperature of the average RHP char yield between 2 to 3 hrs. Duplicate runs are plotted.....	89
Figure 3-8: Effect of pyrolysis temperature on the mode red intensity of PSR woodchip derived biochars. Arrow provides a possible range of pyrolysis temperatures corresponding of the RHP derived chars.....	90
Figure 3-9: Effect of temperature on the red intensity coefficient of variance. Dotted line represents an empirical curve fit. Dashed line represents the corresponding PSR pyrolysis temperature of the average RHP char red intensity coefficient of variation between 2 to 3 hrs. Triplicate measurements are plotted.....	91
Figure 3-10: Effect of temperature on electrical conductivity (EC) of Soxhlet extracted liquids with reference to raw woodchip feedstock EC. Dotted line represents an empirical curve fit. Dashed line represents the corresponding PSR pyrolysis temperature of the average	

EC of RHP char Soxhlet extracted liquids between 2 to 3 hrs. Average of duplicate measurements are plotted.....	92
Figure 3-11: Effect of pyrolysis temperature on methylene blue adsorption. Dotted line represents an empirical curve fit. Dashed line represents the corresponding PSR pyrolysis temperature of the average RHP biochar methylene blue adsorption capacity produced between 2-3 hours.....	93
Figure 3-12: Comparison between all the properties characterized for RHP char processed for the average between 2 to 3 hrs processing time.	95
Figure 4-1: Schematic drawing of Pyrolytic Shaker Reactor (PSR). (a) Trimetric view (b) Front view	102
Figure 4-2: RHP Schematic.	103
Figure 4-3: RGB peak intensity.	106
Figure 4-4: Soxhlet extractor (Adapted from Dolinowski(23))	109
Figure 4-5: PSR biochar yields for SFD and BFD feedstock. Dotted lines represent an empirical curve fit.....	111
Figure 4-6: RHP biochar yields for SFD and BFD feedstock.....	112
Figure 4-7: Red mode intensity of SFD and BFD derived biochars produced with the PSR between 250 °C to 500 °C. Dotted lines represent an empirical curve fit.	113
Figure 4-8: Red intensity coefficient of variation of SFD and BFD derived biochars produced with the PSR between 250-500°C.	113
Figure 4-9: Red mode intensity of SFD and BFD derived biochars produced with the RHP between 1 to 4 hrs.....	114
Figure 4-10: Red intensity coefficient of variation of SFD and BFD derived biochars produced with the RHP between 1 to 4 hrs.....	114

Figure 4-11: Comparison between the ash content of SFD and BFD derived biochars produced with the PSR between 250-500°C. Dotted lines represent an empirical curve fit.	115
Figure 4-12: Comparison between the ash contents of SFD and BFD RHP derived biochars produced between 1-4 hrs.	116
Figure 4-13: Comparison between the skeletal density of SFD and BFD derived biochars produced with the PSR between 250-500°C.....	118
Figure 4-14: Comparison between the skeletal density of SFD and BFD RHP derived biochars produced between 1-4 hrs.	118
Figure 4-15: Comparison between the electrical conductivity of Soxhlet extract of SFD and BFD derived biochars produced with the PSR between 250-500°C. Dotted lines represent an empirical curve fit.....	120
Figure 4-16: Comparison between the electrical conductivity of Soxhlet extract of SFD and BFD RHP derived biochars produced between 1-4 hrs. Dotted lines represent an empirical curve fit.	121
Figure 4-17: Comparison between the methylene blue adsorption of SFD and BFD derived biochars produced with the PSR between 250-500°C. Dotted lines represent an empirical curve fit.	122
Figure 4-18: Comparison between the methylene blue absorption of SFD and BFD RHP derived biochars produced between 1-4hrs. Dotted lines represent an empirical curve fit. ..	122
Figure A-1: Gast air motor product specification sheet.....	131
Figure B-1: Still frames of video taken showing PSR mixing capabilities taken at (a) 0 s; (b) 10 s and (c) 30 s.....	132
Figure C-1: Effect of pyrolysis temperature on the ash content of PSR WCP derived chars. Point at 25 °C is ash content of raw woodchip biomass.....	133
Figure C-2: Skeletal density of PSR WCP derived biochars as a function of pyrolysis temperature.....	133

Figure D-1: Effect of temperature on EC of Soxhlet extracted liquids with reference to raw woodchip feedstock EC. The estimated Soxhlet EC from Nespresso EC using the correlation determined in Figure 3-5..... 135

Figure E-1: Effect of temperature on SFD PSR biochar yield. The corresponding pyrolysis temperature of the RHP char yield processed for 4 hrs is also shown. Duplicate runs are shown..... 136

Figure E-2: Effect of temperature on BFD PSR biochar yield. The corresponding pyrolysis temperature of the RHP char yield processed for 4 hrs is also shown. Duplicate runs are shown..... 137

Figure E-3: Effect of pyrolysis temperature on the mode red intensity of PSR SFD derived biochars. Dashed line corresponds to the red mode intensity of RHP SFD char processed at 4 hrs..... 137

Figure E-4: Effect of pyrolysis temperature on the mode red intensity of PSR BFD derived biochars. Dashed line corresponds to the red mode intensity of RHP char processed at 4 hrs. 138

Figure E-5: Effect of temperature on the red intensity coefficient of variance on PSR SFD derived chars. Dashed line represents RHP SFD char processed at 4 hrs. 138

Figure E-6: Effect of temperature on the red intensity coefficient of variance on PSR BFD derived chars. Dashed line represents RHP BFD char processed at 4 hrs. 139

Figure E-7: Effect of pyrolysis temperature on the ash content of PSR SFD derived chars. Dashed line represents RHP SFD char processed at 4 hrs..... 139

Figure E-8: Effect of pyrolysis temperature on the ash content of PSR BFD derived chars. Dashed line represents RHP BFD char processed at 4 hrs..... 140

Figure E-9: Skeletal density of PSR SFD derived biochars as a function of pyrolysis temperature. Dashed line represents RHP SFD char processed at 4 hrs 140

Figure E-10: Skeletal density of PSR BFD derived biochars as a function of pyrolysis temperature. Dashed line represents RHP BFD char processed at 4 hrs. 141

Figure E-11: Effect of temperature on PSR SFD electrical conductivity of Soxhlet extracted liquids with reference to raw SFD feedstock EC. EC = Electrical conductivity. Dashed line represents RHP SFD char processed at 4 hrs..... 141

Figure E-12: Effect of temperature on PSR BFD EC of Soxhlet extracted liquids with reference to raw BFD feedstock EC. EC = Electrical conductivity. Dashed line represents RHP BFD char processed at 4 hrs..... 142

Figure E-13: Effect of temperature on PSR SFD biochar methylene blue adsorption capacity. Dashed line represents RHP SFD char processed at 4 hrs..... 142

Figure E-14: Effect of temperature on PSR BFD biochar methylene blue adsorption capacity. Dashed line represents RHP BFD char processed at 4 hrs..... 143

List of Appendices

Appendix A: Gast Air Motor Product Specifications	131
Appendix B: PSR Mixing Images	132
Appendix C: Skeletal Density and Ash Content of WCP Biochars	133
Appendix D: Nespresso™ Extraction.....	134
Appendix E: Equivalent PSR Temperatures for PSR Digestate Derived Biochars	136

Chapter 1

1 Introduction and Literature Review

Present day greenhouse gas levels have reached a point where reducing emissions is not enough to reach pre-Industrialization levels. Instead, we must begin to remove greenhouse gases from the atmosphere by delaying their release using carbon sequestration technologies such as biochar. Canada has abundant resources of biomass available from the agricultural and forestry industries, and municipal food waste which can provide an inexpensive feedstock for biomass conversion. In fact, approximately 6 million tons of food waste alone are discarded each year in Canada, representing a significant resource for renewable energy through anaerobic digestion (1).

1.1 Pyrolysis and Biochar

Biochar is the solid product produced during the process known as pyrolysis. Pyrolysis is the thermal decomposition of organic matter in the absence of oxygen at elevated temperatures, and produces a solid called biochar, condensable vapours referred to as bio-oil and gases (mostly carbon monoxide, carbon dioxide and methane). Biomass feedstocks for pyrolysis are provided by sustainable sources of biomass, which are organic resources that do not compete with food sources or require land use changes with negative environmental impacts (2). Examples of feedstocks include agricultural and forestry waste, food waste, and animal waste.

In the past, the liquid co-product, referred to as bio-oil, has been the main product of interest due to its potential as a green fuel and ability to be refined into value added chemicals. However, recently, focus has shifted towards investigating the applications of the solid product, known as biochar. Biochar is a carbon rich fine black powder and is also comprised of inorganics (ash). It is important to note that varying pyrolysis conditions such as feedstock, pyrolysis temperature and exposure time play an important role on biochar properties, therefore, biochar is characterized by end use.

Biochar feedstock sources are available globally and are relatively inexpensive as they are generally regarded as waste resources. In addition, biochar can be used as a carbon sequestering technology, and releases carbon neutral emissions when combusted.

Biomass carbon dioxide emissions are considered zero or negative because any carbon dioxide released during combustion was originally captured during photosynthesis, thereby reducing overall CO₂ emissions (3).

1.2 Pyrolysis Technologies

The carbonization of biomass is a process that has existed for thousands of years.

Evidence of the use of carbonization technologies in ancient civilizations are present in areas such as the Terra Preta (Portuguese meaning “black earth”) a region in the Amazon basin containing a very fertile black soil. The characteristic dark colour of the soil is caused by the addition of charcoal to the soil over hundreds of years through indigenous slash and char agriculture practices. The coal product present within the Terra Preta soils was made in a similar fashion to how biochar is produced. In indigenous slash and char agriculture practices, agricultural waste is burned at low temperatures over a long period of time, with minimal oxygen present (4). With the progression of modern research and growing interest in pyrolysis products, pyrolysis technologies have been developed into several highly specialized units.

Choosing the appropriate reactor design is essential to successfully produce pyrolysis products for any application. All pyrolysis reactors operate under the same general principle where heat is supplied to a reaction vessel under oxygen limiting conditions, with the heat delivery system and gas-solid contact being the main defining trait between reactors. Each reactor has its own advantages and disadvantages depending on the pyrolysis product of interest. The commonly used lab-scale reactors are summarized below in the context of biochar production (Table 1-1).

1.2.1 Jiggle Bed Reactor

The jiggle bed reactor (JBR) is a batch microreactor in which biomass particles are fluidized by mechanically vibrating the reaction vessel with a linear actuator. Heat is supplied to the unit through an induction heating mechanism. Metal rods referred to as internal heating wires are placed inside a ceramic reactor vessel. The induction heating system provides a magnetic field inducing eddy currents on the surface of the wires, providing heat to the system (5). The JBR provides exceptional fluidization/mixing of solid particles with minimal temperature difference between the wires and reactor bed (6). The major drawback of this reactor is that it can only process feedstocks in the order of a few grams (5).

1.2.2 Fluidized Bed Reactors

Fluidized bed reactors have been extensively used in the petroleum and chemical industries. They provide fluidization and mixing by injecting inert gas vertically upward through a bed of solid particles. For pyrolysis to take place, a solid medium (often sand) is heated to provide effective heat transfer to biomass particles as few feedstocks can be fluidized on their own. Heat from the heated medium is transferred to biomass particles by gas and particle convection (7). Fluidized bed reactors have the advantage of being well known technology with relatively simple and effective process controls, scale up and construction. Fluidized beds are utilized for fast pyrolysis processes, ultimately favoring high liquid yields typically ranging, for woody feedstocks, between 70-75 wt.% and biochar yields around 15 wt.% (8). Biomass feedstocks need to be sieved and/or ground into small particle sizes ranging between 2-3 mm to achieve high biomass heating rates. Vapour and solid residence times are very fast and in the order of seconds (9). The biochar product, which is contaminated with the heating medium, requires elutriation and separation by one or more cyclones (8,10). In some fluidized bed processes, the mixture of heating medium and biochar is conveyed to a burner vessel where char is combusted to provide heat for the pyrolysis process (11).

1.2.3 Auger Reactors

In auger reactors, biomass is mechanically moved through a hot cylindrical reactor tube by a screw or auger. Heat can be supplied by heating the exterior reactor wall, which disperses heat into the reactor, or using a heat carrier such as sand, steel shot, or ceramic balls. Vapours are collected from the top of the reactor while solids are collected from the reactor outlet. Liquid product yields are generally lower than yields from fluidized beds at around 50 wt% yield with biochar yields of approximately 30 wt.%. This is because the vapour and solid residence times are longer, ranging between 10-30 s and minutes, respectively. The temperature inside the cylindrical reactor raises the biomass feedstock to the desired temperature.

Auger reactors provide good heat transfer at smaller scales and are relatively simple to design and construct. They can process a wide variety of feedstocks; however significant attrition of biomass and char particles can occur leading to plugging and a significant energy and torque requirements to operate the auger (12). Another major drawback of this reactor design is that the scale-up of available heat transfer surface area is poor as it is limited to the inner diameter of the reaction tube covered by the biomass particles. Heat carrier particles can improve the heat transfer coefficient, but char must then be separated from the carrier-biochar mixture exiting the reactor.

1.2.4 Mechanically Fluidized Reactor (MFR)

The MFR provides vigorous mechanical agitation of biomass throughout the reactor and, especially, near the reactor wall through a vertical blade stirrer. Heat is provided to the outer wall and transferred to the pure char bed. Biomass particles sizes ranging between 4-8 mm can be processed in this reactor, allowing for a variety of feedstocks to be processed. Since biomass particles are injected into a well-agitated bed of hot particles, fast pyrolysis conditions can be achieved, if the biomass particles are small enough.

The MFR is geared towards liquid production rather than maximizing biochar production, with char yields between 20-30 wt.% depending on feedstock and operating conditions (13). Although excellent heat transfer can be achieved with this reactor, it shares similar disadvantages to auger reactors. The vertical blades can cause significant attrition to the biomass and biochar particles, leading to plugging and requiring high energy and torque for processing. During scale up, the heat transfer surface area is also limited by the inner diameter of the reaction vessel, which provides heat to the bed of char particles. Because heat is supplied externally from the reaction vessel wall, insulation is required to minimize heat losses to the environment.

1.2.5 Rotary Kiln Reactor

In rotary kiln reactors, feedstock is fed into a slightly inclined rotating horizontal cylindrical vessel. The rotating motion of the kiln facilitates the agitation of biomass. Heat is provided to the biomass indirectly by heating the exterior of the kiln via an electrical furnace and is mainly transferred through radiative conduction. A major advantage of this technology is that it can process a wide variety of feedstocks with relative ease and without significant attrition to the biomass particles. This technology is also relatively simple and easy to scale up, however the available heat transfer surface area is limited by the inner diameter of the kiln in contact with the solids (7).

Table 1-1: Summary of operating conditions and heat capacities of different lab scale pyrolysis reactors.

Reactor Type	Pyrolysis Condition	Wall-to-bed Heat Transfer Coefficient	References
JBR	Slow	50-500 $\text{W m}^{-2} \text{ } ^\circ\text{C}^{-1}$	(5,13)
FCR	Fast	150-350 $\text{W m}^{-2} \text{ K}^{-1}$	(7)
Auger	Intermediate	50-300 $\text{W m}^{-2} \text{ K}^{-1}$	(7)
MFR	Intermediate or Fast	50-585 $\text{W m}^{-2} \text{ K}^{-1}$	(13,14)
Rotary Kiln	Slow	50-100 $\text{W m}^{-2} \text{ K}^{-1}$	(7)

1.2.6 Laboratory Reactor Needs For the Development of Biochar Products

There is a need for laboratory reactors that can quickly provide sufficient quantities of biochar. Biochar quantities of hundreds of grams of biochar are required for testing in applications such as soil amendment, fillers for concrete or polymers, coke substitution or pollutant capture. Intermediate pyrolysis reactors are preferred for processes focused on the production of high-quality biochar. Many laboratory reactors are scaled-down versions of industrial reactors and the main types include rotary drums and augers (15). These reactors are not suitable for quick laboratory studies on the impact of pyrolysis conditions of biochar properties due to the significant time required to reach steady-state operation. The mechanically complex reactor designs along with a significant heat of pyrolysis greatly influence the time to reach steady-state operations.

To obtain a high quality, homogeneous biochar product, all particles should be exposed to the same temperature history, which means good radial mixing and near plug flow of solids in the axial direction, with negligible axial back-mixing(16,17,18). Therefore, industrial

reactors can be simulated in a lab environment using batch reactors that provide the same temperature evolution of the biomass particles.

1.3 Biochar Applications

Applications of biochar with interesting potential include carbon sequestration, soil amendment, activated carbon production, metallurgical applications, power generation, addition to composites, and catalysis. This thesis focuses on the production of biochar for soil amendment and the relevant literature is reviewed in depth in Section 1.4. A brief overview of interesting biochar applications is provided below.

1.3.1 Biochar for Carbon Sequestration

Carbon sequestration involves the long-term storage of atmospheric carbon to delay the accumulation of greenhouse gases (GHG) within the atmosphere. Carbon dioxide is captured naturally through chemical, biological and physical processes, however, due to the mass generation of GHG, artificial carbon capture technologies have been implemented globally. Figure 1-1 below lists both implemented and potential carbon sequestration methods.

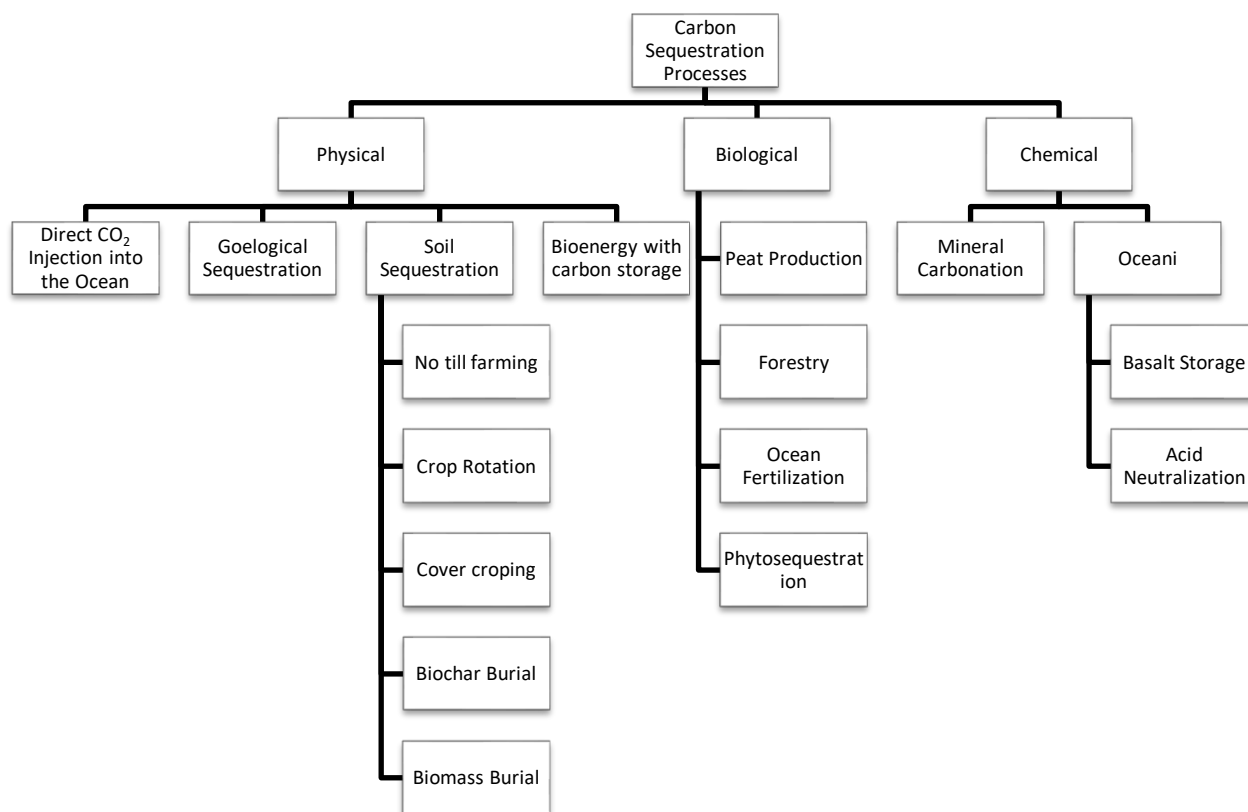


Figure 1-1: Carbon Sequestration Processes and Methods (Adapted from Nogia et al. (17))

Biochar creates a carbon sink when incorporated into the soil through agricultural practices. During photosynthesis, biomass captures carbon dioxide from the atmosphere, which is then stored within biochar. The amount of carbon stored in biochar during pyrolysis is highly dependent on pyrolysis feedstock. On average, approximately 50% of initial biomass carbon is sequestered into biochar (18). Due to their highly aromatic composition, biochars have high C-stability and are less available for microbial degradation (19).

Many biochars have been documented as having high soil stability, especially when produced at high temperatures (20,21). However, the effects of aging on biochar properties, including C-sequestration, are still under debate and studies have been showing contrary results. De la Rosa et al. (22) tested the effects of aging on a number of

biochars produced from a variety of feedstocks. Field experiments over a period of 24 months were conducted, and it was found that carbon losses varied based on biochar feedstocks, ranging between 11-27% of the initial carbon. Another field experiment conducted by Wang et al. (23) suggested that as opposed to prior belief that soil C-sequestration was attributed to biochar recalcitrance, biochar simulates C-sequestration through the stabilization and physical protection of soil organic matter with aggregates.

1.3.2 Biochar as Soil Amendment

Adding charcoal to soils has been shown to have numerous beneficial effects on soil fertility, with the fertility of the Terra Preta soils being a prime example (4). This has inspired a large interest in using biochar to replicate the effects of charcoal in Terra Preta soils.

Biochar has been shown to have several beneficial effects on soils through increased water availability to plants (24), increased cation exchange capacity (25), and decreased soil leaching of nutrients (26). The mechanisms of biochar-soil interactions are still unclear and is a major focus of research in this field. More details are provided in Section 1.4.

1.3.3 Activated Carbon

Activated carbon is the most commonly used adsorbent material in numerous industries. The most common applications of activated carbon are for wastewater pollution removal, air purification and contamination removal. Activated carbon can be divided according to four primary feedstock sources; wood-based, coal-based, coconut shell-based and nutshell-based. Growing public environmental concerns have created a shift within the activated carbon market (27). According to the Freedonia group, the global demand for activated carbon in the year 2016 was 1.65 million tons and is predicted to increase steadily by 3.5% each year until the year 2020. The main driving forces for the growth in the renewable activated carbon market is caused by environmental regulations within the

US and China, who are the two largest contributors to this market (28). Market demands for renewable activated carbon feedstocks, especially coconut shell activated carbons, have increased because of environmental regulations, whereas the coal activated carbon markets have experienced downward trends, which are predicted to continue (27) .

As the activated carbon demand continues to grow, there is a need for inexpensive feedstock alternatives. Biochar produced from globally available forestry and agricultural waste products can provide a suitable precursor material for activated carbon production. In addition, import/export costs would be greatly reduced due to the abundance of locally available waste biomass from numerous industries. The major research focus in this field is on modifying biochar properties through physical or chemical techniques, commonly referred to as activation. Activation techniques have been shown to increase surface area through the development of micro-pores, creating more absorption sites, resulting in faster adsorption rates (29–31).

1.3.4 Biocoke for Metallurgical Applications

The metallurgical industry (such as iron and steel production) produces large amounts of greenhouse gasses using coke as both a fuel and reducing agent. According to Natural Resources Canada (NRC) (32), an average of 3.7 Mt/yr of coke is used in blast furnaces, resulting in 13.7 Mt/yr of CO₂ emissions. Currently, the governing energy sources used for metallurgical applications are derived from fossil fuels (coal and natural gas).

Replacing commercially available reducing agents and non-renewably sourced coke with raw biomass or biochar can reduce greenhouse gas emissions significantly since biochar emissions are CO₂ neutral. While the majority of research in this field has a strong focus on replacing coke with raw biomass within the blast furnace and sintering process for fuel as opposed to using biochar, biochar has been investigated as an alternative for coke and reducing agents (33,34).

Although the ultimate goal is to replace coke derived from non-renewable resources with bio-coke as a fuel source, it is currently not feasible due to the reduced hot strength of the resulting coke, caused by the high mineral content of biochar (35). Through lab scale and

pilot plant experiments conducted by the NRC, it was proven that replacing up to 20% of coke fuels with renewable carbon sources is achievable, potentially reducing CO₂ emissions by 2.8 Mt/yr (32).

1.3.5 Biochar as Bio-coal

In recent years, coal fired power plants have been required to reduce GHG emissions through the implementation of government regulations. In 2012, the Government of Canada implemented the Reductions of Carbon Dioxide from Coal-Fired Generation of Electricity regulation (36). Within the regulation, an emission intensity limit of 420 tonnes CO₂ from the combustion of fossil fuels per GWh electricity produced was set in order to entice coal-fired plants to reduce GHG emissions. In addition, starting in 2019, Canada will be implementing a carbon tax, starting at 20\$/tonne CO₂ equivalent emissions and set to increase to 50\$/tonne CO₂ by 2020. Both policies provide an economic incentive to reduce GHG emissions. However, when compared to natural gas, bio-coal

One method of reducing CO₂ emissions is through the use of biomass as either a direct or indirect fuel alternative due to the carbon neutral nature of biomass. However, raw biomass is not suitable as a coal replacement due to its high moisture retention, non-homogeneous combustion, perishable nature, low energy density and poor grindability (12,37). Many of these issues can be alleviated through the pre-treatment of raw biomass by pyrolysis or torrefaction to produce biochar (38).

Although, the end goal application for biochar as a solid fuel is to completely replace coal as a fuel source, it would require a new plant infrastructure and large capital investment. Since the technology to convert biomass into a solid fuel for coal replacement with high energy efficiencies close to that of coal has not yet been perfected, implementing co-firing into existing power plants is an attractive alternative (39).

Implementing co-firing plants have been shown to help mitigate the non-homogeneous combustion effects that can occur when using biomass. As well, by replacing a fraction of

the coal, overall greenhouse gas emissions of the power plant are lowered. Co-firing can be implemented into existing coal power plants with minimal capital and operational costs, however operation and maintenance costs increase with increasing biomass to coal ratios. Investment costs for direct co-firing are in the range of 300-700 USD/kW, and operational costs are typically 2.5-3.5% of the capital investment (2). According to an estimation made by the International Energy Agency, by the year 2035 the CO₂ emissions from coal firing plants could be reduced between 45-450 million tonnes per year with 1-10% coal replacement with biomass (40).

1.3.6 Biochar as a Catalyst

Biochar can be used as a catalyst for syngas cleaning, converting syngas to liquid hydrocarbons (Fischer-Tropsch synthesis) and as a solid acid catalyst for biodiesel production. One of the most important biochar properties to make a successful catalyst is the ash content within the feedstock. The inorganic elements present in the biomass feedstock are further concentrated in the biochar and serve as active sites in hydrogen recovery systems and methane degradation (41).

1.3.6.1 Syngas cleaning

Syngas produced from biomass gasification contains tars that are extremely harmful to further downstream processes. Traditionally, syngas is cleaned by catalytic cracking, oil or water scrubbing, or thermal cracking. Catalytic cracking is the most commonly used method within industry since it is the least energy intensive process and more environmentally conscious (no wastewater is produced unlike with other syngas cleaning methods, with the exception of thermal cracking). When using the right catalyst, the process is less energy intensive because high tar removal efficiencies (above 90%) can be achieved at low temperatures (below 700 °C).

Multiple studies have tested the use of biochar as a direct catalyst as well as catalyst in the form of biochar supported on an active metal loading. The catalytic activity of

biochar is related to the following properties; pore size, surface area and mineral content (42). In a study conducted by Mani, Kastner and Juneja (43), pine bark biochar was used as a direct catalyst to decompose tar (toluene). The activation energy (91 kJ/mol) and removal efficiency (90%) are comparable with traditional syngas cleaning catalysts, thereby indicating that biochar is a contending catalyst alternative.

1.3.6.2 Fischer-Tropsch Synthesis Catalyst

The use of the right catalyst is the key to a successful conversion of biomass into liquid hydrocarbon fuels (also known as Fischer-Tropsch synthesis). Fischer-Tropsch reactions combine hydrogen and carbon monoxide provided from biomass through a process known as gasification. These gases are then turned into a synthetic fuel. Nano-sized iron particles is a commonly used catalyst for this process because they are inexpensive, have a low hydrogen to carbon monoxide loading rate and a high selectivity towards olefin production. The issue with nano-sized iron catalysts is that there is a low product selectivity, and particle agglomeration accompanied by sintering can become an issue due to the high temperatures in the Fischer-Tropsch synthesis process (44). To overcome these issues, different carbon sources such as activated carbon, saccharides and biochar have been tested as supports for the iron catalyst (45,46). Biochar has been a large interest as a potential carbon support because of its low cost and sustainability. In a study conducted by Yan et al. (47), biochar produced from pine wood was used as a carbon support for the synthesis of carbon encapsulated iron Nano- particles and used to carry out a Fischer-Tropsch synthesis conversion. Through extensive testing over a period of 1500 h, the nanoparticles showed to have an overall CO conversion of 95 % and a liquid hydrocarbon selectivity of 68 %. These values are much higher than for other tested carbon supported iron catalysts.

1.3.6.3 Solid Acid Catalyst for Biodiesel Production

One method of producing biodiesel is through the esterification and transesterification of vegetable oil and animal fat with the use of either an acid or alkaline catalyst. Alkali-catalyzed transesterification is the most common method of biodiesel production because it is an inexpensive catalyst and has shorter reaction times than acid catalysts. There is a need to develop low cost acid catalysts for this process because alkaline catalysts are highly sensitive to both water and free fatty acids present within the oils, whereas acid catalysts are not as sensitive. Studies conducted by Kastner, Mani and Juneja (48) and Dehkhoda, West and Ellis (49) have shown that biochar is a suitable foundation material to produce catalysts for this process. It was shown through these studies that biochar based acid catalyst provided high surface area, particle strength, hydrophobicity and sulphonic group acid density, which attributed to high catalytic activity as well as the ability to reuse the catalyst.

1.3.7 Biochar as a Filler for Composite Materials

Synthetic polymers are heavily used in commercial production of plastics, elastomers, adhesives and surface coatings. There is a high demand for thermoplastic materials, as they provide an inexpensive material often used in packaging, bags and bottles along with many other everyday products. Commercial polymers are often a combination of solid materials (fillers) blended with polymers referred to as composite materials. Fillers are added to composite materials to improve the chemical and mechanical properties of the resultant polymers. Common commercially used fillers include calcium carbonate, talc, aluminum silicate, alumina trihydrate, carbon black and calcium sulfate to name a few. There is a growing interest in replacing non-renewable fillers such as carbon black (which is derived from petrochemical materials) with a bio-composite such as biochar (50). Biochar provides an attractive alternative due to low costs and local feedstock availability. Biochar has the potential to improve polymer matrices electrical, mechanical and thermal properties. This can be attributed to biochars porous structure, high surface area, high carbon content, high thermal stability and potential electrical conductivity

(51,52). In fact biochars hydrophobic nature allow for more stable polymer matrices to form, making it better suited as a filler over other natural fibres (51). Biochar properties can be easily altered through the conditions of pyrolysis, allowing biochar properties to be fine-tuned to obtain a product with greater compatibility with the polymer matrix.

1.4 Biochar for Soil Amendment

1.4.1 Biochar Formation and Characteristics

Biochar is the solid co-product produced during the thermochemical decomposition of biomass in the absence of oxygen. There are three main thermochemical processes that produce biochar: pyrolysis, torrefaction and gasification. Slow pyrolysis and torrefaction reactions are geared towards maximum biochar production. Torrefaction reaction temperatures typically range between 200°C-300°C, whereas pyrolysis reactions occur between 350°C-900°C.

An important balance between maximizing biochar yield without sacrificing quality is essential to producing a successful soil amendment. Biochar yields and characteristics vary widely, and are highly dependent on pyrolysis conditions including feedstock, pyrolysis temperature heating rate and exposure time. Although specific values vary based on feedstock, the effects of pyrolysis temperature on biochar properties usually follow the following trends; with increasing pyrolysis temperature, yield, volatile matter, hydrogen content, and H/C ratio decrease, whereas, ash, aromaticity, carbon content, pH, and surface area increase (53,54). The feedstock also plays an important role on determining biochar properties. Singh et al. (55) investigated the influence of 11 feedstock sources on biochar characteristics for soil amendment. Overall, wood derived biochars have higher carbon content, lower ash content (N, P, K, S, Ca, Mg, Al, Na and Cu) and lower potential cation exchange capacity (CEC) followed by leaf based biochars, then manure based biochars. Heating rate also has an influence on char yields. Slower heating rates increase char productions whereas higher heating rates produce more volatiles (56). Due to their versatile properties, biochar soil amendments must be customized to meet the specific needs of individual soil profiles.

1.4.2 Biochar Effects on Soil Fertility

Biochar has been shown to improve soil fertility when used as a soil amendment, although the exact mechanism between biochar and soil interactions are still unclear. Biochar can improve soil structure and nutrient availability to plant roots, however it is extremely important to properly match biochar properties with the appropriate soils.

1.4.2.1 Nutrient Properties (Chemical Properties)

Biochar itself can provide more nutrients to soils and make nutrients more available for plant uptake. The chemical composition of biochar is dependent on the feedstock, however, inorganic nutrients essential for plant development are concentrated in the final product during pyrolysis. Prakongkep et al. (57) investigated the forms and water solubility of plant nutrient elements in tropical plant waste biochars. As expected, biochar feedstocks provided different nutrients however it was found that plant nutrients were most available in crystalline minerals embedded within the biochar structure and surface. The different biochars provided nutrients in diverse crystallized forms. Calcium was often presented as calcite (CaCO_3), whereas potassium (K) was present in several mineral forms (KH_2PO_4 , KCaCl_3 , KHCO_3 , KCl , $\text{K}_2\text{MgP}_2\text{O}_7$). Solubility testing showed that potassium was highly water soluble and available for immediate plant uptake however, calcium and phosphorous were less water soluble than potassium and therefore unavailable for immediate plant uptake (57). A study conducted by Limwikran et al. (58) found similar results when testing nutrient dissolution into soils as opposed to water solubility. Nutrient dissolution from nine different tropical plant waste biochars was investigated in ten different soil profiles, and it was determined that potassium crystals diffused from the biochar matrix into soils, whereas calcium and phosphorous mostly remained within the structure (58).

In addition to providing additional nutrients, biochar can also improve soil nutrient retention, ultimately reducing eutrophication caused by nutrient leaching. Lehmann et al. (59) found that nutrient leaching of an applied fertilizer was significantly decreased with

biochar soil amendment. Increased plant uptake of P,K,Ca, Zn and Cu was also observed with increasing biochar amendment (59,60). An increase in the soils cation exchange capacity is responsible for improved nutrient retention. Soil cation exchange capacity is a soils ability to hold on to essential nutrients. Biochar addition improves soil cation exchange capacity through the combination of two mechanisms: 1) higher SOM oxidation 2) increased soil surface area for cation adsorption (25). Biochars ability to improve soil nutrient retention is an important factor for the co-application of biochar with chemical fertilizers to improve efficiency. Table 1-2 below outlines recent studies investigating the co-application of fertilizer and biochar.

Soil salinization is a potential disadvantage to amending soils with biochar and occurs when salt concentrations accumulate within soils. Nutrients leached from biochar can accumulate within soils. High salinity effects the metabolism of soil organisms and reduces the amount of plant available water, ultimately reducing crop yields.

Table 1-2: Recent studies investigating the co-application of biochar and fertilizer a soil amendment. Agronomic responses are based on a comparison of soils amended exclusively with biochar vs. fertilizer biochar mixtures.

Reference	Biochar Feedstock	Crop	Fertilizer	Agronomic Response of Biochar Fertilizer Mixture in Comparison to Exclusive Biochar Amendment
(61)	Farmyard manure, poultry manure, woodchips, kitchen waste	Wheat	Chemical Fertilizer	Wheat grain yields increased
(62)	<i>Acacia ssp</i>	Barley	Urea	Grain yield increased
(63)	Poultry litter	Corn (<i>Zea mays</i> L.)	Urea	Plant height aboveground and root biomass increased
(64)	Kunai grass (<i>Imperata cylindrical</i>)	Chinese cabbage (<i>Brassica rapa</i> L. <i>ssp. chinensis</i> L)	Urea	Aerial biomass (stalk + leaf) yield increased approximately 3x
(65)	Kunai grass (<i>Imperata cylindrical</i>)	Sweet potato (<i>Ipomoea batatas</i> L. Lam)	NPK mineral fertilizer	Sweet potato total tuber yield increased by 100% and above ground biomass yield increased 75%

1.4.2.2 Soil Structure and Properties

Soil physical properties have a great influence on soil behaviours, ultimately affecting soil fertility. Biochar amendment can improve soil physical properties when the correct biochar formulation is paired with the right soil profile. Biochar-soil interactions are a major area of research and not fully understood, since every soil profile interacts differently with each type of biochar. Blanco-Canqui, (66) and Omondi et al. (67) both conducted thorough reviews on the effects of biochar amendment on soil physical properties. Overall, both reviews came to the conclusion that when biochar and soil

profiles are properly paired, biochar amendment improves soil bulk density, soil water retention capacity, and wet soil aggregate stability (66,67) .

Bulk density is an indication of a soils ability to function for plant root structural support, water and solute movement, and soil aeration. Soils with high bulk density poor soil porosity, can lead to limitations in plant root growth and development, negatively impacting crop yields. Based on the meta-analysis reviews conducted by Blanco-Canqui (66) and Omondi et al. (67), in general, biochar amended soils reduced bulk density in all soil profiles, however the extent of reduction varied significantly between soil profiles and biochar feedstock. The reduction in soil bulk density with biochar amendment is attributed to three main mechanisms. First, due to biochars low density and high porosity, soil bulk density is reduced through dilution. Because of this mechanism, the impact of biochar amendment is highly dependent on soil density, with the greatest effects occurring between biochars and soils with larger differences in bulk density. Overall data suggested that biochar application has greater effects on the bulk density of course textured soils rather than fine textured soils, further proving that biochar reduces bulk density through dilution. Secondly, biochar could also reduce bulk density by increasing soil porosity through increased aggregate stability. Lastly, Burrell et al. (68) and Laird et al. (69) suggested that biochar acts as a soil conditioner by supporting microbial communities within the soil biota that are associated with maintaining soil structure.

Soil water retention has also been shown to increase with biochar amendment, as it is a function of bulk density (70). In addition, Quin et al. (71) hypothesized that biochar pores can hold water, contributing to improved water retention. Gray et al. (72) then investigated to distinguish the effects of biochar porosity and surface hydrophobicity on water uptake. To do this, water and ethanol absorption of hazelnut and Douglas fir biochars produced at different pyrolysis temperatures were compared. It was found that with increasing pyrolysis temperature, water absorption decreased, however, ethanol absorption remained constant suggesting that water uptake is related to surface hydrophobicity rather than porosity (72). These results are supported by those of Kinney et al. (73) who determined that biochar hydrophobicity is reduced with increasing pyrolysis temperature (73). Increasing the plant available water in soils can contribute to

the reduction of water usage for crop irrigation, with the potential to greatly benefit water-limited regions globally.

Soil aggregate stability signifies a soil ability to resist erosion from natural (wind, rainfall etc.) and agricultural forces (tillage, cropping etc.). The effect of biochar amendment on soil aggregate stability has been investigated with mixed results. Once again, soil-biochar interactions are not fully understood, and pairing specific soil profiles with the correct biochar formulation is the key to producing a successful soil amendment. Blanco-Canqui (66) evaluated the results of studies investigating biochar effects on wet aggregation stability over 34 different soil profiles worldwide. Overall, biochar has been shown to increase wet soil aggregate stability, although the significance varied based specific soil profiles. Burrell et al. (68) indicated that biochar amendment in sandy soils will provide better soil aggregate stability than in clay soils by providing inorganic binding agents to promote soil agglomeration.

1.4.3 Effects of Aging on Biochar

Determining the effects of aging on biochar composition and structure is important to determine its stability in soils over long periods of time. Initially, biochar was thought to be highly resistant to degradation, with a similar timeline to the charcoal present in the Terra Preta soils. However, recent research has shown contradicting results, implying that the stability of biochars over time is much shorter than initially anticipated. The contradicting results about biochar stability in soils is crucial information from an economic standpoint. The value of carbon credits is highly dependent on biochars ability to sequester soil into the soil for as long a time as possible.

De la Rosa et al. (22) studied the effects of five different biochars (pinewood, paper sludge, sewage sludge, old vineyard wood, mixed wood chips) aging over a 24-month field experiment. The study found that initial C content for all biochars decreased with time, ranging between 11-27% C loss for the different biochar types. The pH for each char varied based on the initial feedstock, however they all decreased over time,

indicating the potential use of biochar as a soil acidification treatment. It was also determined that aged biochars are less aromatic, and more functionalized than new chars.

Cross and Sohi (74) used accelerated aging techniques through a combination of thermal and chemical oxidation to determine the effect of pyrolysis temperature on biochar long-term stability. The C-stability of a number of biochars derived from different feedstocks at varying pyrolysis temperatures was tested and a clear relationship was observed; with increasing pyrolysis temperature, C-stability increases as well.

1.4.4 Current Challenges

Biochar can be a very fine powder, which can lead to difficulty when handling and incorporating into soils. Due to its particulate size, biochar is easily susceptible to airborne or soil erosion or dissolution and mobilization through runoff, leading to considerable losses (75–77). It is estimated that approximately 30% of biochar is lost and becomes airborne when cultivated into soils using standard farming equipment (78). Biochar granulation is one method of reducing biochar losses during application, as the larger biochar granules are less susceptible to becoming airborne and washed away. Two studies conducted by Bowden-Green and Briens (79,80) showed that the drum granulation of biochar is possible, however challenges lie in finding an appropriate and inexpensive binding agent. Due to the hydrophobic nature of biochar, water based binding agents do not penetrate the powder bed, forming liquid marbles during granulation resulting in a unique granulation method.

Another major concern with using biochar is the formation of polycyclic aromatic hydrocarbons (PAH) during pyrolysis. Animal studies have shown that PAH are carcinogenic compounds and can also affect the immune and reproductive systems (81). Plants can absorb PAH from soils through their roots and accumulate until ingested by humans and animals (82,83). PAH uptake in plants have been directly linked to PAH concentrations present in contaminated soils (82,84).

A study conducted by De la Rosa et al. (85) conducted a risk assessment of different biochars due to PAH contamination and explored the influence of feedstock, reactor type and operating conditions. Rice husk, wood, wheat and sewage sludge derived biochars were produced in three different pyrolysis reactors (kiln, batch and rotary) at different temperatures (400, 500 and 600 °C). Biochar extractions were performed by Soxhlet extraction with toluene, followed by gas chromatography and mass spectroscopy analysis. The study concluded that the key factors influencing PAH concentrations when producing biochar are the type of reactor and pyrolysis temperature, while feedstock was shown to have minimal effect. The concentration of PAH decreased with increasing pyrolysis temperature, with a drastic decrease in concentration between 400 °C and 500 °C for all char and reactor types (85). The continuous rotary reactor produced the safest biochars compared to the two batch reactors (kiln and batch). It was hypothesized that the immediate separation of the vapours prevents PAH condensation into biochar.

1.5 Granulation

Granulation is used in several industries to reduce dustiness to minimize losses and reduce inhalation and exposure risks; improve flowability and handling; minimize caking of powdered products; and improve bulk density. Wet granulation is the process of agglomerating particles together through the addition of a liquid binder. Binder is sprayed onto a moving powder bed surface, which can be agitated using a mechanical mixer, tumbling drum or fluidization. Binder droplets penetrate the powder bed to bind the particles together by a combination of capillary and viscous forces to form small agglomerates called nuclei. The nuclei then grow through a granulation mechanism into larger granules. More permanent bonds between the particles are then formed following drying or sintering (86).

1.5.1 Hydrophilic Granulation Mechanism

Wet granulation of hydrophilic powders includes three main stages: (i) wetting and nucleation, (ii) consolidation and coalescence and (iii) attrition and breakage. All three stages of granulation can occur together, and do not follow a sequential order. During the wetting and nucleation stage, liquid binder is brought to contact with a dry powder bed and dispersed within the powder bed by mechanical mixing to form small agglomerates called nuclei. Nuclei formation is a function of wetting thermodynamics and kinetics, whereas binder dispersion is a function of, and controlled by process variables (87). Nuclei formation may follow one of two mechanisms proposed by Shaefer and Mathiesen (88). The dispersion mechanism occurs when liquid binder droplets are smaller than the particulates and coat the surface of the particulates causing the individual particulates to agglomerate into a nuclei. When liquid binder droplets are larger than the particulates, the immersion mechanism occurs, and the particulates coat the droplet, and eventually penetrate and fill the droplet to form a nuclei (88). The rate of nuclei growth is highly dependent on the distribution of the binding liquid, as good binder dispersion will provide uniform wetting and controlled nucleation (89–91). There are two broad classes of granule growth behaviour; steady growth and induction or consolidation time growth (92). The deformation of granule is the differentiating factor between the two growth mechanisms. Steady growth behaviour occurs when weaker granules deform during collision, creating a large contact area between granules. The liquid binder is then moved to the surface within the contact zone forming a strong bond between the granules. Contrarily, during consolidation time growth, granules do not deform during collision to form a strong contact bond, causing granules to break apart leading to a period of little to no growth. Liquid binder is continually added until there is enough binder on the surface of the granules to form strong bonds during granule collision, triggering a period of rapid growth. The type of growth behavior is dependent on powder characteristics and granulation parameters such as agitation intensity, liquid viscosity, particle size and liquid surface tension (80,93,94). The third stage in granulation is attrition and breakage. Breakage occurs when wet granules break apart in the granulator, while attrition is the fracture caused by surface wear of dry granules in the granulator or during handling (95).

1.5.2 Granulation of Hydrophobic Powders Mechanism

Granulation mechanisms of hydrophobic powders are currently not well understood. A few studies have examined nucleation mechanisms by drop penetration of liquid binders onto static beds of hydrophobic powders. Contrary to hydrophilic powders, the droplet does not immediately penetrate the powder bed and instead forms a liquid marble structure. The liquid droplet remains intact and powder particles are drawn up and around the surface of the droplet (96,97). A theory to explain this mechanism is based on the solid spreading coefficient model developed by Rowe (98). Hapgood and Khanmohammadi (96) also suggested that bulk motion of the drop due to rolling and impact is required for this type of nucleation to occur. It was also determined that particle size, liquid binder viscosity and surface tension effect the formation of liquid marbles). Hapgood and Khanmohammadi (96) found that liquid marbles were only able to be formed using only the finer grades of PEG200. Decreasing particle sizes creates more stable liquid marbles because as particle size, along with mass, is increased, gravitational forces overcome the forces pulling particles up and around the surface of the liquid marble. Lower viscosity polyethylene glycol (PEG) solutions were also found to form more stable liquid marbles than higher viscosity PEG solutions. However glycerol which had the highest viscosity of all the solutions tested was able to form a stable liquid marble. Lastly, liquid solutions with low surface tensions formed marbles that would collapse while high surface tension liquids formed marbles that were able to maintain their shape.

Mundozah et al. (99) investigated two competing spreading mechanisms of single liquid droplets onto static hydrophilic and hydrophobic beds. The droplet spreading mechanisms investigated are constant drawing area (τ_{CDA}) and decreasing drawing area (τ_{DDA}). τ_{CDA} assumes that horizontal drop diameter remains constant throughout the spreading process while the contact angle decreases, contrary to τ_{DDA} which assumes that contact angle remains unchanged, while horizontal droplet diameter decreases throughout the spreading process. Results showed that horizontal droplet spreading time rate into static hydrophilic powder beds was driven by capillary forces when the liquid droplet is

at maximum horizontal spreading, following the τ_{CDA} mechanism. As the contact angle between the liquid droplet and powder bed increased (due to increased powder hydrophobicity), the droplet penetration process transitioned from the τ_{CDA} to τ_{DDA} mechanism, which occurs via site percolation theory.

1.5.3 Granulation of Biochar

Drum granulation is one type of wet granulation, commonly used in the fertilizer industry to produce granular nitrogen, phosphorus and NPK fertilizer. In this process, agitation of the powdered bed occurs through the rotation of an axially mounted cylinder (drum). In the case of hydrophilic powders, a liquid binder is sprayed, forming nuclei which then tumble to create solid spherical pellets. Drum granulation operating parameters that can be controlled include drum fill volume, liquid binder spray rate and distribution and drum rotation speed. It is important to also note the binder formulation can also impact granulation and granule properties.

Drum rotational speed is one of the fundamental parameters impacting the extent of size enlargement and physical properties of granules through improved opportunity for coalescence to occur. With low drum rotational speed, the powder bed slips at the bottom of the drum with little movement, while high rotational speeds can cause a cataracting flow and wall build up. A cascading flow motion is most desired to provide the greatest probability for granule coalescence to occur (95). It has been suggested that the optimal drum speed is half the critical speed (100), which is defined as follows:

$$N_c = \sqrt{(g \sin \beta) / 2 \pi^2 D} \quad (1-1)$$

Where g : gravitational constant; β : angle of the drum; D : diameter of the drum

The effect of drum volume load was studied by Santomaso et al. (101), where a drum was filled at 10, 15 and 25 % v/v. It was determined that the transition between the rolling and cascading flow pattern was achieved at 25 % v/v fill level.

Viscosity and liquid tension of the added binder also plays an important role on the consolidation rate and resultant granule properties. In a study conducted by Iverson and Litster (92), the consolidation rate for the granulation of glass ballotini particles was found to be a complex function of both binder viscosity and solid particle properties. Consolidation rate was found to increase as particle size decreased, and binder viscosity increased. It was also determined that interparticle friction, capillary and viscous forces all affect granule consolidation. Interparticle forces acts as a lubricant between particles, and are therefore reduced with increasing binder content, while also viscous forces.

Bowden-Green and Briens (79,80) were able to successfully granulate three different biochar feedstocks (birchbark, miscanthus and cornstalk) in a drum granulator using hydroxypropyl methylcellulose (HPMC) as the binding agent. Binder concentration, total binder solution volume and drum rotational speed were all found to affect granule size, while drum rotational speed and liquid binder concentration affected granule strength. Increased drum rotational speed and liquid volume increased biochar size in all three feedstocks, however binder concentration had a negative effect due to increased viscous forces. Consolidation was promoted by increased binder concentration leading to overall increased granule strength. Although drum granulation was successfully achieved, granulation parameters need to be optimized to produce granules with characteristics that can withstand handling and distribution methods of the agricultural industry. It would be ideal to produce granules with characteristics similar to fertilizer granules, allowing for the simple integration of biochar granules into current industrial practices.

1.5.4 Thesis Objectives

The following thesis can be divided into three main research stages. Each of the research stages are represented in chapters 2, 3 and 4, respectively. The main objective for the first research stage (Chapter 2) was to design, develop and build a new lab scale pyrolysis reactor capable of producing kg quantities of biochars required for further testing to develop biochar products. Stage 2 (Chapter 3) focused on the validation of the new pyrolysis reactor (referred to as the Rotating Heater Pyrolyzer (RHP)), through the comparison of biochar quality between the RHP and a small-scale lab reactor. The final research stage (Chapter 4) provided an example of a potential application for RHP produced biochar, and the potential for soil amendment between two different digestate feedstocks was investigated.

1.6 References

1. Biogas Association. Canadian Biogas Study: Benefits to the Economy, Environment and Energy [Internet]. 2013 [cited 2019 Jun 16]. Available from: https://biogasassociation.ca/images/uploads/documents/2014/biogas_study/Canadian_Biogas_Study_Summary.pdf
2. Lempp P. Biomass Co-Firing in Coal Power Plants [Internet]. 2013 [cited 2019 Jun 8]. Available from: www.irena.org
3. Schmidt H-P, Anca-Couce A, Hagemann N, Werner C, Gerten D, Lucht W, et al. Pyrogenic carbon capture and storage. *GCB Bioenergy* [Internet]. 2019 Apr 1 [cited 2019 May 28];11(4):573–91. Available from: <http://doi.wiley.com/10.1111/gcbb.12553>
4. Winklerprins AMGA. Terra Preta The Mysterious Soils of the Amazon [Internet]. 2014 [cited 2019 Jun 8]. Available from: <https://pdfs.semanticscholar.org/1d8d/a796a7ccacea70e05f6251dbe131ca238337.pdf>
5. Latifi M, Berruti F, Briens C. Non-catalytic and catalytic steam reforming of a bio-oil model compound in a novel Jiggle Bed Reactor. *FUEL* [Internet]. 2014 [cited 2019 May 27];129:278–91. Available from: <http://dx.doi.org/10.1016/j.fuel.2014.03.053>
6. Latifi M, Berruti F, Briens C. Gasification of Bio-oils to Syngas in Fluidized Bed Reactors [Internet]. 2012 [cited 2019 May 27]. Available from: <https://ir.lib.uwo.ca/etdhttps://ir.lib.uwo.ca/etd/490>
7. Funke A, Grandl R, Ernst M, Dahmen N. Modelling and improvement of heat transfer coefficient in auger type reactors for fast pyrolysis application. *Chem Eng Process - Process Intensif* [Internet]. 2018 Aug 1 [cited 2019 May 28];130:67–75. Available from: <https://www.sciencedirect.com/science/article/pii/S0255270118302538>

8. Bridgwater A V. Review of fast pyrolysis of biomass and product upgrading. 2012 [cited 2019 May 27].
9. Colomba A, Berruti F, Briens C. Production Of Activated Carbons From Pyrolytic Char For Environmental Applications [Internet]. 2015 [cited 2019 May 28]. Available from: <https://ir.lib.uwo.ca/etdhttps://ir.lib.uwo.ca/etd/2978>
10. Shen J, Wang X-S, Garcia-Perez M, Mourant D, Rhodes MJ, Li C-Z. Effects of particle size on the fast pyrolysis of oil mallee woody biomass. *Fuel* [Internet]. 2009 Oct 1 [cited 2019 May 27];88(10):1810–7. Available from: <https://www.sciencedirect.com/science/article/pii/S0016236109002117>
11. Streff M. Rapid Thermal Processing (RTP TM): A Proven Pathway to Renewable Liquid Fuel [Internet]. 2009 [cited 2019 Jun 7]. Available from: <https://www.tappi.org/content/events/09IBBC/papers/34.pdf>
12. Dai J, Grace JR. A model for biomass screw feeding. *Powder Technol* [Internet]. 2008 Aug 1 [cited 2019 May 28];186(1):40–55. Available from: <https://www.sciencedirect.com/science/article/pii/S0032591007005578?via%3Dihub>
13. Fiore S, Berruti F, Briens C. Investigation of innovative and conventional pyrolysis of ligneous and herbaceous biomasses for biochar production. *Biomass and Bioenergy* [Internet]. 2018 Dec 1 [cited 2019 May 28];119:381–91. Available from: <https://www.sciencedirect.com/science/article/pii/S0961953418302769?via%3Dihub>
14. Kankariya DM, Briens C, Pjontek D. Agglomerate Formation and Heat Transfer study in a Novel Mechanically Fluidized Reactor [Internet]. 2016 [cited 2019 May 29]. Available from: <https://ir.lib.uwo.ca/etdhttps://ir.lib.uwo.ca/etd/4146>
15. Garcia-Nunez JA, Pelaez-Samaniego MR, Garcia-Perez ME, Fonts I, Abrego J, M Westerhof RJ, et al. Historical Developments of Pyrolysis Reactors: A Review.

- 2017 [cited 2019 Apr 2]; Available from: <https://pubs.acs.org/sharingguidelines>
16. Babler MU, Phounglamcheik A, Amovic M, Ljunggren R, Engvall K. Modeling and pilot plant runs of slow biomass pyrolysis in a rotary kiln. *Appl Energy*. 2017 Dec 1;207:123–33.
 17. Nogia P, Sidhu GK, Mehrotra R, Mehrotra S. Capturing atmospheric carbon: biological and nonbiological methods. [cited 2019 Jun 16]; Available from: <https://academic.oup.com/ijlct/article-abstract/11/2/266/2198361>
 18. Lehmann J, Gaunt J, Rondon M. Mitigation and Adaptation Strategies for Global Change (2006) 11: 403-427 BIO-CHAR SEQUESTRATION IN TERRESTRIAL ECOSYSTEMS-A REVIEW. 2006 [cited 2019 Jun 8]; Available from: http://www.css.cornell.edu/faculty/lehmann/publ/MitAdaptStratGlobChange_11_403-427_Lehmann_2006.pdf
 19. Sohi SP, Krull E, Lopez-Capel E, Bol R. A Review of Biochar and Its Use and Function in Soil. *Adv Agron* [Internet]. 2010 Jan 1 [cited 2019 Jun 8];105:47–82. Available from: <https://www.sciencedirect.com/science/article/pii/S0065211310050029>
 20. Yu X, Wu C, Fu Y, Brookes PC, Lu S. Three-dimensional pore structure and carbon distribution of macroaggregates in biochar-amended soil. *Eur J Soil Sci* [Internet]. 2016 Jan [cited 2019 Jun 8];67(1):109–20. Available from: <http://doi.wiley.com/10.1111/ejss.12305>
 21. Zimmerman AR. Abiotic and Microbial Oxidation of Laboratory-Produced Black Carbon (Biochar). *Environ Sci Technol* [Internet]. 2010 Feb 15 [cited 2019 Jun 8];44(4):1295–301. Available from: <https://pubs.acs.org/doi/10.1021/es903140c>
 22. de la Rosa JM, Rosado M, Paneque M, Miller AZ, Knicker H. Effects of aging under field conditions on biochar structure and composition: Implications for biochar stability in soils. *Sci Total Environ* [Internet]. 2018 Feb 1 [cited 2019 Jun 8];613–614:969–76. Available from:

<http://www.ncbi.nlm.nih.gov/pubmed/28946384>

23. Wang D, Fonte SJ, Parikh SJ, Six J, Scow KM. Biochar additions can enhance soil structure and the physical stabilization of C in aggregates. *Geoderma* [Internet]. 2017 Oct [cited 2019 Jun 8];303:110–7. Available from: <https://linkinghub.elsevier.com/retrieve/pii/S0016706117304627>
24. Obia A, Mulder J, Martinsen V, Cornelissen G, Børresen T. In situ effects of biochar on aggregation, water retention and porosity in light-textured tropical soils. *Soil Tillage Res* [Internet]. 2016 Jan 1 [cited 2019 Jun 8];155:35–44. Available from: <https://www.sciencedirect.com/science/article/pii/S0167198715001798>
25. Liang B, Lehmann J, Solomon D, Kinyangi J, Grossman J, O’neill B, et al. Black Carbon Increases Cation Exchange Capacity in Soils. *Soil Sci Soc Am* [Internet]. 2006 [cited 2019 Jun 8];(70):1719–30. Available from: http://xrm.phys.northwestern.edu/research/pdf_papers/2006/liang_sssaj_2006.pdf
26. Major J, Rondon M, Molina D, Riha SJ, Lehmann J. Nutrient Leaching in a Colombian Savanna Oxisol Amended with Biochar. *J Environ Qual* [Internet]. 2012 [cited 2019 Jun 8];41(4):1076. Available from: <http://www.ncbi.nlm.nih.gov/pubmed/22751049>
27. Research and Markets. Global and China Activated Carbon Industry Report, 2018-2023 [Internet]. 2018 [cited 2019 Jun 8]. Available from: <https://www.researchandmarkets.com/reports/4605170/global-and-china-activated-carbon-industry>
28. Freedonia Group. Activated Carbon - Market Size, Market Share, Market Leaders, Demand Forecast, Sales, Company Profiles, Market Research, Industry Trends and Companies [Internet]. 2016 [cited 2019 Jun 8]. Available from: <https://www.freedoniagroup.com/industry-study/activated-carbon-3467.htm>
29. Tan X, Liu Y, Zeng G, Wang X, Hu X, Gu Y, et al. Application of biochar for the removal of pollutants from aqueous solutions. *Chemosphere* [Internet]. 2015 Apr 1

- [cited 2019 Jun 8];125:70–85. Available from:
<https://www.sciencedirect.com/science/article/pii/S0045653514015008>
30. Nair V, Vinu R. Peroxide-assisted microwave activation of pyrolysis char for adsorption of dyes from wastewater. *Bioresour Technol* [Internet]. 2016 Sep 1 [cited 2019 Jun 8];216:511–9. Available from:
<https://www.sciencedirect.com/science/article/pii/S0960852416307106>
 31. Colomba A, Berruti F, Briens C. Production Of Activated Carbons From Pyrolytic Char For Environmental Applications [Internet]. 2015 [cited 2019 Jun 4]. Available from: <https://ir.lib.uwo.ca/etdhttps://ir.lib.uwo.ca/etd/2978>
 32. Natural Resources Canada. Bio-Coke [Internet]. 2013 [cited 2019 Jun 9]. Available from:
<https://www.nrcan.gc.ca/energy/efficiency/industry/processes/energy-systems/5611>
 33. Wei R, Zhang L, Cang D, Li J, Li X, Xu CC. Current status and potential of biomass utilization in ferrous metallurgical industry. *Renew Sustain Energy Rev* [Internet]. 2017 Feb 1 [cited 2019 Jun 9];68:511–24. Available from:
<https://www.sciencedirect.com/science/article/pii/S1364032116306657>
 34. Adrados A, De Marco I, López-Uriónabarrenechea A, Solar J, Caballero BM, Gastelu N. Biomass Pyrolysis Solids as Reducing Agents: Comparison with Commercial Reducing Agents. *Mater* (Basel, Switzerland) [Internet]. 2015 Dec 23 [cited 2019 Jun 9];9(1). Available from:
<http://www.ncbi.nlm.nih.gov/pubmed/28787805>
 35. Ng KW, Giroux L, MacPhee T. Biofuel Ironmaking Strategy from a Canadian Perspective: Short-Term Potential and Long-Term Outlook [Internet]. 2011 [cited 2019 Jun 16]. Available from:
http://www.cancarb.ca/pdfs/CCRA_papers/METEC2011_EECR2011_Biofuel.pdf
 36. Government of Canada. Reduction of Carbon Dioxide Emissions from Coal-fired

- Generation of Electricity Regulations [Internet]. 2012 [cited 2019 Jun 9]. Available from: <https://laws-lois.justice.gc.ca/PDF/SOR-2012-167.pdf>
37. Cruz DC, Franco Berruti S, Supervisor Cedric Briens J. Production of Bio-coal and Activated Carbon from Biomass Recommended Citation [Internet]. 2012 [cited 2019 Jun 9]. Available from: <https://ir.lib.uwo.ca/etd://ir.lib.uwo.ca/etd/1044>
 38. Agar D, Wihersaari M. Bio-coal, torrefied lignocellulosic resources – Key properties for its use in co-firing with fossil coal – Their status. *Biomass and Bioenergy* [Internet]. 2012 Sep 1 [cited 2019 Jun 9];44:107–11. Available from: <https://www.sciencedirect.com/science/article/pii/S0961953412002103>
 39. Dai J, Sokhansanj S, Grace JR, Bi X, Lim CJ, Melin S. Overview and some issues related to co-firing biomass and coal. *Can J Chem Eng.* 2008;86(3):367–86.
 40. International Energy Agency. *World Energy Outlook 2011* [Internet]. 2011 [cited 2019 Jun 9]. Available from: <https://www.iea.org/newsroom/news/2011/november/world-energy-outlook-2011.html>
 41. Yao D, Hu Q, Wang D, Yang H, Wu C, Wang X, et al. Hydrogen production from biomass gasification using biochar as a catalyst/support. *Bioresour Technol* [Internet]. 2016 [cited 2019 Jun 9];216:159–64. Available from: <http://dx.doi.org/10.1016/j.biortech.2016.05.011>
 42. Abu El-Rub Z, Bramer EA, Brem G. Experimental comparison of biomass chars with other catalysts for tar reduction. 2008 [cited 2019 Jun 9]; Available from: www.fuelfirst.com
 43. Mani S, Kastner JR, Juneja A. Catalytic decomposition of toluene using a biomass derived catalyst. *Fuel Process Technol* [Internet]. 2013 [cited 2019 Jun 9];114:118–25. Available from: <http://dx.doi.org/10.1016/j.fuproc.2013.03.015>
 44. Qian K, Kumar A, Zhang H, Bellmer D, Huhnke R. Recent advances in utilization of biochar. *Renew Sustain Energy Rev* [Internet]. 2014 [cited 2019 Jun 9]

- 9];42:1055–64. Available from: <http://dx.doi.org/10.1016/j.rser.2014.10.074>
45. Chen W, Fan Z, Bao X. Effect of Confinement in Carbon Nanotubes on the Activity of Fischer-Tropsch Iron Catalyst. [cited 2019 Jun 9]; Available from: <https://pubs.acs.org/doi/10.1021/ja8008192>.
 46. Yan Q, Street J, Yu F. Synthesis of carbon-encapsulated iron nanoparticles from wood derived sugars by hydrothermal carbonization (HTC) and their application to convert bio-syngas into liquid hydrocarbons. 2015 [cited 2019 Jun 9]; Available from: <http://dx.doi.org/10.1016/j.biombioe.2015.09.002>
 47. Yan Q, Wan C, Liu J, Gao J, Yu F, Zhang J, et al. Green Chemistry Iron nanoparticles in situ encapsulated in biochar-based carbon as an effective catalyst for the conversion of biomass-derived syngas to liquid hydrocarbons. Cite this Green Chem [Internet]. 2013 [cited 2019 Jun 9];15:1631. Available from: www.rsc.org/greenchem
 48. Kastner JR, Mani S, Juneja A. Catalytic decomposition of tar using iron supported biochar. 2015 [cited 2019 Jun 9]; Available from: <http://dx.doi.org/10.1016/j.fuproc.2014.09.038>
 49. Dehkhoda AM, West AH, Ellis N. Biochar based solid acid catalyst for biodiesel production. *Appl Catal A Gen.* 2010;382:197–204.
 50. Matthew Cuthbertson D, Berruti S, Briens C-S. The Production of Pyrolytic Biochar for Addition in Value-Added Composite Material [Internet]. 2018 [cited 2019 Jun 16]. Available from: <https://ir.lib.uwo.ca/etd://ir.lib.uwo.ca/etd/5182>
 51. Das O, Sarmah AK, Bhattacharyya D. A novel approach in organic waste utilization through biochar addition in wood/polypropylene composites. *Waste Manag [Internet]*. 2015 [cited 2019 Jun 16];38:132–40. Available from: <http://dx.doi.org/10.1016/j.wasman.2015.01.015>
 52. Li X, Lei B, Lin Z, Huang L, Tan S, Cai X. The utilization of bamboo charcoal enhances wood plastic composites with excellent mechanical and thermal

- properties. *Mater Des* [Internet]. 2014 [cited 2019 Jun 16];53:419–24. Available from: <http://dx.doi.org/10.1016/j.matdes.2013.07.028>
53. He X, Liu Z, Niu W, Yang L, Zhou T, Qin D, et al. Effects of pyrolysis temperature on the physicochemical properties of gas and biochar obtained from pyrolysis of crop residues. 2018 [cited 2019 Jun 9]; Available from: <https://doi.org/10.1016/j.energy.2017.11.062>
54. Suman S, Gautam S. Pyrolysis of coconut husk biomass: Analysis of its biochar properties. *Energy Sources, Part A Recover Util Environ Eff* [Internet]. 2017 Apr 18 [cited 2019 Jun 9];39(8):761–7. Available from: <https://www.tandfonline.com/doi/full/10.1080/15567036.2016.1263252>
55. Singh B, Singh BP, Cowie AL. Characterisation and evaluation of biochars for their application as a soil amendment. *Soil Res* [Internet]. 2010 Oct 19 [cited 2019 Jun 9];48(7):516. Available from: <http://www.publish.csiro.au/?paper=SR10058>
56. Gheorghe C, Marculescu C, Badea A, Dinca C, Apostol T. Effect of Pyrolysis Conditions on Bio-Char Production from Biomass Effect of Pyrolysis Conditions on Bio-Char Production from Biomass. *Renew Energy Sources*. 2015;(January 2015):239–42.
57. Prakongkep N, Gilkes RJ, Wiriyakitnatekul W. Forms and solubility of plant nutrient elements in tropical plant waste biochars. *J Plant Nutr Soil Sci*. 2015;178(5):732–40.
58. Limwikran T, Kheoruenromne I, Suddhiprakarn A, Prakongkep N, Gilkes RJ. Dissolution of K, Ca, and P from biochar grains in tropical soils. *Geoderma* [Internet]. 2018 [cited 2019 Jun 9];312:139–50. Available from: <http://dx.doi.org/10.1016/j.geoderma.2017.10.022>
59. Lehmann J, Pereira da Silva Jr J, Steiner C, Nehls T, Zech W, Glaser B. Nutrient availability and leaching in an archaeological Anthrosol and a Ferralsol of the Central Amazon basin: fertilizer, manure and charcoal amendments [Internet]. Vol.

- 249, *Plant and Soil*. 2003 [cited 2019 Jun 9]. Available from: <https://link-springer-com.proxy1.lib.uwo.ca/content/pdf/10.1023%2FA%3A1022833116184.pdf>
60. Lehmann J, Joseph S. *Biochar for Environmental Management* [Internet]. 2009 [cited 2019 Jun 9]. Available from: [http://www.css.cornell.edu/faculty/lehmann/publ/First proof 13-01-09.pdf](http://www.css.cornell.edu/faculty/lehmann/publ/First%20proof%2013-01-09.pdf)
61. Sadaf J, Shah A, Shahzad K, Ali N, Shahid M, Ali S, et al. Improvements in wheat productivity and soil quality can accomplish by co-application of biochars and chemical fertilizers. *Sci Total Environ* [Internet]. 2017 [cited 2019 Jun 9];607–608:715–24. Available from: <http://dx.doi.org/10.1016/j.scitotenv.2017.06.1780048-9697/>
62. Agegnehu G, Nelson PN, Bird MI. The effects of biochar, compost and their mixture and nitrogen fertilizer on yield and nitrogen use efficiency of barley grown on a Nitisol in the highlands of Ethiopia. *Sci Total Environ* [Internet]. 2016 [cited 2019 Jun 9];569–570:869–79. Available from: <http://dx.doi.org/10.1016/j.scitotenv.2016.05.0330048-9697/>
63. Brantley KE, Savin MC, Brye KR, Longer DE. Nutrient availability and corn growth in a poultry litter biochar-amended loam soil in a greenhouse experiment. *Soil Use Manag*. 2016;32(3):279–88.
64. Baiga R, Rajashekhar Rao BK. Effects of biochar, urea and their co-application on nitrogen mineralization in soil and growth of Chinese cabbage. *Soil Use Manag*. 2017;33(1):54–61.
65. Walter R, Rao BKR. Biochars influence sweet-potato yield and nutrient uptake in tropical Papua New Guinea. *J Plant Nutr Soil Sci*. 2015;178(3):393–400.
66. Blanco-Canqui H. Biochar and Soil Physical Properties. *Soil Sci Soc Am J*. 2017;81(4):687.
67. Omondi MO, Xia X, Nahayo A, Liu X, Khan Korai P, Pan G. Quantification of biochar effects on soil hydrological properties using meta-analysis of literature

- data. *Geoderma* [Internet]. 2016 [cited 2019 Jun 9];274:28–34. Available from: <http://dx.doi.org/10.1016/j.geoderma.2016.03.029>
68. Burrell LD, Zehetner F, Rampazzo N, Wimmer B, Soja G. Long-term effects of biochar on soil physical properties. 2016 [cited 2019 Jan 10]; Available from: <http://dx.doi.org/10.1016/j.geoderma.2016.07.019>
 69. Laird DA, Fleming P, Davis DD, Horton R, Wang B, Karlen DL. Impact of biochar amendments on the quality of a typical Midwestern agricultural soil. 2010;
 70. Burrell LD, Zehetner F, Rampazzo N, Wimmer B, Soja G. Long-term effects of biochar on soil physical properties. *Geoderma* [Internet]. 2016 [cited 2019 Jun 9];282:96–102. Available from: <http://dx.doi.org/10.1016/j.geoderma.2016.07.019>
 71. Quin PR, Cowie AL, Flavel RJ, Keen BP, Macdonald LM, Morris SG, et al. Oil mallee biochar improves soil structural properties-A study with x-ray micro-CT. *"Agriculture, Ecosyst Environ* [Internet]. 2014 [cited 2019 Jun 9];191:142–9. Available from: <http://dx.doi.org/10.1016/j.agee.2014.03.022>
 72. Gray M, Johnson MG, Dragila MI, Kleber M. Water uptake in biochars: The roles of porosity and hydrophobicity. 2014 [cited 2019 Jun 9]; Available from: <http://dx.doi.org/10.1016/j.biombioe.2013.12.010>
 73. Kinney TJ, Masiello CA, Dugan B, Hockaday WC, Dean MR, Zygourakis K, et al. Hydrologic properties of biochars produced at different temperatures. 2012 [cited 2019 Jun 9]; Available from: <http://www.unipress.waw.pl/fityk/>
 74. Cross A, Sohi SP. A method for screening the relative long-term stability of biochar. *GCB Bioenergy*. 2013;5(2):215–20.
 75. Jaffé R, Ding Y, Niggemann J, Vähätalo A V, Stubbins A, Spencer RGM, et al. Global Charcoal Mobilization from Soils via Dissolution and Riverine Transport to the Oceans. [cited 2019 Jun 9]; Available from: www.sciencemag.org/cgi/content/full/340/6130/345/DC1

76. Rumpel C, Alexis M, Chabbi A, Chaplot V, Rasse DP, Valentin C, et al. Black carbon contribution to soil organic matter composition in tropical sloping land under slash and burn agriculture. 2005 [cited 2019 Jun 9]; Available from: www.elsevier.com/locate/geoderma
77. Peng X, Zhu QH, Xie ZB, Darboux F, Holden NM. The impact of manure, straw and biochar amendments on aggregation and erosion in a hillslope Ultisol. *Catena* [Internet]. 2016 [cited 2019 Jun 9];138:30–7. Available from: <http://dx.doi.org/10.1016/j.catena.2015.11.008>
78. Major J. Guidelines on Practical Aspects of Biochar Application to Field Soil in Various Soil Management Systems Photo by Josiah Hunt [Internet]. [cited 2019 May 29]. Available from: www.biochar-international.org
79. Bowden-Green B, Briens L. An investigation of drum granulation of biochar powder. *Powder Technol* [Internet]. 2016;288:249–54. Available from: <http://dx.doi.org/10.1016/j.powtec.2015.10.046>
80. Bowden-Green B, Briens L. A comparison of drum granulation of biochars. *Powder Technol* [Internet]. 2019 Feb 1 [cited 2019 May 29];343:723–32. Available from: [https://www.sciencedirect-com.proxy1.lib.uwo.ca/science/article/pii/S0032591018309938?via%3Dihub#bb0060](https://www.sciencedirect.com.proxy1.lib.uwo.ca/science/article/pii/S0032591018309938?via%3Dihub#bb0060)
81. Agency for Toxic Substances and Disease Registry. PUBLIC HEALTH STATEMENT [Internet]. 1995 [cited 2019 Jun 9]. Available from: www.atsdr.cdc.gov/
82. Fismes J, Perrin-Ganier C, Empereur-Bissonnet P, Morel JL. Soil-to-Root Transfer and Translocation of Polycyclic Aromatic Hydrocarbons by Vegetables Grown on Industrial Contaminated Soils. *J Environ Qual* [Internet]. 2002 [cited 2019 Jun 9];31(5):1649. Available from: <https://www.agronomy.org/publications/jeq/abstracts/31/5/1649>

83. Lin H, Tao S, Zuo Q, Coveney RM. Uptake of polycyclic aromatic hydrocarbons by maize plants. [cited 2019 Jun 9]; Available from: www.elsevier.com/locate/envpol
84. Gworek B, Klimczak K, Kijen´ska M, Kijen´ska K. The Relation between Polyaromatic Hydrocarbon Concentration in Sewage Sludge and Its Uptake by Plants: *Phragmites communis*, *Polygonum persicaria* and *Bidens tripartita*. 2014 [cited 2019 Jun 9]; Available from: www.plosone.org
85. De la Rosa JM, Sánchez-Martín AM, Campos P, Miller AZ. Effect of pyrolysis conditions on the total contents of polycyclic aromatic hydrocarbons in biochars produced from organic residues: Assessment of their hazard potential. *Sci Total Environ* [Internet]. 2019;667:578–85. Available from: <https://doi.org/10.1016/j.scitotenv.2019.02.421>
86. Ennis BJ, Litster JD. Particle Size Enlargement. In: *Perry's Chemical Engineers' Handbook*. 7th edn. New York: McGraw-Hill; 1997. p. 20-56-20–89.
87. Iveson SM, Litster JD, Hapgood K, Ennis BJ. Nucleation, growth and breakage phenomena in agitated wet granulation processes: a review [Internet]. Vol. 117, *Powder Technology*. 2001 [cited 2019 May 25]. Available from: www.elsevier.com/locate/powtec
88. Schaefer T, Mathiesen C. *international journal of pharmaceutics: Melt pelletization in a high shear mixer*. IX. Effects of binder particle size. Vol. 139, *International Journal of Pharmaceutics*. 1996.
89. Mort PR, Tardos GI. Scale-up of agglomeration processes using transformation. *Kona Powder Sci Technol Japan*. 1999;17:64–75.
90. Holm P, Jungersen O, Schaefer T, Kristensen HG. Granulation in high speed mixers: Part 1. Effects of process variables during kneading. *Pharm Ind*. 1983;45:806–11.
91. Holm P, Jungersen O, Schaefer T, Kristensen HG. Granulation in high speed

- mixers: Part 2. Effects of process variables during kneading. *Pharm Ind.* 1984;46:97–101.
92. Iveson SM, Litster JD. Growth regime map for liquid-bound granules. *AIChE J.* 1998;44(7):1510–8.
93. Pitt K, Peña R, Tew JD, Pal K, Smith R, Nagy ZK, et al. Particle design via spherical agglomeration: A critical review of controlling parameters, rate processes and modelling. 2017 [cited 2019 May 29]; Available from: <https://doi.org/10.1016/j.powtec.2017.11.052>
94. Probst K V, Iilejeji KE. The effect of process variables on drum granulation behavior and granules of wet distillers grains with solubles. 2016 [cited 2019 May 29]; Available from: <http://dx.doi.org/10.1016/j.ap.2016.04.029>
95. Lister J, Ennis B. *The Science and Engineering of Granulation Processes* - Jim Litster, Bryan Ennis - Google Books [Internet]. Springer Science + Business Media Dordrecht; 2004 [cited 2019 May 29]. 221–134 p. Available from: [https://books.google.ca/books?id=WDbyCAAQBAJ&pg=PA121&lpg=PA121&dq=wet+granule+breakage&source=bl&ots=EUUOKw3BBk&sig=ACfU3U0jQ6hSqTnCzsK44zh4KIUEiU4OPQ&hl=en&sa=X&ved=2ahUKEwiUlbbN6LHiAhUCH6wKHQxlCm8Q6AEwCXoECAkQAQ#v=onepage&q=wet granule breakage&f=](https://books.google.ca/books?id=WDbyCAAQBAJ&pg=PA121&lpg=PA121&dq=wet+granule+breakage&source=bl&ots=EUUOKw3BBk&sig=ACfU3U0jQ6hSqTnCzsK44zh4KIUEiU4OPQ&hl=en&sa=X&ved=2ahUKEwiUlbbN6LHiAhUCH6wKHQxlCm8Q6AEwCXoECAkQAQ#v=onepage&q=wet%20granule%20breakage&f=false)
96. Hapgood KP, Khanmohammadi B. Granulation of hydrophobic powders. *Powder Technol.* 2008;189:253–62.
97. Nguyen T, Shen W, Hapgood K. Drop penetration time in heterogeneous powder beds. *Chem Eng Sci* [Internet]. 2009 [cited 2019 Jul 4];64:5210–21. Available from: www.elsevier.com/locate/ces
98. Rowe RC. Binder-substrate interactions in granulation: a theoretical approach based on surface free energy and polarity. *Int J Pharm* [Internet]. 1989 Jun 1 [cited 2019 May 25];52(2):149–54. Available from:

<https://www.sciencedirect.com/science/article/pii/0378517389902895>

99. Mundozah AL, Cartwright JJ, Tridon CC, Hounslow MJ, Salman AD. Hydrophobic/hydrophilic static powder beds: Competing horizontal spreading and vertical imbibition mechanisms of a single droplet. *Powder Technol* [Internet]. 2018 May [cited 2019 Jul 4];330:275–83. Available from: <https://linkinghub.elsevier.com/retrieve/pii/S0032591018301542>
100. Walker GM. Chapter 4 Drum Granulation Processes. *Handb Powder Technol* [Internet]. 2007 Jan 1 [cited 2019 Aug 31];11:219–54. Available from: <https://www.sciencedirect.com/science/article/pii/S016737850780039X>
101. Santomaso AC, Ding YL, Lickiss JR, York DW. Investigation of the Granular Behaviour in a Rotating Drum Operated over a Wide Range of Rotational Speed. *Chem Eng Res Des* [Internet]. 2003 Sep [cited 2019 Aug 31];81(8):936–45. Available from: <https://linkinghub.elsevier.com/retrieve/pii/S0263876203723831>

Chapter 2

2 Rotating Heater Pyrolysis Reactor (RHP) Design and Development

2.1 Introduction

Biochar is the solid product from biomass pyrolysis. In this process, sustainable and renewable biomass feedstocks are thermally decomposed in the absence of oxygen, and produce solid, liquid and gas products. In the past, the liquid co-product referred to as bio-oil has been the main product of interest due to its potential as a green fuel and ability to be refined into value-added chemicals. Research focus has shifted towards the production of biochar due to the growing number of attractive industrial applications. Examples of the potential applications include biochar as a soil amendment, carbon sequestration technology, activated carbon for wastewater and air purification, bio-coke fuel source for metallurgical applications and as a filler for composite/polymer materials (1–6).

Biochar has been shown to improve soil fertility when used as a soil amendment by increasing plant available nutrients and improving soil structure. Biochar has water soluble crystalline minerals embedded within its structure and surface, providing additional nutrition for plant uptake (7,8). In addition, biochar can also improve soil nutrient retention and reduce eutrophication caused by nutrient leaching (9,10). Increased soil nutrient retention is caused by an increase in soil cation exchange capacity. Biochar addition increases soil cation exchange capacity by a combination of increasing solid organic material (SOM) oxidation and increasing in surface area for cation adsorption (11). Soils physical structure and properties are also influenced by biochar addition. When biochars are properly paired with a soil, biochar amendment has been shown to improve soil bulk density, water retention capacity, and wet aggregate stability (12,13).

The physical and chemical properties of biochar are influenced by pyrolysis parameters such as highest treatment temperature (HTT), heating rate, residence time and feedstock. Differences in feedstock elemental composition and lignin, cellulose and hemicellulose content also impact the properties of the resultant biochar after pyrolysis. Although

specific values vary based on feedstock, the effects of pyrolysis treatment temperature on biochar properties usually follow the following trends; with increasing pyrolysis temperature, yield, volatile matter, hydrogen content, and hydrogen to carbon ratio (H/C) decrease, whereas, ash, aromaticity, carbon content, pH, and surface area increase (14,15). Slower heating rates increase char productions whereas higher heating rates produce more volatiles (16). Singh et al. (34) investigated the influence of 11 feedstock sources on biochar characteristics for soil amendment. Overall, wood derived biochars have higher carbon content, lower ash content (N, P, K, S, Ca, Mg, Al, Na and Cu) and lower potential cation exchange capacity (CEC) followed by leaf based biochars, then manure based biochars. Due to the range of possible properties, biochar as a soil amendment can be customized to meet the specific needs of individual soil profiles.

Biochar can be a very fine powder, making it difficult to incorporate into large agricultural fields as it can be easily blown away and is susceptible to erosion or mobilization through runoff, leading to considerable losses (17–20). For biochar to be an effective soil amendment, it must be a powder with relatively fine particles to provide a large surface for the growth of beneficial bacteria (21) and to enhance the rate of transfer of beneficial minerals from the char to the soil (22). Granulation is one method of transforming biochar powders into a product that can be easily applied to agricultural fields; an additional advantage of granulation is that biochar granules can be formulated to include mineral fertilizer powders. Granulation is the agglomeration of biochar through the addition of a binder solution and is effective at reducing dust emissions of fine powders. With proper binder selection, biochar granules can be designed to disintegrate into individual particles after added to soil and in contact with water.

Evidence of the use of carbonization technologies in ancient civilizations are present in areas such as the Terra Preta (Portuguese meaning “black earth”), a region in the Amazon basin containing a very fertile black soil. The characteristic dark colour of the soil is caused by the addition of charcoal to the soil over hundreds of years through indigenous slash and char agriculture practices. With the progression of modern research and growing interest in pyrolysis products, pyrolysis technologies have been developed into highly specialized units.

As biochar was initially considered the waste product of pyrolysis, most traditional lab scale pyrolysis reactors are designed to maximize bio-oil production. However, in many applications, biochar is more valuable and reactors that maximize the biochar yield and quality are required. While some traditional slow pyrolysis reactors maximize biochar yield (23,24), they do not provide biochar that releases its minerals quickly (25).

Traditional lab scale pyrolysis reactors are often not capable of handling large biomass loadings, thereby producing small quantities of biochar. Larger amounts of biochar in the approximate range of 2-5 kg are required to develop granulation methods, and to test for soil amendment applications.

For this research, a new Rotating Heater Pyrolysis reactor (RHP) has been developed to process a variety of feedstocks and create batches of biochar of several kilograms. The RHP allows for the production of biochar that is representative of traditional biochar reactors and can operate under similar conditions. The focus of this chapter is to provide an in-depth description for the RHP technology and characterize the reactors features.

2.2 Rotating Heater Pyrolyzer (RHP)

2.2.1 Principles of the RHP Design

The RHP was designed to meet the following requirements:

- Process biomass batches of 20 L.
- Inexpensive and easy to build.
- Easy, low cost operation.
- Low dust entrainment.
- Low energy consumption.
- Produces char with similar yield, homogeneity and characteristics to standard high temperature (400-500°C), and laboratory batch reactor (See Chapter 3).

Accordingly, the following design decisions were made:

- Avoid the use of a solid heat carrier such as sand or steel shot, which would contaminate the char product.
- Avoid the use of a fluidizing or carrier gas. Such a gas would be costly, require additional energy for heating, and entrain dust and oil vapors out of the reactor.
- Keep the heating surfaces away from the walls. This would minimize heat losses to reduce energy consumption and allow for the use of inexpensive wall material.
- Keep the heating surfaces away from the gas and vapors exhaust. Ideally, the reactor regions near the gas exhaust should be at a relatively low temperature so that heavy tars can be condensed and recycled to the reactor for further conversion to char, light vapors and gas. This would maximize char production and minimize tar production.
- Avoid the use of mechanical mixers. For large lab reactors, mechanical mixers are expensive and consume energy. Mechanical mixers also promote dust generation by attrition of the biochar. Ideally, gravity could be used to provide enough mixing for the production of homogenous biochar: as they react, particles in a pile of biomass will shrink and move towards the bottom of the vessel.

2.2.2 Design and Set-up

The RHP is comprised of four sections: the reactor vessel, the induction heating system, the rotating heater and the air motor. Figure 2-1 shows the schematic structure of the RHP.

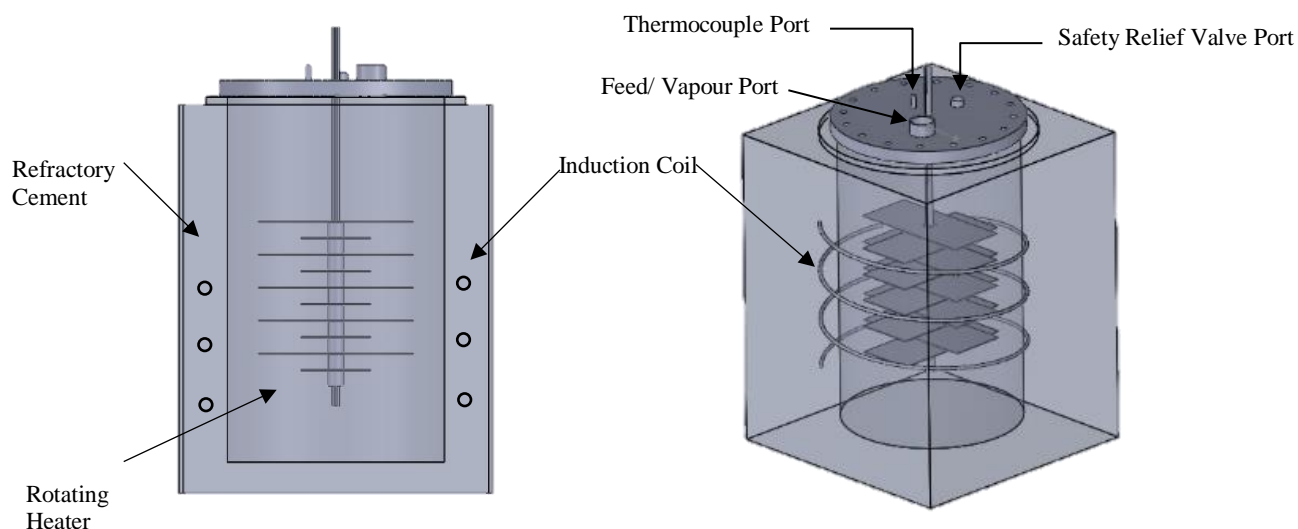


Figure 2-1: RHP Schematic.

The reactor vessel is a cylindrical vessel cast from refractory cement and has a diameter of 45 cm and length of 60 cm (Figure 2-2). Refractory cement was chosen because it does not interact with or shield the induction magnetic fields from the rotating heater. In addition, refractory cement provides additional insulation, and can withstand high process temperatures while maintaining its mechanical strength. The reactor vessel top flange has a diameter of 50 cm and is made from stainless steel. The vessel was designed to these dimensions so that approximately 20 L of feedstock can be processed per batch and produce several kilograms of char required for granulation trials.

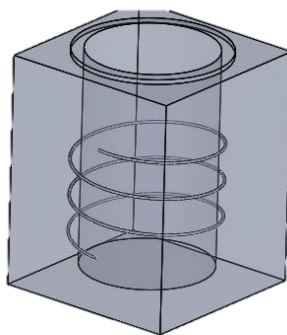


Figure 2-2: Reactor Vessel Drawing.

The top flange is attached by screws drilled into the refractory cement vessel and lined with high temperature silicone to ensure the vessel is sealed. The reactor lid is made from 2.5 cm thick stainless steel with a diameter of 48 cm and is attached to the reactor vessels top flange by 16 bolts (0.10 cm diameter, 5.84 cm length). The surface of the lid exposed to the inside of the reactor is lined with a 0.64 cm thick layer of refractory cement. To prevent any leakage, a gasket is placed between the top flange and lid. There are 4 ports located on the lid; a 2.5 cm diameter vapour exhaust port/ biomass feeding port, 0.32 cm thermocouple housing port (Type K) 1.3 cm pressure safety relief valve housing port, and lastly a 2.5 cm port to house the shaft of the rotating heater.

Copper induction coils of 0.64 cm inner diameter are wrapped around the reaction vessel and embedded within a rectangular concrete frame of 64 cm height x 80 cm length. The induction coil system is made up of three turns spanning over $\frac{2}{3}$ of the reactor vessel volume. The coil is connected to a SI-12 kW Induction heating system by The Superior Induction Company with a maximum output of 12 kW and a frequency range of 30-80 KHz.

The basic principle for heating in this reactor is to distribute heat to the solids by placing the heating element within the reactor. In conventional pyrolysis reactors, the reaction vessel walls are heated, and solids are displaced to contact the heated surface with either a mechanical mixer or the use of a fluidizing gas, requiring large mechanical energy. The rotating heater was designed to maximize the surface area of the heating element, while

minimizing frictional forces between the element and solid particles during heat distribution. Figure 2-1 illustrates the rotating heater design. The rotating heater is an assembly of 10 carbon steel plates stacked perpendicularly from one another and placed 5 cm apart along a shaft.

Carbon steel was chosen for blade material because it is significantly less expensive than stainless steel; ferromagnetic and therefore able to react with the induction magnetic field; and able to maintain its shape and strength at high temperatures. Each blade is 25 cm long, 11.5 cm wide and 0.16 cm thick. The plates are strategically placed to maximize the power input from the induction unit into the heating element while also lessening frictional forces between the plates and solids. This configuration maximizes the metal area exposed to the induction magnetic field while minimizing shielding effects between the plates.

Biomass particles contract when converted into biochar due to the removal of chemically bound water and volatile organic compounds, combustible hydrocarbons and tars from the biomass structure. As biomass is converted into biochar, the reactor bed volume continually decreases, ensuring that the solids in contact with the heater surface are constantly renewed to provide a uniform biochar product.

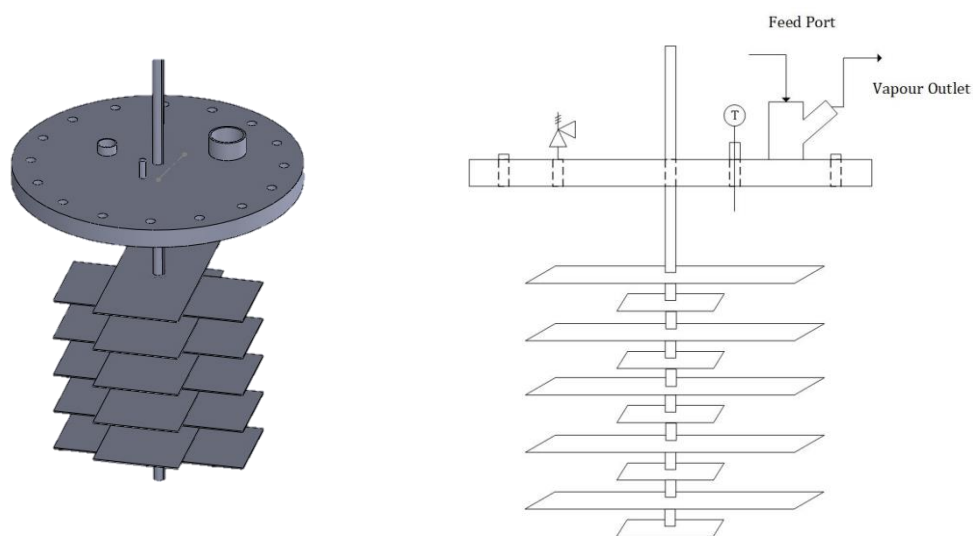


Figure 2-3: Reactor lid and rotating heater diagram.

2.3 Materials and Methods

2.3.1 Methods to Characterize RHP Performance

2.3.1.1 Rotating Heater Power Optimization

Three different rotating heaters were designed, built and tested to determine which design would provide the greatest induction power input into the system. The reactor vessel was filled 1/3 of the volume with sand, which acted as a support to hold each of the heating elements tested in place. An ammeter was connected to the induction unit to provide an accurate reading of the maximum current that could enter the system before the induction unit protected itself. Power provided to the induction unit was then calculated using the current from the following Equation:

$$P = 3(V \times I)/\sqrt{3} \quad (2-1)$$

Where P = power in kW, V = voltage in volts and I = current in amps. The induction unit operates with three phase alternating current (AC). The induction first converts the three phase AC into a direct current (DC) and then converts it once again into an alternating current with a frequency of up to 80,000 Hz.

2.3.1.2 Actual Power to the Bed and Heat Losses

Energy is supplied to the reactor via an induction heating system described in Section 2.2.2. The power output displayed on the induction unit does not exclusively go towards the pyrolysis reaction. Heat losses within the reactor consume a fraction of the power supplied from the induction unit. The lid of the reactor is also electromagnetic, and therefore some of the induction power is used to heat the lid.

Prior to biomass feeding, the energy supplied to the reactor is equal to the heat losses of the reactor as described by Equation 2-2:

$$Q_{in} = Q_{loss} \quad (2-2)$$

Once the reactor is filled with biomass the energy supplied to the reactor is equal to the energy required for pyrolysis to take place, along with the sum of all heat losses, as described in Equation 2-3:

$$Q_{in} = Q_{loss} + H_{pyrolysis} \quad (2-3)$$

The assumption is commonly made that heat losses between the two scenarios described above are equal, often leading to an overestimation for the enthalpy of pyrolysis. In fact, with the additional power supplied from the induction unit for pyrolysis process to take place, there is a corresponding increase in the reactor wall temperature, resulting with an increase in reactor heat losses.

The method to determine the power input from the rotating heater into the particulate bed was adapted from the method developed by Barry et al. (26), to provide an estimate of the heat losses. Water was injected using a peristaltic pump into the reactor filled with silica sand, operating under the same steady state conditions as experimental pyrolysis runs. The flow rate of water was adjusted until the bed temperature of the sand was reduced and maintained at 100 °C. Under these conditions the energy into the reaction bed is equal to the energy required to vaporize the known flowrate of water (Equation 2-4):

$$H_{pyrolysis} = \frac{\dot{m}_{water}}{H_{vapourization}} \quad (2-4)$$

2.3.1.3 Energy to Rotate Heater

The reactor vessel was filled to approximately 2/3 volume with unreacted biomass feedstock, then sealed and operated under pyrolysis conditions described in Section 2.3.3. The air motor was set at an air supply pressure of 101.3 kPa and the rotational speed of the heater was recorded. Using data provided by the air motor manufacturing company (Appendix A), the measured rotational speed was converted to determine the corresponding power and torque required to turn the heating element.

2.3.2 Feedstock

Three main feedstocks are used in the scope of this thesis. The first objective for this thesis was to design, develop and characterize the RHP reactor. Woodchip (WCP) biomass was used to develop and characterize the RHP reactor as conversion of this type of feedstock to biochar has been extensively studied in literature (27–31). Woodchip feedstocks are relatively expensive, therefore once the RHP technology had been developed, the focus of this thesis shifted towards converting anaerobic digestate into biochar. The first digestate was provided from Bayview Flowers greenhouse (BFD) located in St. Catharines, ON, and the second from Storm Fisher Environmental (SFD), a food waste anaerobic digestion facility located in London, ON. The three feedstocks have distinct particle shape and size distribution, which can be seen in Figure 2-4 and Table 2-1, respectively.



Figure 2-4: (a) Woodchips (b) Storm Fisher Digestate (c) Bayview Flowers Digestate.

Table 2-1: Particle Size Distributions of Feedstocks.

Particle Size Distribution Parameters (mm)	WCP	BFD	SFD
Dp₁₀	0.4	0.3	0.1
Dp₅₀	1.6	1.4	0.7
Dp₉₀	3.5	2.3	2.7
Distribution Span	1.9	1.5	3.7

2.3.3 RHP Experimental Procedure

RHP pyrolysis experiments are based on process time rather than bed temperature. This is due to the nature of the rotating heater, which means that there is no uniform bed temperature. Prior to pyrolysis, all components of the RHP are assembled and the reactor lid is sealed. Compressed air is used to turn on the air motor, which rotates the shaft attached to the rotating heater. The compressed air is controlled by an Arduino system programmed to rotate the shaft similar to a washing machine motion; 3 s clockwise, 3 s counter-clockwise with a specified stationary period of 30 s between each rotation motion.

The biomass sample is fed into the reactor through a feeding port located on the lid until 2/3 of the reactor volume is filled (approximately 20 L). The induction heating system is then turned on, set to the maximum frequency and maintained at a nominal input power of 7.5 kW. The vapour temperature is monitored and recorded throughout the duration of the procedure.

The biomass is heated until the vapour temperature reaches 120 °C to ensure that all moisture in the biomass sample has been removed. Once the vapour temperature has reached 120 °C, the RHP heater remains on for the desired processing time varying between 1 to 4 hours. The gaseous product is continually passed through a condenser that is cooled with water throughout the entire procedure.

Once the desired process time is reached, the induction heating and the compressed air to the rotating heater are turned off, and the entire reactor is left to cool to room temperature over 15 hours (typically overnight).

2.3.4 Biochar Production Conditions

Four biochars were produced from wood chips in the RHP, with varying process times of 1, 2, 3 and 4 hours.

2.3.5 Methods to Characterize Biochar

The following methods were chosen to characterize biochar properties because they are sensitive to pyrolysis temperature and heating rate.

2.3.5.1 Reactor Yield

Char yield was determined by comparing the biomass batch weight fed to the reactor with the weight of the char bed at the end of each run.

$$\text{BC yield (\%)} = \frac{\text{Weight of Collected Biochar (g)}}{\text{Weight of Biomass (g)}} \times 100 \quad (2-5)$$

2.3.5.2 Red, Green & Blue (RGB) Imaging

2.3.5.2.1 RGB Mode Intensity

The RGB intensity of biochar samples was used as a tool to compare biochars based on colour. As biomass is pyrolyzed into biochar, the colour of biochar gradually becomes darker. Due to the nature of the rotating heater in the RHP, the maximum temperature of the char bed is unknown, and the main operating parameter is processing time. By analyzing biochar colour, a correlation between processing time in the RHP and bed temperature was made to provide a maximum pyrolysis temperature range. The RGB intensity was determined using ZEISS Axiocam 105 colour microscope and software. The Axiocam 105 colour software analyzes each individual pixel from the image taken by the microscope and assigns an RGB intensity between 0 to 255, with zero assigned as pure black and 255 assigned as pure white. The frequency of all the pixels were plotted, with the mean RGB intensity displayed as the peak of the curve (Figure 2-5).

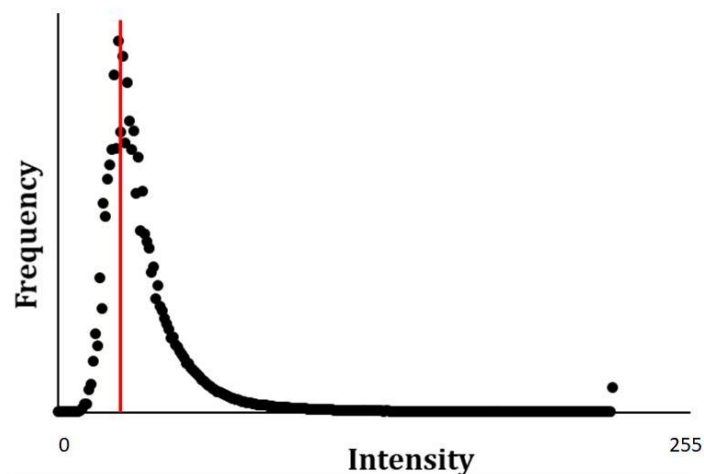


Figure 2-5: RGB peak intensity.

2.3.5.2.2 RGB Intensity Variance

The red intensity was used to determine biochar sample uniformity because it displayed the greatest difference in mode intensity between biochar samples. The more uniform in colour a sample product is, the narrower the distribution spread of the RGB intensity curve. The RGB intensity was determined using ZEISS Axiocam 105 colour microscope and software. The Axiocam 105 colour software analyzes each individual pixel from the image taken by the microscope and assigns an RGB intensity between 0 to 255, with zero assigned as pure black and 255 assigned as pure white. The frequency of all the pixels were plotted, with the mode RGB intensity displayed as the peak of the curve. The coefficient of variation is used to analyze the biochars and is defined as follows:

$$\text{Coefficient of Variation} = \frac{\sqrt{\text{Variance}}}{\text{Mean}} \quad (2-6)$$

2.3.5.3 Ash Content

The procedure to determine the ash content complies with ASTM D1762-84: samples of 1 g were placed in a crucible and dried in an oven at 105 °C for 2 hours, then placed in a muffle furnace 750 °C for 4 hours.

2.3.5.4 Skeletal Density

Sample density was measured by volume displacement. Prior to measurements, each volumetric flask was calibrated. Biochar samples were ground in a burr mill, then sieved to 500 µm. 1 g of the biochar powder is placed into a 120 ml volumetric flask along with 20 ml of dispersant (Finish Quantum dishwasher detergent). The flask was mixed until the biochar powder was immersed within the dispersant solution to form a slurry, then filled with de-ionized water to the 120 ml indicator line and weighed. Biochar volume can then be determined based on the volume of the solution displaced, allowing to calculate the density using the following equations:

$$\text{Liquid Solution in Volumetric Flask (g)} = (\text{Volumetric flask with BC and liquid solution (g)}) - \text{BC (g)} - \text{Dry volumetric flask (g)} \quad (2-7)$$

$$\text{Biochar Volume} = \text{Volume Displaced (cm}^3\text{)} = \frac{[\text{Calibrated liquid (g)} - \text{Liquid solution in volumetric flask (g)}]}{\rho_{\text{water}}} \quad (2-8)$$

$$\text{Skeletal Density} \left(\frac{\text{g}}{\text{cm}^3} \right) = \frac{\text{BC (g)}}{\text{Biochar Volume (cm}^3\text{)}} \quad (2-9)$$

Where the density of water (ρ_{water}) at 25 °C is taken as 0.997 g/cm³.

2.3.5.5 Electrical Conductivity and Heavy Metals Analysis

Leaching of heavy metals and nutrients was studied using a Soxhlet extractor, which continuously washes a sample with fresh recycled solvent, water in this case, over a period of 16 hours.

Electrical conductivity was measured using a High Range Hanna Instruments Combo pH/Conductivity/TDS tester. Electrical conductivity measured in mS/cm were corrected based on biochar sample weight and volume of the extraction liquid as follows:

$$\text{Corrected EC} = \frac{EC}{\left(\frac{BC}{V_{\text{extract}}}\right)} \quad (2-10)$$

Where EC is the measured electrical conductivity in mS/cm; BC is the weight of biochar sample in g; and V_{extract} is the volume of the Soxhlet extraction liquid in cm^3 .

Figure 2-6 shows a diagram of a Soxhlet extractor, which can be separated into three sections: a boiling flask, extraction chamber and condenser. The boiling flask is placed in an oil bath of 140 °C and heated to boil the solvent, ensuring only pure solvent evaporates. The vaporized solvent bypasses the extraction chamber and enters the condenser. Cooling water flowing through the condenser then condenses the solvent into the extraction chamber. The extraction chamber houses a cellulose thimble filled with biochar sample that is continuously washed with fresh condensed solvent. This solvent collects in the extraction chamber until a volume of 75 mL is reached, then siphoned through a tube back into the boiling flask to be recycled.

The leaching experiment described above has been adapted from EPA Method 3540C and Chegini (2017) used to extract heavy metals and nutrients from solids such as soils, sludges and wastes using a Soxhlet extractor. Deionized water was used to simulate real world conditions of rainfall on agricultural soils.

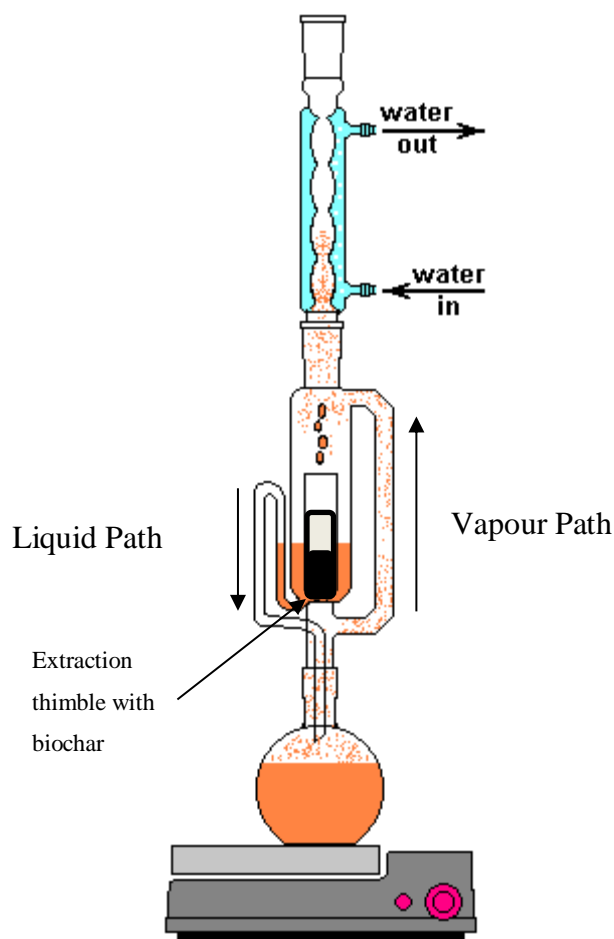


Figure 2-6: Soxhlet extractor (Adapted from Dolinowski (32))

2.3.5.6 Methylene Blue Adsorption

Methylene blue adsorption capacity was used to measure the porosity of biochar. Methylene blue adsorption was chosen over Brunauer-Emmett-Teller (BET) adsorption to characterize porosity because liquid adsorption is more reliable over gas adsorption as biochar interaction with water is more of a concern. The method described was adapted from Raposo et al. (33). All biochars were washed with 95°C deionized water and dried overnight at 105°C to remove impurities and clear pore structures prior to measurements. Based on preliminary studies conducted with activated carbon, an initial methylene blue and deionized water solution of 800 ppm and biochar to methylene blue solution ratio of

1:75 was used for all adsorption experiments. 0.2 g of biochar was combined with 15 mL of methylene blue solution and agitated in a shaker for 48 hrs. Once this stage was complete, 3 mL of the resulting solution was centrifuged at 5000 rpm for 10 min to separate the biochar from the used methylene solution. The spent methylene blue solution was then diluted with deionized water ratio of 1:7.5 into a cuvette and analyzed using a spectrophotometer. The spectrophotometer analyzed the solution at 664 nm, and a calibration curve was used to determine the diluted solutions methylene blue concentration (Equation 2-11).

$$\text{Calibration Curve Concentration} = 4.6724(\text{Abs}) - 0.1465 \quad (2-11)$$

where Abs is the absorbance reading from the spectrophotometer in nm.

2.4 Results and Discussion

2.4.1 RHP Characterization and Performance

The RHP reactor has high feedstock processing flexibility. Three different biomass feedstocks were processed; woodchips (WCP), Storm Fisher digestate (SFD) and Bayview Flowers digestate (BFD). All three feedstocks were successfully converted to biochar, regardless of the differences in physical properties between the biomass feedstocks. Table 2-2 provides the bulk densities of each biomass feedstock and Table 2-3 provides the biomass loadings used in all the RHP experimental pyrolysis runs. Biomass batches between 6-12 kg were processed, with biomass loadings depending on feedstock type.

Table 2-2: Bulk density of feedstocks.

Feedstock	Bulk Density (g/cm³)
Woodchips (WCP)	0.176
Storm Fisher Digestate (SFD)	0.694
Bayview Flowers Digestate (BFD)	0.588

Table 2-3: Biomass loadings for different RHP runs.

RHP Process Time (hr)	Biomass Loading (kg)		
	Woodchips (WCP)	Storm Fisher Digestate (SFD)	Bayview Flowers Digestate (BFD)
1	6.0	11.4	9.3
2	6.0	12.3	11.9
3	6.0	11.1	10.1
4	6.0	12.4	10.6

Three different heating element designs were constructed and tested using the method described in 2.3.1.1. The three designed referred as (i) Spiral heater, (ii) Tube heater and (iii) Plate heater are shown in Figure 2-7.

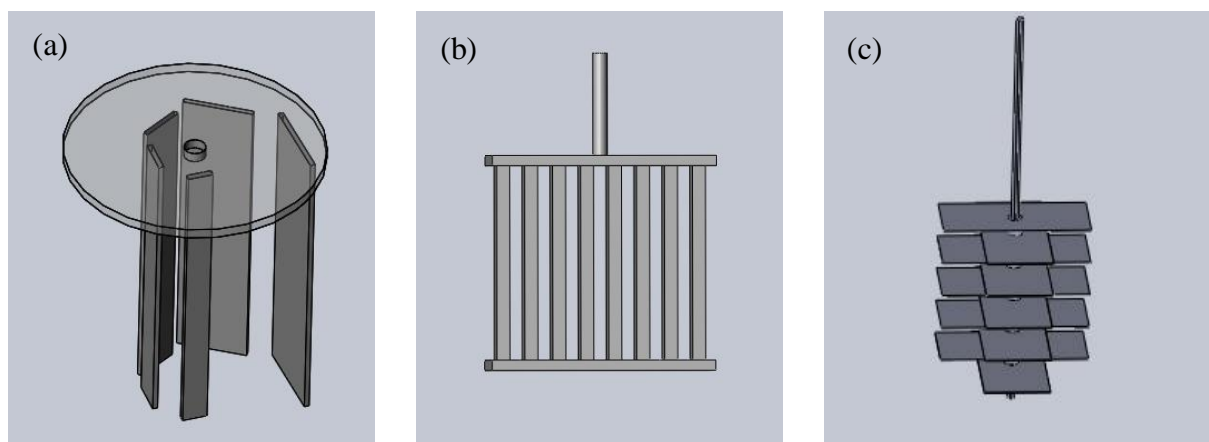


Figure 2-7: Rotating heater designs (a) Spiral Heater; (b) Tube Heater; (c) Plate Heater.

The three heater designs were created based on a preliminary study investigating the effects of metal geometry and weight on the current passing through the induction system. Based on the preliminary study it was determined that geometry and thickness of the metal also affect power provided to the bed. It is important to note that the relationship between power provided to the system and metal surface area is not linear. Geometry plays an important role with respect to active shielding effects that can occur within an induction magnetic field. In this specific case, active shielding is when counter fields opposite to the main field are produced around a magnetic element within the main

induction field. Therefore, two or more magnetic elements placed next to one another can create an active shield and reduce the heating effects created by the induction magnetic field. The mass of metal also plays an important role in optimizing the power provided to the heating element, and it was determined that lighter metals were able to heat to higher temperatures at faster rates. Based on these preliminary results, it was determined that the rotating heater needs to follow the following constraints:

- Maximize power through the induction system, while also maximizing the surface area available for biomass-to-heater surface contact
- Minimize the effect of shielding between metallic elements of the heater
- Minimize metal element weight, while also being durable enough to withstand mechanical wear and tear
- During rotation, the heating element needs to be able to move aerodynamically through the bed (frictional forces need to be minimized between the heating element and biomass particles to reduce the power required by the motor to turn the heating element. The goal is not to distribute the solids to the heat source, rather distribute the heat source to the solid particles.)

Each of the heating elements were designed with the following constraints in mind. Using the current passed through the induction system with each of the individual heater designed the power passed through the induction system was calculated. Table 2-4 provides the power provided to the unit and the corresponding surface area of each heater design.

Table 2-4: Current through the induction system with the spiral heater, tube heater and plate heater.

Rotating Heater Design	Current Through Induction System (Amps)	Nominal Power through the induction system (kW)	Surface Area of Working Metal (m²)
Spiral	21.2	7.6	0.43
Tube	15.0	5.4	0.15
Plate (10 plate design)	22.0	7.9	0.58

The plate design provides the highest power through the induction system while maximizing the surface area of the heater. It is important to provide as large a surface area for contact with biomass particles, as biomass particles become reactive when in contact with the heating surface. In addition, the plate design can provide the most aerodynamic movement through the bed of solids. The spiral and tube heaters were less aerodynamic and mechanically ground the feedstocks into a fine dust.

The actual power supplied to the reaction bed was determined using the method described in Section 2.3.1.2. Figure 2-8 provides the conversion of power supplied by the induction unit and the actual power supplied to the sand bed based on the latent vaporization of water. During pyrolysis production runs, the induction unit is set to the maximum allowable power input of 3 kW. The peristaltic pump was unable to provide the flowrate of water required to maintain the bed temperature at 100°C and was interpolated from the relationship shown in Figure 2-8.

It was determined that 2 kW of power are transferred from the heating element to the bed when supplied with 3 kW of power from the induction unit. 1/3 of power supplied to the system is lost due to heat losses from the system and heating of the cooling water passed through the induction coils surrounding the reaction vessel.

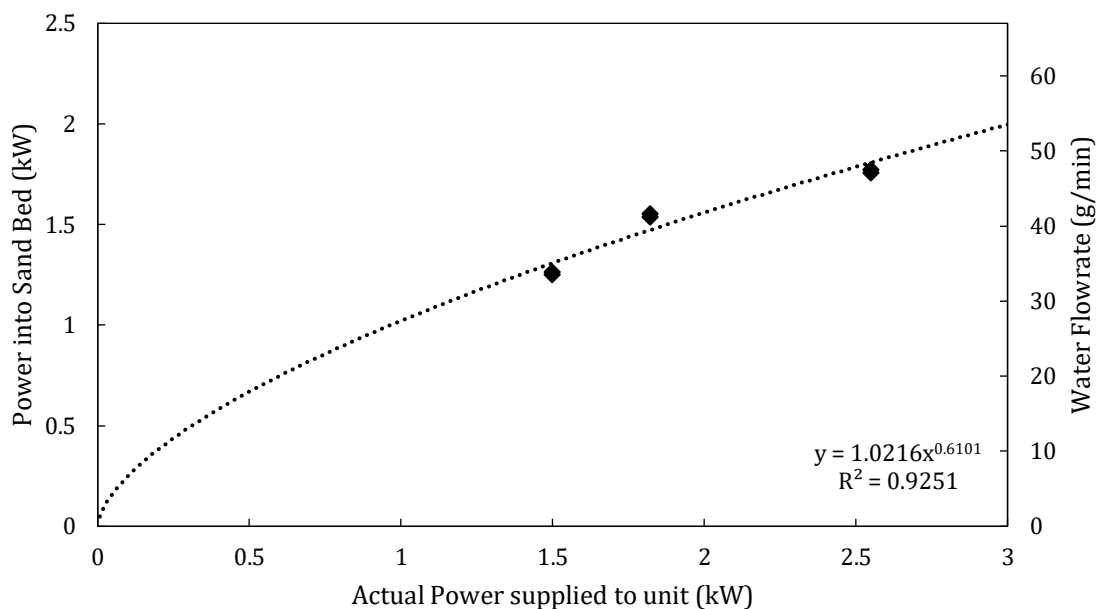


Figure 2-8: Power supplied to the reaction bed with the plate heater. Empirical curve fit was used.

The energy required to operate the rotating heater was determined using the methods described in section 2.3.1.3. The operating pressure, heater rpm in the clockwise and counter-clockwise rotation is listed in

Table 2-5 along with the corresponding air consumption, torque and power consumption using the information provided from the air motor manufacturing company.

Table 2-5: Energy consumption required to operate the rotating heater.

	Clockwise Rotation	Counter-clockwise Rotation
Rotation per minute (rpm)	145	215
Air line pressure (bar)	7	7
Air consumption (l/s)	7	9
Torque (N.m)	4.8	5.5
Power consumption (kW)	0.02	0.1

One of the design objectives for this reactor was to keep the heating element at a distance from the walls to have vapours exiting the reactor through the exhaust at relatively low temperatures. The purpose behind this design decision was to condense heavy tars to be further converted to char, vapours and gas. Deposits of condensed heavy tars are shown in Figure 2-9, verifying that heavy tars are being condensed and recycled throughout pyrolysis.

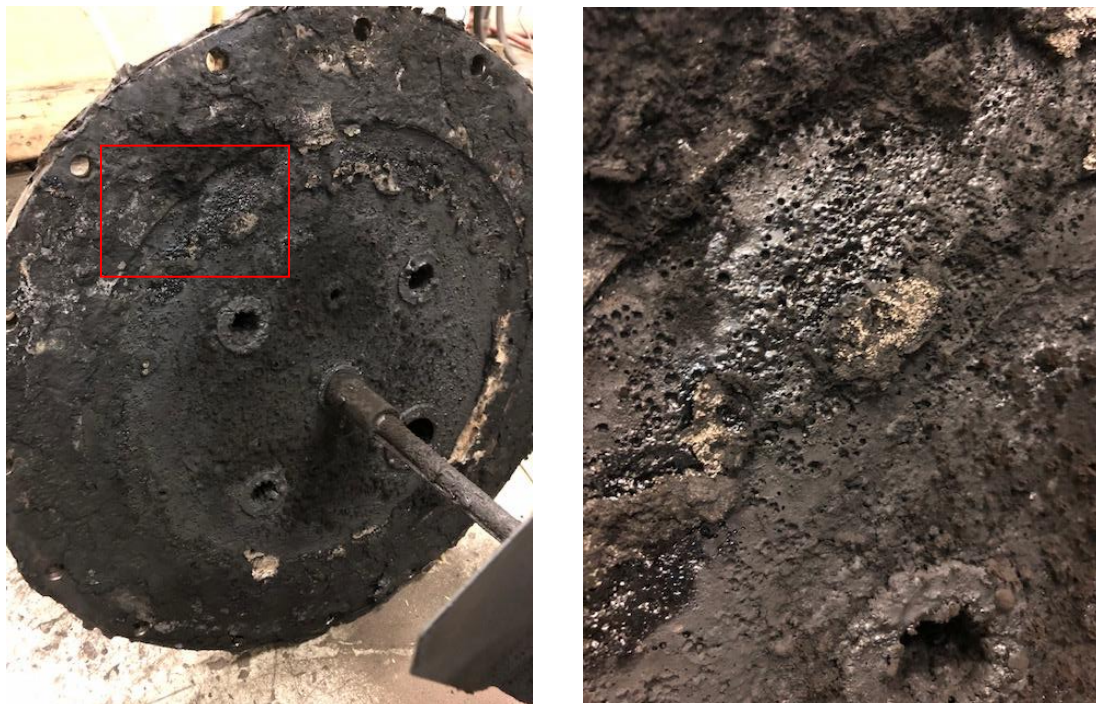


Figure 2-9: Tar deposits along lid of RHP.

2.4.2 Effect of Process Time on Biochar Properties

As shown in Figure 2-10, the yield of biochar decreases with a decrease in processing time. The yield of biochar decreases from 73.2% to 43.8% from process time of 0.5 hrs to 2 hrs and remains relatively constant between 2 to 4 hrs. A 0.4% increase in biochar yield occurs between process times of 2 to 3 hrs. This is contradictory as biochar yield generally increases with increasing processing time. The increase in yield could be attributed to the condensation of tars on the lid of the reactor. As reaction time proceeds, the lid gets progressively hotter and the condensed tars on the lid may be drying and falling into the bed, making a minor contribution to the overall yield.

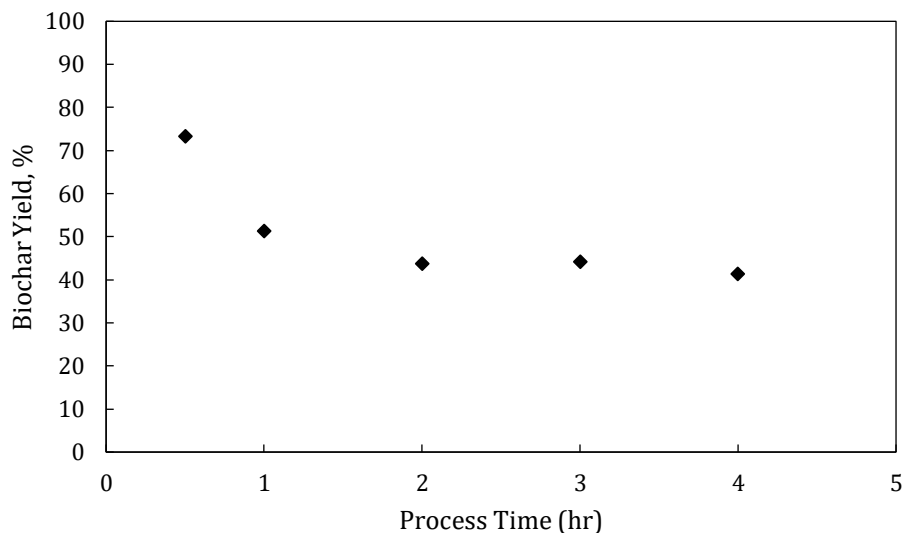


Figure 2-10: Effect of RHP process time (hrs) on biochar yield.

Figure 2-11 depicts the effect of RHP process time on the mode red intensity. The mode red intensity is used to detect changes in colour within the biochar, as described in Section 2.3.5.2. The woodchip feedstock is represented at a process time of 0 hrs and has a mode red intensity of 255. Figure 2-11 clearly illustrates that there is a significant change in red colour intensity between the raw feedstock and biochars processed between 1 to 4 hours. Regardless of processing time, the red intensity remains relatively constant for all chars, potentially indicating that the pyrolysis reaction occurs within 1 hr of processing time, however longer holding times may be required to achieve specific char property goals, depending on the end use applications.

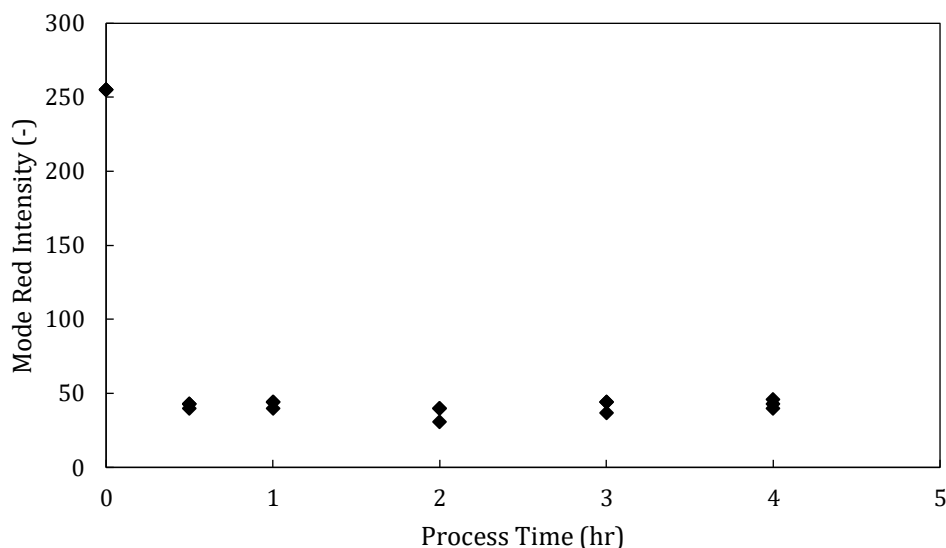


Figure 2-11: Effect of process time (hrs) on mode red intensity of woodchip derived biochar. Raw woodchip feedstock mode red intensity is represented at a process time of 0 hrs, Triplicate results are displayed.

Figure 2-13 shows the effect of RHP process time on the ash content of the biochars. The relatively large variation between the triplicate ash content measurements are attributed to inhomogeneities such as small rocks, sand and soil present within the woodchip feedstock. The reproducibility for the ash content measurements are greatly affected by inhomogeneities present within the feedstock at the 1 g sampling level. However, some general trends are still observed. As expected, ash content increases from with increasing processing time between 1 to 3 hrs. A significant drop in ash content is observed between processing time of 3 to 4 hrs. The drop in ash content is unexpected as mineral concentration within a biochar sample should increase with increasing pyrolysis temperature/ processing time or plateau and remain relatively constant in the case that after a certain process time is reached, the pyrolysis temperature does not change.

The coefficient of variation of the mode red intensity was also analyzed to determine the uniformity of the biochar products. Figure 2-12 demonstrates the effects of RHP process time on the red mode intensity coefficient of variation. The variance of the RHP char remains relatively constant around a coefficient of variation of approximately 0.5,

indicating that regardless of processing time, the resultant products are all processed similarly and have a comparable homogeneity. The homogeneity of RHP derived chars compared to chars produced with a traditional lab scale batch reactor is investigated in Chapter 3.

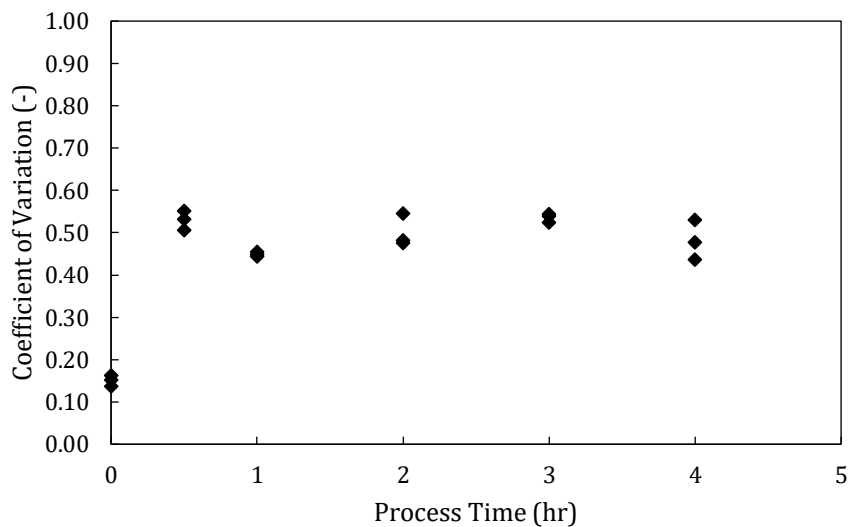


Figure 2-12: Effect of RHP process time (hrs) on the red mode intensity coefficient of variation. Triplicate results are displayed.

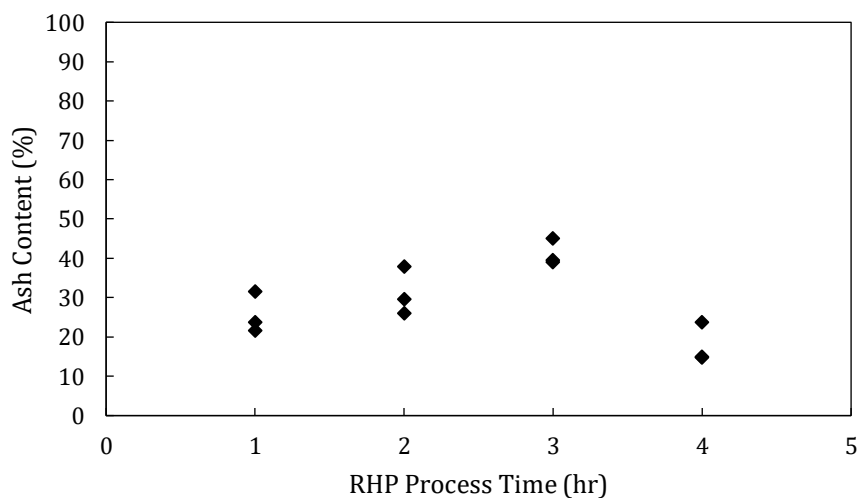


Figure 2-13: Effect of RHP process time (hrs) on the ash content of woodchip derived biochar. Triplicate results are displayed.

Figure 2-14 displays the effect of RHP process time on the skeletal density of woodchip derived chars. Due to inhomogeneities such as sand, small rocks and soil present within the feedstock, skeletal density measurements showed some variation. Rock and sand particles affect the skeletal density measurements on the 1 g sampling level, as these are high density and non-porous materials.

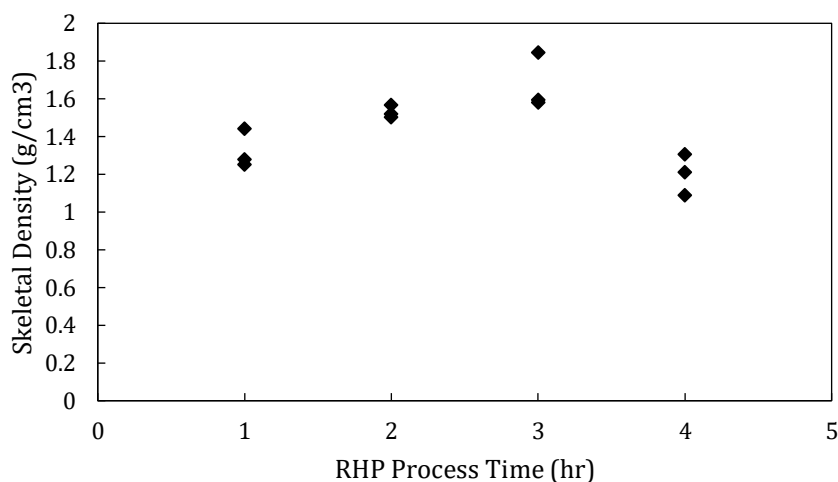


Figure 2-14: Effect of RHP process time (hrs) on the skeletal density of woodchip derived biochar. Triplicate results are displayed.

Figure 2-15 illustrates the effect of process time on the electrical conductivity of biochar Soxhlet extract with respect to the electrical conductivity of raw woodchip Soxhlet extract. As shown in Figure 2-15, processing the feedstock in the RHP increases the electrical conductivity of biochar extract regardless of process time. At lower processing times between 1 to 2 hours, the electrical conductivity of the biochar extract with respect to the electrical conductivity of biomass extract increased by a factor of 1.35. Then a decrease in electrical conductivity is observed from process times of 3 to 4 hrs and approaches the baseline electrical conductivity of the raw woodchip feedstock. The decrease in electrical conductivity is unexpected as the concentration of mineral content was shown to increase with increasing process time (Figure 2-13). The initial increase in electrical conductivity may have been caused by the formation of pore structures within

the biochar providing better contact between water and the water-soluble metals. While the decrease in electrical conductivity starting at 3 hr process time may be caused by tars plugging the biochar pore structures, reducing access to water soluble minerals.

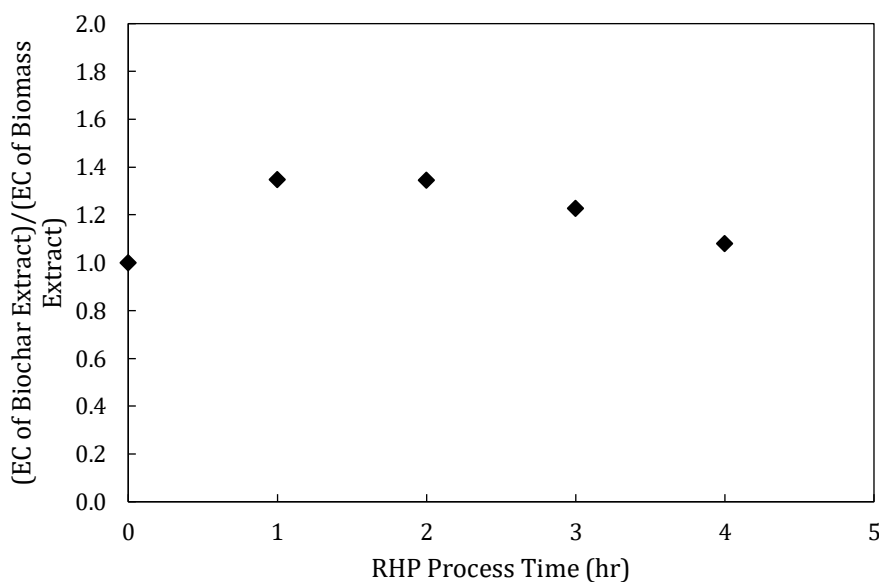


Figure 2-15: Effect of RHP process time on the electrical conductivity of biochar Soxhlet extract from biochar with respect to the electrical conductivity of raw woodchip Soxhlet extract. Average of duplicate measurements displayed.

Methylene blue adsorption capacity is related to macropore and mesopore distribution and can be used as a tool to interpret the level of porosity in activated carbons and biochars. Figure 2-16 portrays the effect of RHP process time on methylene blue adsorption capacity. An overall decrease in methylene blue adsorption is observed between processing times of 1 to 4 hrs. This decreasing trend resembles the trend observed in Figure 2-15, and implies that the production of tars may be clogging the pore structures, leading to reduced electrical conductivities and methylene blue adsorption.

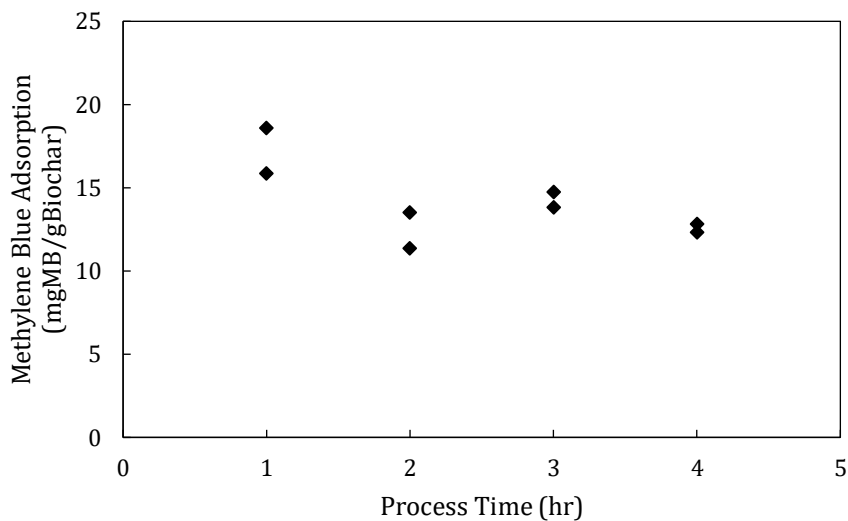


Figure 2-16: Effect of RHP processing time (hrs) on methylene blue adsorption of woodchip derived biochar.

2.5 Conclusions

The Rotating Heater Pyrolyzer (RHP) is a new batch reactor with characteristics that make it suitable for lab scale biochar production. One of the main features of the RHP is that heat is distributed to the solids via a rotating heating element instead of the other way around as is the case in most traditional lab scale pyrolysis reactors. A number of design objectives for the RHP were set and ultimately met. The RHP is capable of successfully processing a wide variety of feedstocks and producing batches of biomass within the 10-12 kg range, depending on feedstock. The RHP has a relatively low energy consumption, as it relies on gravity for mixing, leading to low air consumption rates required to turn the rotating heater, and contains efficient heating with only 1/3 of the power lost due to environmental heat losses. In addition, capital and operating expenses are minimized as no solid heat carrier or fluidization gas are required for pyrolysis to effectively take place. Condensation and recycling of heavy tars from the vapour stream occurs, contributing to the reactor biochar yields.

2.6 References

1. Giorcelli M, Khan A, Pugno NM, Rosso C, Tagliaferro A. Biochar as a cheap and environmental friendly filler able to improve polymer mechanical properties. *Biomass and Bioenergy* [Internet]. 2019 Jan [cited 2019 May 30];120:219–23. Available from: <https://linkinghub.elsevier.com/retrieve/pii/S0961953418303325>
2. Peterson SC, Chandrasekaran SR, Sharma BK. Birchwood biochar as partial carbon black replacement in styrene-butadiene rubber composites. [cited 2019 May 30]; Available from: <https://journals.sagepub.com/doi/pdf/10.1177/0095244315576241>
3. Qian K, Kumar A, Zhang H, Bellmer D, Huhnke R. Recent advances in utilization of biochar. *Renew Sustain Energy Rev* [Internet]. 2014 [cited 2019 Jun 9];42:1055–64. Available from: <http://dx.doi.org/10.1016/j.rser.2014.10.074>
4. Fiore S, Berruti F, Briens C. Investigation of innovative and conventional pyrolysis of ligneous and herbaceous biomasses for biochar production. *Biomass and Bioenergy* [Internet]. 2018 Dec 1 [cited 2019 May 28];119:381–91. Available from: <https://www.sciencedirect.com/science/article/pii/S0961953418302769?via%3Dihub>
5. Adrados A, De Marco I, López-Uriónabarrenechea A, Solar J, Caballero BM, Gastelu N. Biomass Pyrolysis Solids as Reducing Agents: Comparison with Commercial Reducing Agents. *Mater (Basel, Switzerland)* [Internet]. 2015 Dec 23 [cited 2019 Jun 9];9(1). Available from: <http://www.ncbi.nlm.nih.gov/pubmed/28787805>
6. Li X, Lei B, Lin Z, Huang L, Tan S, Cai X. The utilization of bamboo charcoal enhances wood plastic composites with excellent mechanical and thermal properties. *Mater Des* [Internet]. 2014 [cited 2019 Jun 16];53:419–24. Available from: <http://dx.doi.org/10.1016/j.matdes.2013.07.028>

7. Limwikran T, Kheoruenromne I, Suddhiprakarn A, Prakongkep N, Gilkes RJ. Dissolution of K, Ca, and P from biochar grains in tropical soils. *Geoderma* [Internet]. 2018 [cited 2019 Jun 9];312:139–50. Available from: <http://dx.doi.org/10.1016/j.geoderma.2017.10.022>
8. Prakongkep N, Gilkes RJ, Wiriyaakitnatekul W. Forms and solubility of plant nutrient elements in tropical plant waste biochars. *J Plant Nutr Soil Sci*. 2015;178(5):732–40.
9. Lehmann J, Pereira da Silva Jr J, Steiner C, Nehls T, Zech W, Glaser B. Nutrient availability and leaching in an archaeological Anthrosol and a Ferralsol of the Central Amazon basin: fertilizer, manure and charcoal amendments [Internet]. Vol. 249, *Plant and Soil*. 2003 [cited 2019 Jun 9]. Available from: <https://link-springer-com.proxy1.lib.uwo.ca/content/pdf/10.1023%2FA%3A1022833116184.pdf>
10. Major J, Rondon M, Molina D, Riha SJ, Lehmann J. Nutrient Leaching in a Colombian Savanna Oxisol Amended with Biochar. *J Environ Qual* [Internet]. 2012 [cited 2019 Jun 8];41(4):1076. Available from: <http://www.ncbi.nlm.nih.gov/pubmed/22751049>
11. Liang B, Lehmann J, Solomon D, Kinyangi J, Grossman J, O’Neill B, et al. Black Carbon Increases Cation Exchange Capacity in Soils. *Soil Sci Soc Am J* [Internet]. 2006;70(5):1719. Available from: <https://www.soils.org/publications/sssaj/abstracts/70/5/1719>
12. Omondi MO, Xia X, Nahayo A, Liu X, Khan Korai P, Pan G. Quantification of biochar effects on soil hydrological properties using meta-analysis of literature data. *Geoderma* [Internet]. 2016 [cited 2019 Jun 9];274:28–34. Available from: <http://dx.doi.org/10.1016/j.geoderma.2016.03.029>
13. Blanco-Canqui H. Biochar and Soil Physical Properties. *Soil Sci Soc Am J*. 2017;81(4):687.
14. He X, Liu Z, Niu W, Yang L, Zhou T, Qin D, et al. Effects of pyrolysis

temperature on the physicochemical properties of gas and biochar obtained from pyrolysis of crop residues. 2018 [cited 2019 Jun 9]; Available from:

<https://doi.org/10.1016/j.energy.2017.11.062>

15. Suman S, Gautam S. Pyrolysis of coconut husk biomass: Analysis of its biochar properties. *Energy Sources, Part A Recover Util Environ Eff* [Internet]. 2017 Apr 18 [cited 2019 Jun 9];39(8):761–7. Available from:
<https://www.tandfonline.com/doi/full/10.1080/15567036.2016.1263252>
16. Gheorghe C, Marculescu C, Badea A, Dinca C, Apostol T. Effect of Pyrolysis Conditions on Bio-Char Production from Biomass Effect of Pyrolysis Conditions on Bio-Char Production from Biomass. *Renew Energy Sources*. 2015;(January 2015):239–42.
17. Jaffé R, Ding Y, Niggemann J, Vähätalo A V, Stubbins A, Spencer RGM, et al. Global Charcoal Mobilization from Soils via Dissolution and Riverine Transport to the Oceans. [cited 2019 Jun 9]; Available from:
www.sciencemag.org/cgi/content/full/340/6130/345/DC1
18. Rumpel C, Alexis M, Chabbi A, Chaplot V, Rasse DP, Valentin C, et al. Black carbon contribution to soil organic matter composition in tropical sloping land under slash and burn agriculture. 2005 [cited 2019 Jun 9]; Available from:
www.elsevier.com/locate/geoderma
19. Peng X, Zhu QH, Xie ZB, Darboux F, Holden NM. The impact of manure, straw and biochar amendments on aggregation and erosion in a hillslope Ultisol. *Catena* [Internet]. 2016 [cited 2019 Jun 9];138:30–7. Available from:
<http://dx.doi.org/10.1016/j.catena.2015.11.008>
20. Major J. Guidelines on Practical Aspects of Biochar Application to Field Soil in Various Soil Management Systems Photo by Josiah Hunt [Internet]. [cited 2019 May 29]. Available from: www.biochar-international.org
21. Judith Martínez E, Rosas JG, Sotres A, Moran A, Cara J, Sánchez ME, et al.

- Codigestion of sludge and citrus peel wastes: Evaluating the effect of biochar addition on microbial communities. *Biochem Eng J* [Internet]. 2018 [cited 2019 Jun 4];137:314–25. Available from: <https://doi.org/10.1016/j.bej.2018.06.010>
22. Chen J, Li S, Liang C, Xu Q, Li Y, Qin H, et al. Response of microbial community structure and function to short-term biochar amendment in an intensively managed bamboo (*Phyllostachys praecox*) plantation soil: Effect of particle size and addition rate. *Sci Total Environ* [Internet]. 2017 [cited 2019 Jun 4];574:24–33. Available from: <http://dx.doi.org/10.1016/j.scitotenv.2016.08.190>
 23. Siddiqui MTH, Nizamuddin S, Mubarak NM, Shirin K, Aijaz M, Hussain M, et al. Characterization and Process Optimization of Biochar Produced Using Novel Biomass, Waste Pomegranate Peel: A Response Surface Methodology Approach. *Waste and Biomass Valorization* [Internet]. 2019 Mar 23 [cited 2019 Jun 3];10(3):521–32. Available from: <http://link.springer.com/10.1007/s12649-017-0091-y>
 24. Hodgson E, Lewys-James A, Rao Ravella S, Thomas-Jones S, Perkins W, Gallagher J. Optimisation of slow-pyrolysis process conditions to maximise char yield and heavy metal adsorption of biochar produced from different feedstocks. 2016 [cited 2019 Jun 3]; Available from: <http://dx.doi.org/10.1016/j.biortech.2016.05.009>
 25. Chegini G, Sanchez Careaga FJ, Pjontek D, Briens C. Impact of Pyrolysis heating characteristics on leachability of biochar minerals. *TCBiomass* [Internet]. 2017; Available from: <http://www.gastechnology.org/tcbiomass/tcbiomass2017/Ghazaleh-Chegini-Thu-tcbiomass2017-presentation.pdf>
 26. Barry DJ, Briens S, Berruti C-S. Pyrolysis as an Economical and Ecological Treatment Option for Solid Anaerobic Digestate and Municipal Sewage Sludge Recommended Citation [Internet]. 2018 [cited 2019 Jul 21]. Available from: <https://ir.lib.uwo.ca/etd://ir.lib.uwo.ca/etd/5187>

27. Kloss S, Zehetner F, Dellantonio A, Hamid R, Ottner F, Liedtke V, et al. Characterization of Slow Pyrolysis Biochars: Effects of Feedstocks and Pyrolysis Temperature on Biochar Properties. *J Environ Qual*. 2012;41(4):990.
28. Keiluweit M, Nico PS, Johnson MG, Kleber M. Dynamic Molecular Structure of Plant Biomass-Derived Black Carbon (Biochar). *Environ Sci Technol* [Internet]. 2010 [cited 2019 Jun 4];44:1247–53. Available from: <https://pubs.acs.org/doi/10.1021/es9031419>.
29. Mukome FND, Zhang X, Silva LCR, Six J, Parikh SJ. Use of Chemical and Physical Characteristics To Investigate Trends in Biochar Feedstocks. 2013 [cited 2019 Jun 4]; Available from: <https://pubs.acs.org/doi/10.1021/jf3049142>.
30. Yargicoglu EN, Sadasivam BY, Reddy KR, Spokas K. Physical and chemical characterization of waste wood derived biochars. *Waste Manag* [Internet]. 2015 Feb [cited 2019 Jun 4];36:256–68. Available from: <https://linkinghub.elsevier.com/retrieve/pii/S0956053X14005133>
31. Jindo K, Mizumoto H, Sawada Y, Sanchez-Monedero MA, Sonoki T. Physical and chemical characterization of biochars derived from different agricultural residues. *Biogeosciences* [Internet]. 2014 [cited 2019 Jun 4];11:6613–21. Available from: www.biogeosciences.net/11/6613/2014/
32. Dolinowski T. Soxhlet Extractor. 2011;
33. Raposo F, De La Rubia MA, Borja R. Methylene blue number as useful indicator to evaluate the adsorptive capacity of granular activated carbon in batch mode: Influence of adsorbate/adsorbent mass ratio and particle size. *J Hazard Mater* [Internet]. 2009 Jun 15 [cited 2019 Aug 23];165(1–3):291–9. Available from: <https://linkinghub.elsevier.com/retrieve/pii/S0304389408014702>
34. Singh B, Singh BP, Cowie AL. Characterisation and evaluation of biochars for their application as a soil amendment. *Soil Res* [Internet]. 2010 Oct 19 [cited 2019 Jun 9];48(7):516. Available from: <http://www.publish.csiro.au/?paper=SR10058>

Chapter 3

3 Comparison of RHP Derived Biochar Properties to Standard Batch Pyrolysis Biochar

3.1 Introduction

Biochar is the solid product produced during the process known as pyrolysis. Pyrolysis is the thermal decomposition of organic matter in the absence of oxygen at elevated temperatures, and produces a solid called biochar, condensable vapours referred to as bio-oil and gases (mostly carbon monoxide, carbon dioxide and methane). Biochar is a porous material comprised of crystallized carbon, inorganics (ash) and polyaromatic hydrocarbons (PAH) originally contained within the biomass feedstock. Biomass feedstocks for pyrolysis are provided by sustainable sources of biomass, which are organic resources that do not compete with food sources or require land use changes with negative environmental impacts (1). Examples of feedstocks include agricultural and forestry waste, food waste, and animal waste. Biochar has gained interest for its potential use as a carbon sequestration technology and soil amendment to improve agricultural output. Biochar is often characterized by end use application, as its physical and chemical properties are highly dependent on pyrolysis conditions including feedstock, pyrolysis temperature heating rate and exposure time (2–4). Biochar can be used in other applications including wastewater treatment, bio-coke fuel source for metallurgical applications, and as a filler for composite/polymer materials (5–10).

Choosing the appropriate reactor design is essential to successfully produce pyrolysis products for any application. Pyrolysis reactors operate under the same general principle where heat is supplied to a reaction vessel under oxygen limiting conditions, with the heat delivery system and gas-solid contact being the main defining trait between reactors. Most lab scale reactors are geared towards the production of bio-oil over biochar. The rotating heater pyrolyzer (RHP) is a lab scale reactor designed specifically to produce several kg of char (Chapter 2). Unlike most lab scale reactors, the RHP does not heat the exterior of the reaction vessel, and instead a metallic heating element is placed inside, and

heated via induction. In addition, the RHP does not require any heat carriers or fluidization gas, and the main body is constructed from concrete.

The aim of this study was to compare biochar produced with the RHP to biochar produced using a standard batch pyrolysis reactor, referred to as the Pyrolytic Shaker Reactor (PSR). Properties related to soil amendment applications are tested and compared between the RHP and PSR technologies.

It is noted that Section 3.3: Feedstock and Biochar Characterization Methods contains the same characterization methods as those outlined in Chapter 2 with the exception of Sections 3.3.1.3, 3.3.1.4, and 3.3.1.5.2

3.2 Materials and Pyrolysis Methods

3.2.1 Feedstock

Three main feedstocks are used in the scope of this thesis. The first objective for this thesis was to design, develop and characterize the RHP reactor. Woodchip (WCP) biomass was used to develop and characterize the RHP reactor as conversion of this type of feedstock to biochar (BC) has been extensively studied in literature (11–15).

Woodchip feedstocks are relatively expensive, therefore once the RHP technology had been developed, the focus of this thesis shifted towards converting two different anaerobic digestates into biochar. The first digestate was provided from Bayview Flowers greenhouse (BFD) located in St. Catherines, ON, and the second from Storm Fisher Environmental (SFD), a food waste anaerobic digestion facility located in London, ON.

3.2.2 Standard Batch Pyrolysis Reactor: Pyrolytic Shaker Reactor (PSR)

The Pyrolytic Shaker Reactor (PSR) is comprised of three sections: the reactor vessel, induction heating system and the mechanical agitation system. Figure 3-1 shows the schematic structure of the PSR.

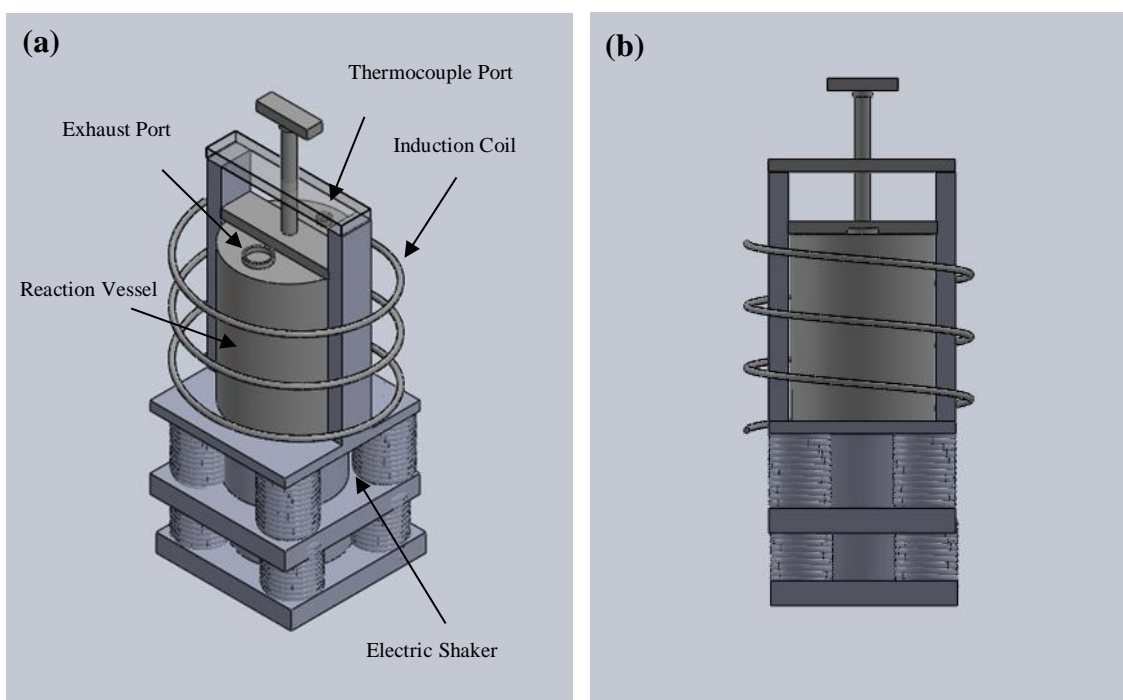


Figure 3-1: Schematic drawing of Pyrolytic Shaker Reactor (PSR): (a) Trimetric view (b) Front view.

Mechanical agitation is provided by a dedicated electric shaker. The shaker measures 29 cm length x 66 cm height x 39 cm wide. The shaker provides axial radial and angular mixing of the solid particles (Appendix B). Due to rapid heating of the solid bed, mixing is assisted by the evolution of gaseous pyrolysis products, which aerate the bed.

The reactor body is made of 0.08 cm thick carbon steel and has a diameter of 17 cm and a height of 19 cm (Figure 3-1). The lid has a diameter of 17 cm. To allow for exhaust of the product vapours during pyrolysis, a 2.5 cm diameter port is added to the lid, with gas pipe tubing attached to a condenser. A second port with a 0.64 cm diameter has a tee valve that houses a 0.32 cm type K/J thermocouple and a pressure safety relief valve.

The thermocouple is used to monitor bed temperature. The induction system is a SI-12kW model from the Superior Induction Company with a maximum nominal output of 12 kW and a frequency range of 30-80 KHz. Copper coil (0.64 cm inner diameter tubing) for the induction system tightly surrounds the reactor vessel and is held in place by the shaker support beams. The coil is made up of 3 turns with an outer diameter of 18 cm, and an insulating sleeve covering the entire length of the coils for safety purposes.

3.2.3 Rotating Heater Pyrolyzer (RHP)

The RHP is comprised of four sections: the reactor vessel, the induction heating system, the rotating heater and the air motor. Figure 3-2 shows the schematic structure of the RHP (Chapter 2). An in-depth description and operation of the RHP design is provided in Chapter 2.

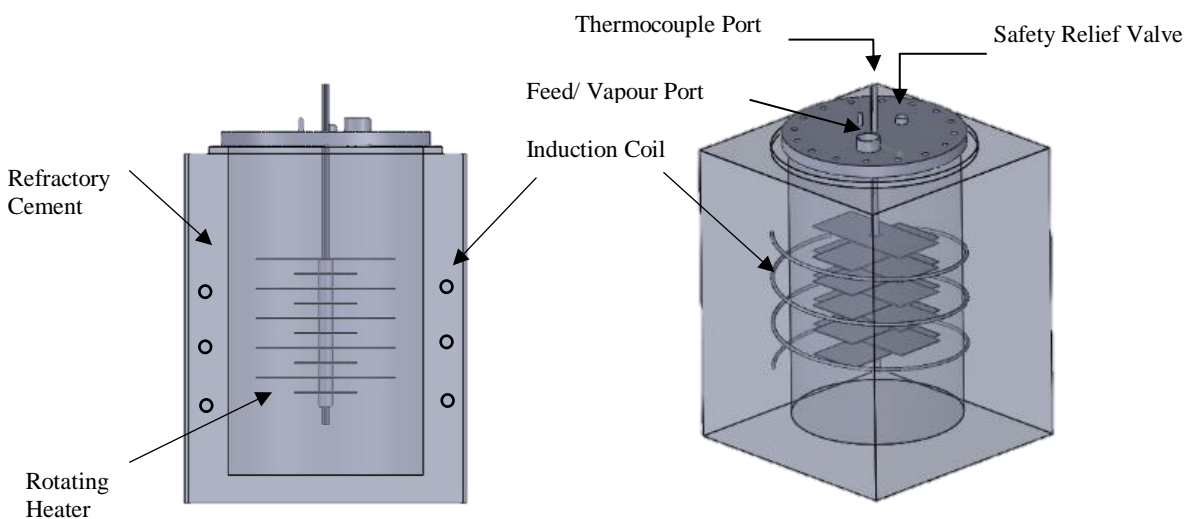


Figure 3-2: RHP Schematic.

3.2.4 Pyrolysis Procedures

3.2.4.1 PSR Procedure

Prior to pyrolysis, 2/3 of the volume of the reaction vessel is filled with biomass feedstock, with the weight of biomass sample recorded. Biomass batches fed to the reactor do not undergo any pre-treatment (for example; sieving or grinding to a specific size distribution) other than air drying over 48 hrs, to reduce the moisture content below 10%. The vessel is then sealed and secured into the shaking device. PSR agitation is started and maintained throughout the duration of the experiment to ensure proper mixing and heat transfer to create a uniform sample bed temperature. The induction heating system is turned on, set to the maximum frequency and maintained at a nominal input power of 8 kW. Samples are then heated to a set bed temperature (between 250 °C and 600 °C). Once the desired temperature is reached, both shaking, and induction heating are turned off, and the reactor and its contents are allowed to cool to room temperature.

3.2.5 Biochar Production Conditions

Twelve different WCP derived biochars were produced for detailed characterization using the PSR, gradually increasing in pyrolysis temperature from 250 to 525 °C, by increments of 25 °C. Two RHP derived chars were produced with WCP at processing times of 2 and 3 hrs for the same detailed characterization.

3.3 Feedstock and Biochar Characterization Methods

The following methods were chosen to characterize biochar properties because they are sensitive to pyrolysis temperature and heating rate.

3.3.1.1 Reactor Yield

Char yield was determined by comparing the biomass batch weight fed to the reactor with the weight of the char bed at the end of each run.

$$\text{BC yield (\%)} = \frac{\text{Weight of Collected Biochar (g)}}{\text{Weight of Biomass (g)}} \times 100 \quad (3-1)$$

3.3.1.2 Red, Green & Blue (RGB) Imaging

3.3.1.2.1 Red Green Blue (RGB) Intensity

The RGB intensity of biochar samples was used as a tool to compare RHP and PSR biochars based on colour. As biomass is pyrolyzed into biochar, the colour of biochar gradually becomes darker. The RGB intensity was determined using ZEISS Axiocam 105 colour microscope and software. The Axiocam 105 colour software analyzes each individual pixel from the image taken by the microscope and assigns an RGB intensity between 0 to 255, with zero assigned as pure black and 255 assigned as pure white. The frequency of all the pixels were plotted, with the mean RGB intensity displayed as the peak of the curve as shown in the example of Figure 3-3.

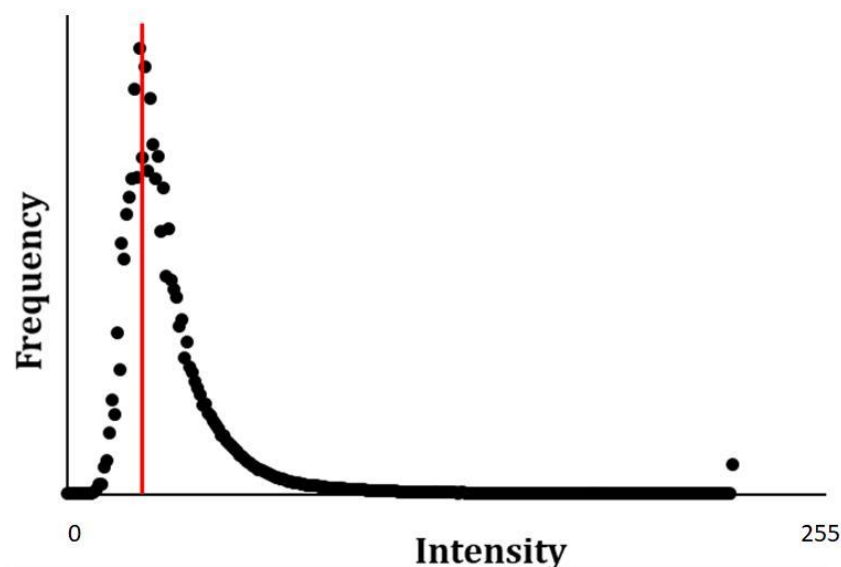


Figure 3-3: RGB peak intensity.

3.3.1.2.2 RGB Intensity Variance

The red intensity was used to determine biochar sample uniformity as preliminary results showed that it provided the greatest difference in mode intensity between biochar samples. The more uniform in colour a sample product is, the narrower the distribution spread of the RGB intensity curve. The RGB intensity was determined using ZEISS Axiocam 105 colour microscope and software. The Axiocam 105 colour software analyzes each individual pixel from the image taken by the microscope and assigns an RGB intensity between 0 to 255, with zero assigned as pure black and 255 assigned as pure white. The frequency of all the pixels were plotted, with the mode RGB intensity displayed as the peak of the curve.

The coefficient of variation is used to analyze the biochars and is defined as follows:

$$\text{Coefficient of Variation} = \frac{\sqrt{\text{Variance}}}{\text{Mean}} \quad (3-2)$$

3.3.1.3 Ash Content

The procedure to determine the ash content complies with ASTM D1762-84: samples of 1 g were placed in a crucible and dried in an oven at 105 °C for 2 hours, then placed in a muffle furnace 750 °C for 4 hours.

The results were not inaccurate/ reproducible due to inhomogeneities within the feedstock such as soil, small rocks and sand. At the 1 g level of sampling, these inhomogeneities have an amplified effect on the results as they are almost completely comprised of ash. A much larger sampling size would be required to minimize these errors. Due to these inaccuracies, the ash content measurements were omitted from the results and discussion section and can be found in Appendix C.

3.3.1.4 Skeletal Density

Sample density was measured by volume displacement. Prior to measurements, each volumetric flask was calibrated. Biochar samples were ground in a burr mill, then sieved to 500 µm. 1 g of the biochar powder is placed into a 120 ml volumetric flask along with 20 ml of dispersant (Finish Quantum dishwasher detergent). The flask was mixed until the biochar powder was immersed within the dispersant solution to form a slurry, then filled with de-ionized water to the 120 ml indicator line and weighed. Biochar volume can then be determined based on the volume of the solution displaced, allowing to calculate the density using the following equations:

$$\begin{aligned} \text{Liquid Solution in Volumetric Flask (g)} = \\ (\text{Volumetric flask with BC and liquid solution (g)}) - \text{BC (g)} - \\ \text{Dry volumetric flask (g)} \end{aligned} \quad (3-3)$$

$$\begin{aligned} \text{Biochar Volume} = \text{Volume Displaced (cm}^3\text{)} = \\ \frac{[\text{Calibrated liquid (g)} - \text{Liquid solution in volumetric flask (g)}]}{\rho_{\text{water}}} \end{aligned} \quad (3-4)$$

$$\text{Relative Density} \left(\frac{g}{cm^3} \right) = \frac{BC (g)}{\text{Biochar Volume} (cm^3)} \quad (3-5)$$

Due to inhomogeneities such as small rocks, sand and soil present within the woodchip feedstock, skeletal density results were not accurate or reproducible. At the 1 g sampling level, the effects of these inhomogeneities greatly affect the measurements, as rock and soil are relatively non-porous materials, leading to inaccurate measurements. The skeletal measurements were omitted from the results and discussion section of this chapter and can be found in Appendix C.

Where the density of water (ρ_{water}) at 25 °C is taken as 0.997 g/cm³.

3.3.1.5 Electrical Conductivity

Leaching of heavy metals and nutrients was studied using two different extraction procedures. The first extraction method was conducted using a Soxhlet extractor, which continuously washes a sample with fresh recycled solvent, water in this case, over a period of 16 hours. A new extraction method referred to as “Nespresso Extraction” was devised to extract heavy metals and nutrients within a much shorter time (30 s). The extraction system uses an espresso coffee machine, where a set volume of very hot, pressurized water (95 °C and 19 bars) is passed through a packed bed of finely ground biochar.

Electrical conductivity was measured for both extraction methods using a High Range Hanna Instruments Combo pH/Conductivity/TDS tester. Electrical conductivity measured in mS/cm were corrected based on biochar sample weight and volume of the extraction liquid as follows:

$$\text{Corrected EC} = \frac{EC}{\left(\frac{BC}{V_{\text{extract}}} \right)} \quad (3-6)$$

Where EC is the measured electrical conductivity in mS/cm; BC is the weight of biochar sample in g; and V_{extract} is the volume of the Soxhlet extraction liquid in cm³.

The electrical conductivity of the resulting extraction liquids from both extraction methods was measured and a correlation was determined. The procedure for both extraction methods is described in further detail below.

3.3.1.5.1 Soxhlet Extraction

Figure 3-4 shows a diagram of a Soxhlet extractor, which can be separated into three sections: a boiling flask, extraction chamber and condenser. The boiling flask is placed in an oil bath of 140 °C and heated to boil the solvent, ensuring only pure solvent evaporates. The vaporized solvent bypasses the extraction chamber and enters the condenser. Cooling water flowing through the condenser then condenses the solvent into the extraction chamber. The extraction chamber houses a cellulose thimble filled with biochar sample that is continuously washed with fresh condensed solvent. This solvent collects in the extraction chamber until a volume of 75 mL is reached, then siphoned through a tube back into the boiling flask to be recycled.

The leaching experiment described above has been adapted from EPA Method 3540C and Chegini (2017) used to extract heavy metals and nutrients from solids such as soils, sludges and wastes using a Soxhlet extractor. Deionized water was used to simulate real world conditions of rainfall on agricultural soils.

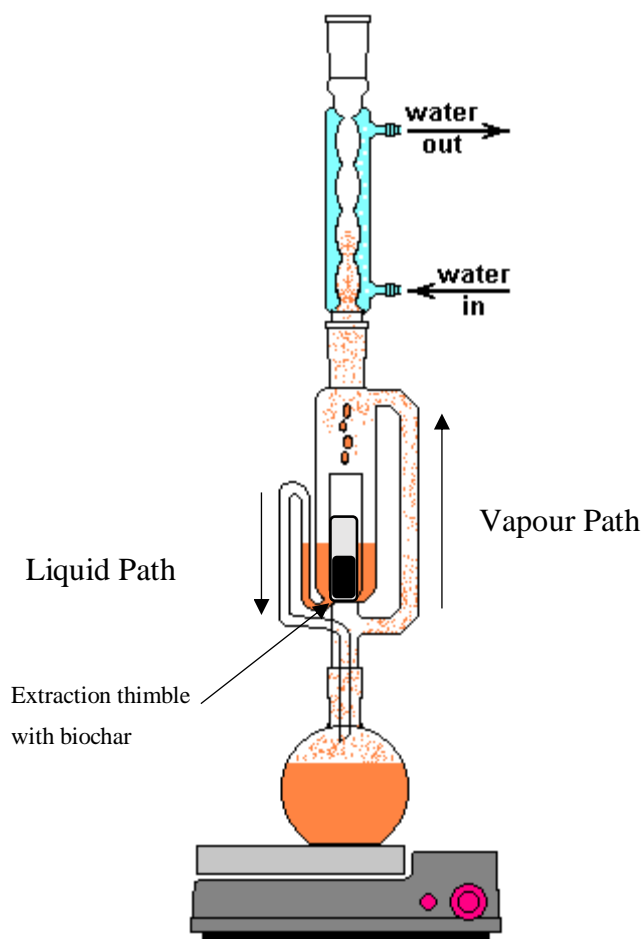


Figure 3-4: Soxhlet extractor (Adapted from Dolinowski(16))

3.3.1.5.2 Nespresso™ Extraction

A new method of extracting heavy metals and nutrients was developed utilizing a Nespresso coffee maker. In this system, 95 °C deionized water is passed through a stainless-steel capsule packed with biochar sample. The capsule contains small pores to allow water to pass through the packed bed with minimal biochar loss. As the deionized water passes through the sample, water-soluble nutrients and heavy metals are removed, and the liquid extract is collected. Preliminary testing showed that there is a strong correlation between Soxhlet and Nespresso extract electrical conductivity (Figure 3-5). The Nespresso extraction method has the potential to provide a very quick tool to

determine biochar extract electrical conductivity, as the extraction time is reduced from 16 hrs via Soxhlet down to 30 s. However, one of the trade offs is that the Nespresso extract electrical conductivity is more sensitive to changes in particulate size than Soxhlet extraction. Because Soxhlet extraction has a long water-biochar contact time, water has more time to penetrate the internal pores of larger particulates allowing for better extraction. Therefore, only Soxhlet extracted electrical conductivities are referred to throughout the remainder of the thesis. Further details on this extraction method can be found in Appendix D.

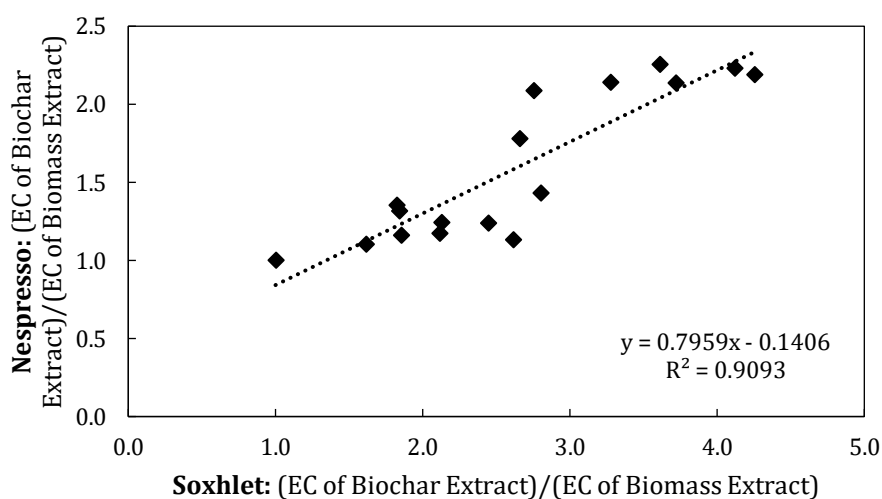


Figure 3-5: Correlation between electrical conductivity (EC) of Soxhlet extracted and Nespresso extracted liquids. BC: Biochar, BM: Biomass.

3.3.1.6 Methylene Blue Adsorption

Methylene blue adsorption capacity was used to measure the porosity of biochar. Methylene blue adsorption was chosen over Brunauer–Emmett–Teller (BET) adsorption to characterize porosity because liquid adsorption is more relatable over gas adsorption as biochar interaction with water is more of a concern. The method described was adapted from Raposo et al. (17). All biochars were washed with 95°C deionized water and dried

overnight at 105°C to remove impurities and clear pore structures prior to measurements. Based on preliminary studies conducted with activated carbon, an initial methylene blue and deionized water solution of 800 ppm and biochar to methylene blue solution ratio of 1:75 was used for all adsorption experiments. 0.2 g of biochar was combined with 15 mL of methylene blue solution and agitated in a shaker for 48 hrs. Once this stage was complete, 3 mL of the resulting solution was centrifuged at 5000 rpm for 10 min to separate the biochar from the used methylene solution. The spent methylene blue solution was then diluted with deionized water ratio of 1:7.5 into a cuvette and analyzed using a spectrophotometer. The spectrophotometer analyzed the solution at 664 nm, and a calibration curve was used to determine the diluted solutions methylene blue concentration (Equation 3-7).

$$\text{Calibration Curve Concentration} = 4.6724(\text{Abs}) - 0.1465 \quad (3-7)$$

where Abs is the absorbance reading from the spectrophotometer in nm.

3.4 Results and Discussion

Figure 3-6 illustrates the effect of RHP process time on biochar yield. Processing times between 2 to 3 hrs produced comparable yields of 43.8% and 44.2%, respectively. The comparable yields imply that the chars are produced at very similar temperatures regardless of the process time between 2 to 3 hours. Therefore, when comparing the rest of the RHP biochar properties to PSR biochar, the average property measurement between chars produced for 2 and for 3 hrs is used throughout the remainder of this chapter.

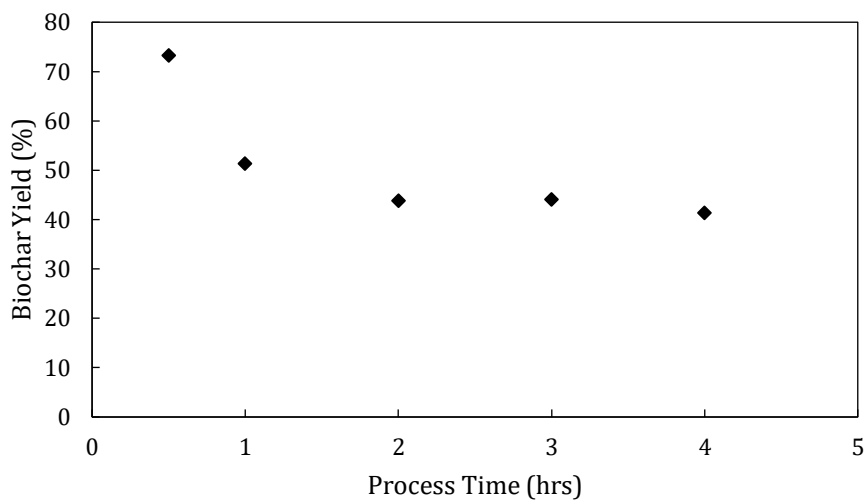


Figure 3-6: Effect of RHP process times on biochar yield.

As shown in Figure 3-7, biochar yields in the PSR decrease from 94.2% to 34.7% with an increase in pyrolysis temperature between 250 °C to 525 °C. The decrease in biochar yield is expected due to the significant mass loss caused by volatilization. Comparing PSR to RHP yields, RHP derived char corresponds to a process temperature of 400 °C (Figure 3-7).

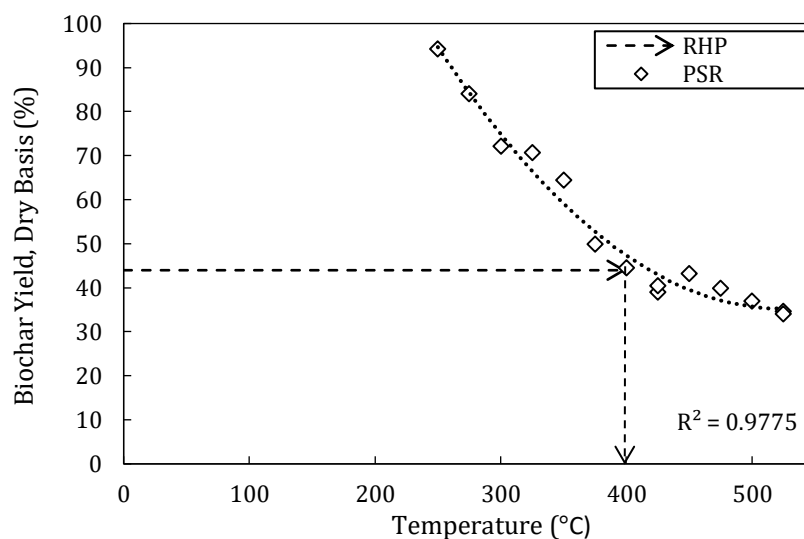


Figure 3-7: Effect of temperature on PSR biochar yield. Dotted line represents an empirical curve fit. Dashed line represents the corresponding PSR pyrolysis temperature of the average RHP char yield between 2 to 3 hrs. Duplicate runs are plotted.

Mode red intensity is used as an indication of the biomass to biochar change in colour with respect to temperature. Figure 3-8 Figure 3-8: Effect of pyrolysis temperature on the mode red intensity of PSR woodchip derived biochars. Arrow provides a possible range of pyrolysis temperatures corresponding of the RHP derived chars. illustrates that with increasing pyrolysis temperature, PSR derived biochars red mode intensity decreased from 183.0 to 37.0. This is because as biochar is formed at higher temperatures, it becomes darker in colour. The red intensity plateaus between 375 °C to 525 °C, indicating that after pyrolysis at 375 °C, biochar colour does not significantly vary. The red intensity of RHP derived biochar is compared to the colour change scale determined for PSR derived chars to provide a temperature range of RHP pyrolysis temperature corresponding to a 2-3 hrs processing time. Figure 3-8 shows that RHP derived biochar are comparable to PSR chars produced at 375 °C or greater.

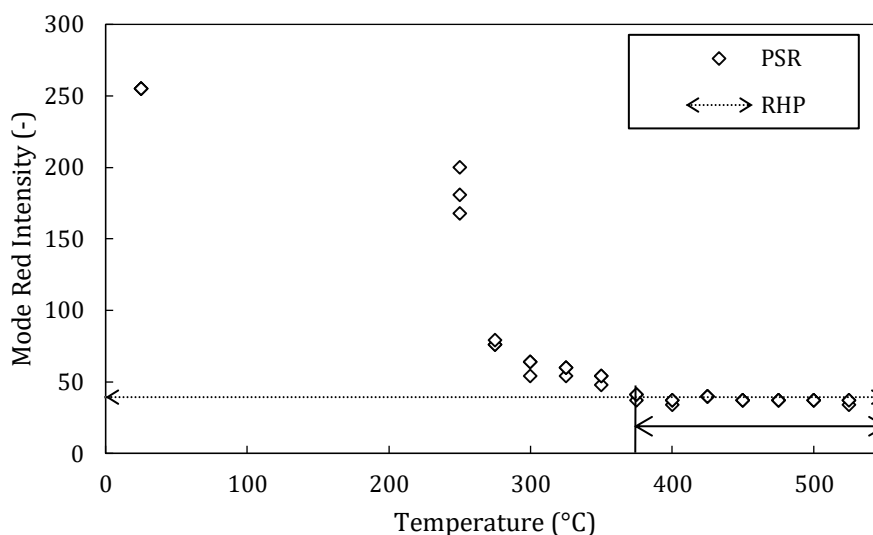


Figure 3-8: Effect of pyrolysis temperature on the mode red intensity of PSR woodchip derived biochars. Arrow provides a possible range of pyrolysis temperatures corresponding of the RHP derived chars.

The variance of the mode red intensity was also analyzed to determine the uniformity of the biochar products. Figure 3-9 depicts the variance of PSR derived chars as a function of pyrolysis temperature. The variance of RHP char produced lies within the range of PSR derived chars, indicating that the RHP produced a product with equivalent homogeneity to the PSR. In addition, by comparison the RHP derived char corresponds to a production temperature of 400 °C.

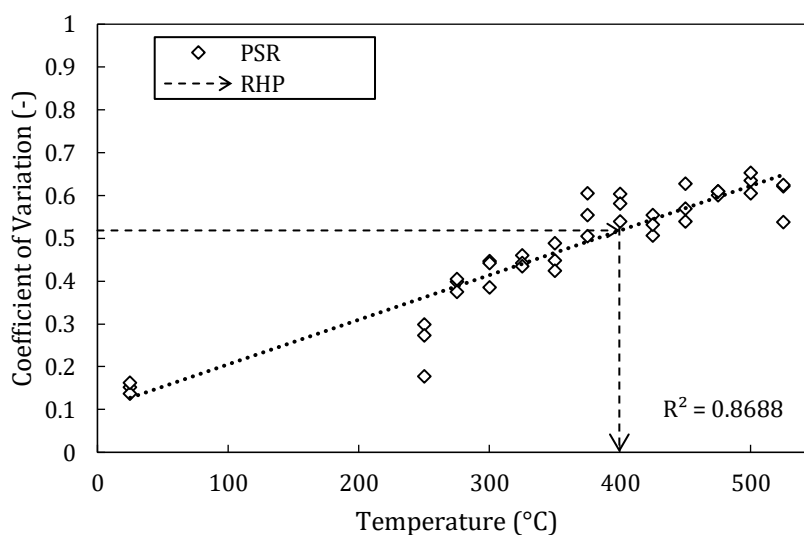


Figure 3-9: Effect of temperature on the red intensity coefficient of variance. Dotted line represents an empirical curve fit. Dashed line represents the corresponding PSR pyrolysis temperature of the average RHP char red intensity coefficient of variation between 2 to 3 hrs. Triplicate measurements are plotted.

The effect of pyrolysis temperature for PSR derived chars and process time for RHP chars on electrical conductivity relative to raw woodchip biomass electrical conductivity was investigated. In Figure 3-10, the electrical conductivity of Soxhlet extracted liquids was observed to increase linearly with pyrolysis temperature. These findings agree with the trends observed by Singh et al. (2010) (4) and Kloss et al. (2012) (11). RHP derived char electrical conductivity lies within the range of PSR derived chars, and has an electrical conductivity equivalent to a PSR derived char produced at 375 °C. These results correspond with the pyrolysis temperature range determined through red colour intensity image analysis in Figure 3-8. Figure 3-8: Effect of pyrolysis temperature on the mode red intensity of PSR woodchip derived biochars. Arrow provides a possible range of pyrolysis temperatures corresponding of the RHP derived chars..

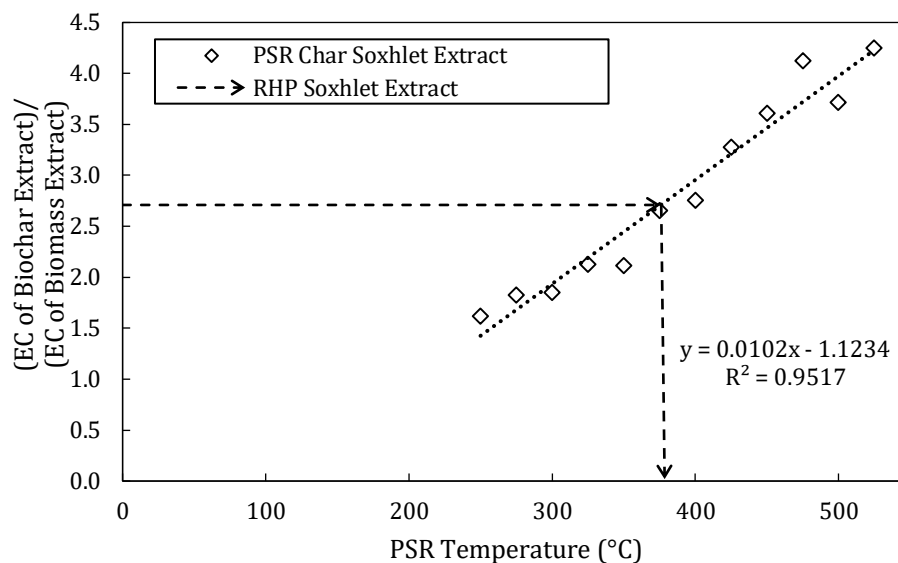


Figure 3-10: Effect of temperature on electrical conductivity (EC) of Soxhlet extracted liquids with reference to raw woodchip feedstock EC. Dotted line represents an empirical curve fit. Dashed line represents the corresponding PSR pyrolysis temperature of the average EC of RHP char Soxhlet extracted liquids between 2 to 3 hrs. Average of duplicate measurements are plotted.

Methylene blue adsorption has been used to approximate the distribution of pores for activated carbons and is related to macropore and mesopore capacity (17). Figure 3-11 shows that methylene blue absorption decreases with increasing pyrolysis temperature. The methylene blue adsorption of the RHP derived char was measured at 14.5 mgMB/gBiochar, and matches a PSR char produced at 365 °C.

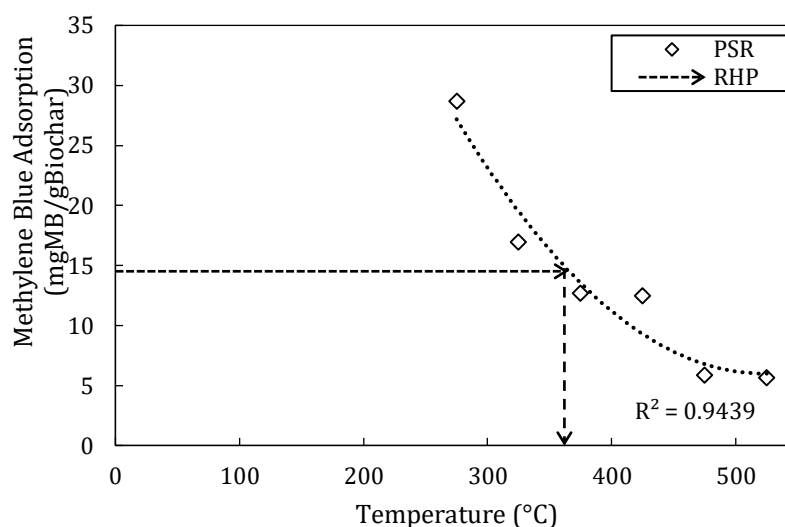


Figure 3-11: Effect of pyrolysis temperature on methylene blue adsorption. Dotted line represents an empirical curve fit. Dashed line represents the corresponding PSR pyrolysis temperature of the average RHP biochar methylene blue adsorption capacity produced between 2-3 hours.

The properties of RHP and PSR derived chars produced under varying pyrolysis temperature and processing time were compared to determine the corresponding RHP temperatures. A dimensionless property comparison parameter was used to allow for the comparison of all the biochar properties tested at once. The parameter is defined as follows:

$$\text{Property Comparison Parameter} = \frac{[R_{\text{avg}} - P_i]}{P_{\text{Max}} - P_{\text{Min}}} \quad (3-8)$$

where R_{avg} is the property measurement average between RHP chars produced at 2 and 3 hrs, P_i is the measured property of PSR derived char at temperature i , P_{Max} and P_{Min} are the range of the measured property of PSR chars produced at 550 and 250 °C, respectively.

Based on Figure 3-12 the RHP chars produced at a processing time of 2 and 3 hrs were equivalent to chars produced with the PSR at 400 °C. The property comparison parameter for most characterization methods (except for methylene blue adsorption and red mode intensity variance) intersect the x-axis at 400 °C, indicating that the characterization measurements were the same. Methylene blue adsorption does not intersect the x-axis of the graph at 400 °C, which is also observed in Figure 3-11 and indicates an equivalent PSR temperature of approximately 375 °C. Contrary to the results determined in Figure 3-12, the red mode intensity variance does correspond to a production temperature of 400 °C in Figure 3-9. The discrepancy between these results occurred because the raw data is used to calculate the property comparison parameter, whereas the results in Figure 3-9 are based on the trendline determined.

The same analysis used to determine the equivalent PSR temperature of RHP derived chars was performed on chars derived from Storm Fisher digestate and Bayview Flower digestate feedstocks (Appendix E). Table 3-1 reports the equivalent PSR temperatures of RHP derived chars for the individual characterizations. The coefficient of variation was not able to provide an equivalent PSR temperature for SFD and BFD feedstocks because the effects of temperature on the coefficient of variance were minimal. For both digestate feedstocks, the properties of RHP char processed for 4 hrs was compared to the range of PSR derived chars. It was determined that RHP chars have an equivalent PSR temperature range between 420 to 450 °C for SFD derived chars, and 400 – 420 °C for BFD derived chars.

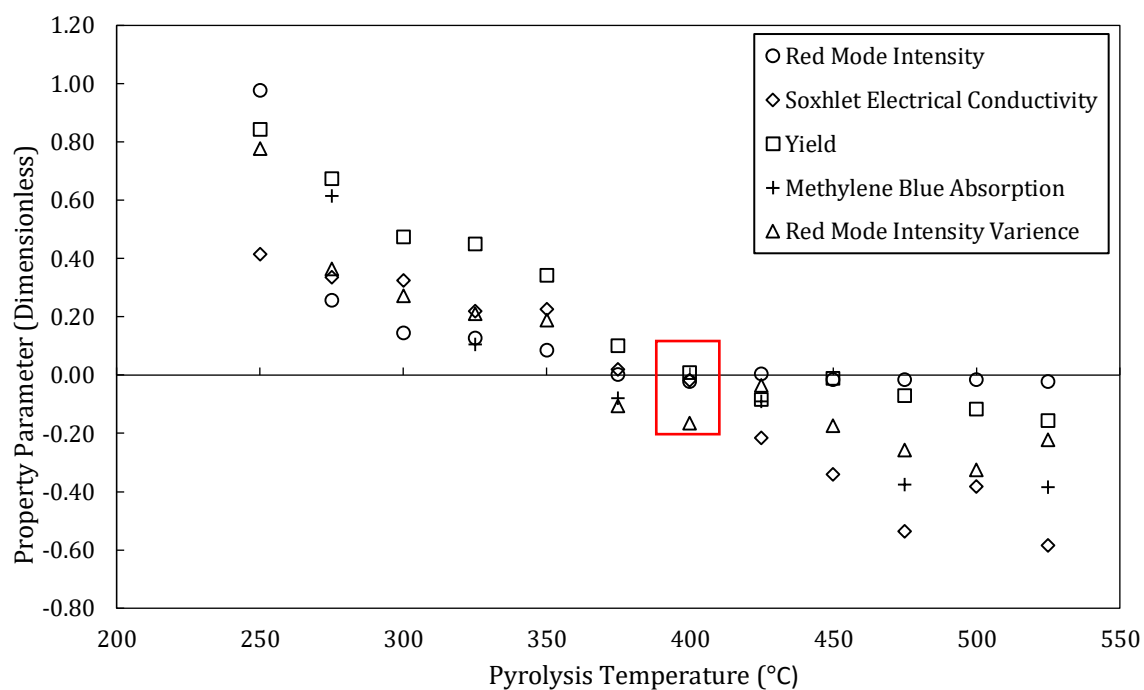


Figure 3-12: Comparison between all the properties characterized for RHP char processed for the average between 2 to 3 hrs processing time.

Table 3-1: Equivalent PSR temperatures of RHP derived chars based on individual biochar characterization for all feedstocks.

Feedstock	WCP	SFD	BFD
Process Conditions (hrs)	Average 2 – 3	4	4
Characterization Method	Equivalent PSR Temperature (°C)		
Yield	400	380	420
Red Mode Intensity	>375	>270	>270
Coefficient of Variance	400	-	-
Ash Content	-	420	>400
Skeletal Density	-	450	400
Soxhlet Electrical Conductivity	375	-	340
Methylene Blue Adsorption	375	450	410

3.5 Conclusions

In this study, physical and chemical properties of woodchip derived biochars produced with a new pyrolysis technology referred to as the Rotating Heater Pyrolyzer (RHP) were compared to chars produced using a standard batch reactor (PSR) to determine if the RHP can produce a char with similar properties to one produced with the PSR at a specific temperature profile. RHP chars processed between 2-3 hrs were compared to PSR chars produced between 250 to 525 °C, and it was determined that the RHP char is equivalent to PSR char produced between 375 - 400 °C.

The equivalent PSR temperature of two digestate feedstocks produced in the RHP at a processing time of 4 hrs was also determined using the analysis method presented for the woodchip feedstock. RHP chars derived from SFD feedstock was found to have an equivalent PSR temperature range between 420 to 450 °C while RHP chars produced from BFD feedstock ranged from 420 to 450 °C.

A new extraction method referred as the Nespresso extraction was developed for this research, to provide a quick and efficient means of determining biochar nutrient and metals leaching based on the extracted liquid electrical conductivity. The Nespresso extraction method can reduce the time required to process samples from 16 hours to 30 s, making it suitable for the monitoring of industrial biochar units.

3.6 References

1. Lempp P. Biomass Co-Firing in Coal Power Plants [Internet]. 2013 [cited 2019 Jun 8]. Available from: www.irena.org
2. Suman S, Gautam S. Pyrolysis of coconut husk biomass: Analysis of its biochar properties. *Energy Sources, Part A Recover Util Environ Eff* [Internet]. 2017 Apr 18 [cited 2019 Jun 9];39(8):761–7. Available from: <https://www.tandfonline.com/doi/full/10.1080/15567036.2016.1263252>
3. Gheorghe C, Marculescu C, Badea A, Dinca C, Apostol T. Effect of Pyrolysis Conditions on Bio-Char Production from Biomass Effect of Pyrolysis Conditions on Bio-Char Production from Biomass. *Renew Energy Sources*. 2015;(January 2015):239–42.
4. Singh B, Singh BP, Cowie AL. Characterisation and evaluation of biochars for their application as a soil amendment. *Soil Res* [Internet]. 2010 Oct 19 [cited 2019 Jun 9];48(7):516. Available from: <http://www.publish.csiro.au/?paper=SR10058>
5. Giorcelli M, Khan A, Pugno NM, Rosso C, Tagliaferro A. Biochar as a cheap and environmental friendly filler able to improve polymer mechanical properties. *Biomass and Bioenergy* [Internet]. 2019 Jan [cited 2019 May 30];120:219–23. Available from: <https://linkinghub.elsevier.com/retrieve/pii/S0961953418303325>
6. Peterson SC, Chandrasekaran SR, Sharma BK. Birchwood biochar as partial carbon black replacement in styrene-butadiene rubber composites. [cited 2019 May 30]; Available from: <https://journals.sagepub.com/doi/pdf/10.1177/0095244315576241>
7. Qian K, Kumar A, Zhang H, Bellmer D, Huhnke R. Recent advances in utilization of biochar. *Renew Sustain Energy Rev* [Internet]. 2014 [cited 2019 Jun 9];42:1055–64. Available from: <http://dx.doi.org/10.1016/j.rser.2014.10.074>
8. Fiore S, Berruti F, Briens C. Investigation of innovative and conventional pyrolysis of ligneous and herbaceous biomasses for biochar production. *Biomass*

and Bioenergy [Internet]. 2018 Dec 1 [cited 2019 May 28];119:381–91. Available from:

<https://www.sciencedirect.com/science/article/pii/S0961953418302769?via%3Dihub>

9. Adrados A, De Marco I, López-Urionabarrenechea A, Solar J, Caballero BM, Gastelu N. Biomass Pyrolysis Solids as Reducing Agents: Comparison with Commercial Reducing Agents. *Mater* (Basel, Switzerland) [Internet]. 2015 Dec 23 [cited 2019 Jun 9];9(1). Available from: <http://www.ncbi.nlm.nih.gov/pubmed/28787805>
10. Li X, Lei B, Lin Z, Huang L, Tan S, Cai X. The utilization of bamboo charcoal enhances wood plastic composites with excellent mechanical and thermal properties. *Mater Des* [Internet]. 2014 [cited 2019 Jun 16];53:419–24. Available from: <http://dx.doi.org/10.1016/j.matdes.2013.07.028>
11. Kloss S, Zehetner F, Dellantonio A, Hamid R, Ottner F, Liedtke V, et al. Characterization of Slow Pyrolysis Biochars: Effects of Feedstocks and Pyrolysis Temperature on Biochar Properties. *J Environ Qual*. 2012;41(4):990.
12. Keiluweit M, Nico PS, Johnson MG, Kleber M. Dynamic Molecular Structure of Plant Biomass-Derived Black Carbon (Biochar). *Environ Sci Technol* [Internet]. 2010 [cited 2019 Jun 4];44:1247–53. Available from: <https://pubs.acs.org/doi/10.1021/es9031419>.
13. Mukome FND, Zhang X, Silva LCR, Six J, Parikh SJ. Use of Chemical and Physical Characteristics To Investigate Trends in Biochar Feedstocks. 2013 [cited 2019 Jun 4]; Available from: <https://pubs.acs.org/doi/10.1021/jf3049142>.
14. Yargicoglu EN, Sadasivam BY, Reddy KR, Spokas K. Physical and chemical characterization of waste wood derived biochars. *Waste Manag* [Internet]. 2015 Feb [cited 2019 Jun 4];36:256–68. Available from: <https://linkinghub.elsevier.com/retrieve/pii/S0956053X14005133>

15. Jindo K, Mizumoto H, Sawada Y, Sanchez-Monedero MA, Sonoki T. Physical and chemical characterization of biochars derived from different agricultural residues. *Biogeosciences* [Internet]. 2014 [cited 2019 Jun 4];11:6613–21. Available from: www.biogeosciences.net/11/6613/2014/
16. Dolinowski T. Soxhlet Extractor. 2011;
17. Raposo F, De La Rubia MA, Borja R. Methylene blue number as useful indicator to evaluate the adsorptive capacity of granular activated carbon in batch mode: Influence of adsorbate/adsorbent mass ratio and particle size. *J Hazard Mater* [Internet]. 2009 Jun 15 [cited 2019 Aug 23];165(1–3):291–9. Available from: <https://linkinghub.elsevier.com/retrieve/pii/S0304389408014702>

Chapter 4

4 A Comparison Between Two Anaerobic Digestate Derived Biochars for Soil Amendment Applications

4.1 Introduction

Biochar is a carbon rich powder produced during a process known as pyrolysis, where organic material is thermally degraded under oxygen limited conditions. In the past, bio-oil was the main pyrolysis product of interest, however the interest has shifted to the industrial and environmental applications of biochar. Some areas of research interest include the application of biochar for carbon sequestration; soil amendment; precursor material for activated carbon used for wastewater and air purification; bio-coke fuel source for metallurgical applications; and as a filler for composite/polymer materials (1–6). Numerous studies have investigated the beneficial effects of biochar as a soil amendment, and shown that biochar amendment can improve plant available nutrients, soil cation exchange capacity and soil water holding capacity (7–11).

There is a growing interest in using biochar as a form of agricultural and animal waste management (12). In Canada alone, approximately 6 million tons of food waste are discarded of each year, representing a significant resource for renewable energy processes such as anaerobic digestate (13). The solid product of anaerobic digestion is referred to as digestate and is the solid concentration of nutrients and organic matter present in the original waste material. Digestate is often sold as an inexpensive fertilizer, however nutrient leaching leading to the pollution of surface and ground water pose serious environmental issues (12,14). The pyrolysis of digestates can minimize the environmental impacts that amending soil with raw digestates pose while continuing to improve soil fertility. In addition, the production of biochar helps mitigate the effects of climate change by sequestering carbon and creating a carbon sink when incorporated into soils. Biochars have a high carbon stability, making them highly resistant to microbial degradation (15–17).

The Rotating HeaterP (RHP) is a lab scale reactor designed to produce several kg of biochar per batch. Unlike most lab scale pyrolysis reactors, the heating source is placed within the reactor and rotated to distribute heat to the solid biomass particles (Chapter 2). Biochar physical and chemical properties are highly dependent on the nature of the feedstock and pyrolysis conditions including temperature, heating rate and exposure time (18–20). Therefore, the objective for this study was to investigate the effects of process conditions on the char properties related to soil amendment on two different anaerobic digestate feedstocks.

It is noted that for Sections 4.2.2 through 4.3.1.6 the pyrolysis methods and biochar characterization methods are the same as those outlined in Chapter 2.

4.2 Materials and Pyrolysis Methods

4.2.1 Feedstock

Two different anaerobic digestates were used to make the biochars studied. The first digestate was procured from Bayview Flowers greenhouse (BFD) located in St. Catharines, ON, and the second from Storm Fisher (SFD), a food waste anaerobic digestion facility located in London, ON. The moisture contents of each feedstock are listed in Table 4-1, and measured in triplicate with a Mettler Toledo Moisture Analyzer.

Table 4-1: Average moisture content of SFD and BFD feedstocks.

Feedstock	Moisture Content (wt %)
SFD	9
BFD	3

4.2.2 Standard batch pyrolysis reactor: Pyrolytic Shaker Reactor (PSR)

The Pyrolytic Shaker Reactor (PSR) is comprised of three sections: the reactor vessel, induction heating system and the mechanical agitation system. Figure 4-1 shows the schematic structure of the PSR.

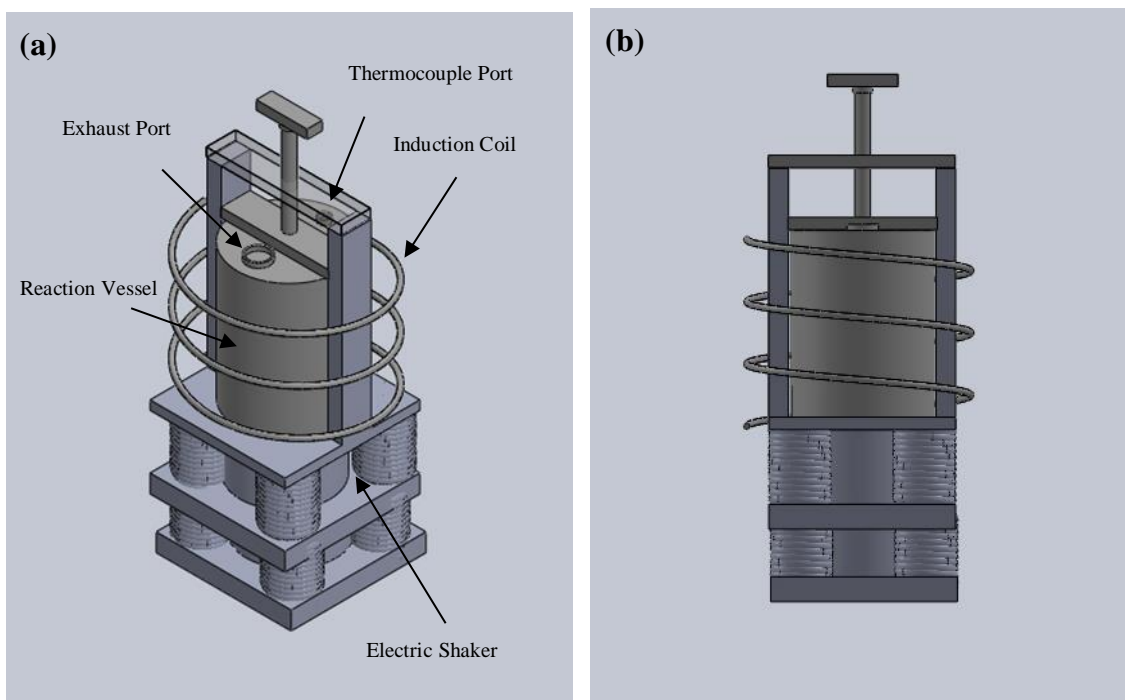


Figure 4-1: Schematic drawing of Pyrolytic Shaker Reactor (PSR). (a) Trimetric view (b) Front view

Mechanical agitation is provided by a dedicated electric shaker. The shaker measures 29 cm length x 66 cm height x 39 cm wide. The shaker provides both axial and radial mixing of the solid particles (Appendix B). Due to rapid heating of the solid bed, additional mixing is assisted by the evolution of gaseous pyrolysis products, which aerate the bed.

4.2.3 Rotating Heater Pyrolyzer (RHP)

The RHP is comprised of four sections: the reactor vessel, the induction heating system, the rotating heater and the air motor. Figure 4-2 shows the schematic structure of the RHP. Refer to Chapter 2 for a more detailed description and characterization of the RHP.

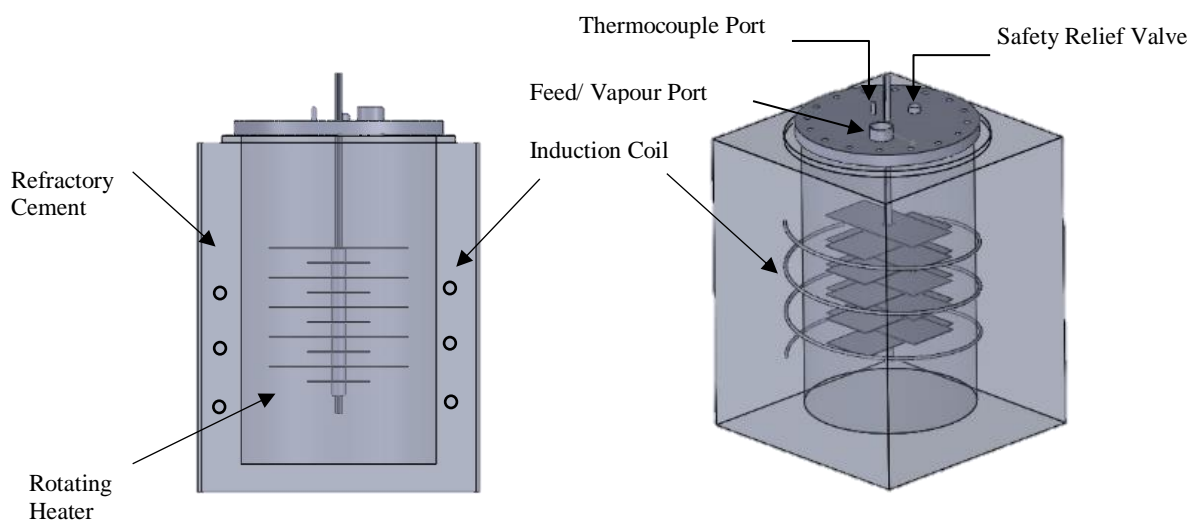


Figure 4-2: RHP Schematic.

4.2.4 PSR Procedure

Prior to pyrolysis, $2/3$ the volume of the reaction vessel is filled with biomass feedstock, with the weight of biomass sample recorded. Biomass batches fed to the reactor do not undergo any pre-treatment (for example; sieving or grinding to a specific size distribution) other than air drying over 48 hrs. The vessel is then sealed and secured into the shaking device. PSR agitation is started and maintained throughout the duration of the experiment to ensure proper mixing and heat transfer to create a uniform sample bed temperature. The induction heating system is turned on and set to the maximum frequency and maintained at an input power of 8 kW. Samples are then heated to a set

bed temperature (between 250 °C and 600 °C). Once the desired temperature is reached, both shaking, and induction heating are turned off and allowed to cool to room temperature.

4.2.5 RHP Procedure

In contrast to the PSR, the RHP pyrolysis experiments are based on process time rather than bed temperature. This is due to the nature of the rotating heater, in which there is no uniform bed temperature. Prior to pyrolysis, all components of the RHP are assembled and the reactor lid is sealed. Compressed air is used to turn on the air motor, which rotates the shaft attached to the rotating heater. The compressed air is controlled by an Arduino system programmed to rotate the shaft similar to a washing machine motion; 3s clockwise, 3s counter-clockwise with a specified stationary period (30 s or 60 s) between each rotation motion.

The biomass sample is fed into the reactor through a feeding port located on the lid until 2/3 of the reactor volume is filled (approximately 25 L). The induction heating system is then turned on, set to the maximum frequency and maintained at an input power of 7.5 kW. The vapour temperature is monitored and recorded throughout the duration of the procedure. The biomass is heated until the vapour temperature reaches 120 °C to ensure that all moisture in the biomass sample has been removed. Once the vapour temperature has reached 120 °C, the RHP heater remains on for the desired processing time varying between 1 to 4 hours. The gaseous product is continually passed through a condenser that is cooled with water throughout the entire procedure.

Once the desired process time is reached, the induction heating and the compressed air to the rotating heater are turned off, and the entire reactor is left to cool to room temperature over 15 hours (typically overnight).

4.2.6 Biochar Production Conditions

For each feedstock, eleven different biochars were produced for detailed characterization using the PSR, gradually increasing in pyrolysis temperature from 250 to 500 °C, by increments of 25 °C. An additional four chars were produced in the RHP, with varying process times of 1, 2, 3, and 4 hours for the same detailed characterization.

4.3 Feedstock and Biochar Characterization Methods

The following methods were chosen to characterize biochar properties because they are sensitive to pyrolysis temperature and heating rate.

4.3.1.1 Reactor Yield

Char yield was determined by comparing the biomass batch weight fed to the reactor with the weight of the char bed at the end of each run.

$$\text{BC yield (\%)} = \frac{\text{Weight of Collected Biochar (g)}}{\text{Weight of Biomass (g)}} \times 100 \quad (4-1)$$

4.3.1.2 Red, Green & Blue (RGB) Imaging

4.3.1.2.1 Red Green Blue (RGB) Intensity

The RGB intensity of biochar samples was used as a tool to compare RHP and PSR biochars based on colour. As biomass is pyrolyzed into biochar, the colour of biochar gradually becomes darker. The RGB intensity was determined using ZEISS Axiocam 105 colour microscope and software. The Axiocam 105 colour software analyzes each individual pixel from the image taken by the microscope and assigns an RGB intensity between 0 to 255, with zero assigned as pure black and 255 assigned as pure white. The frequency of all the pixels were plotted, with the mean RGB intensity displayed as the peak of the curve as shown in the example of Figure 4-3.

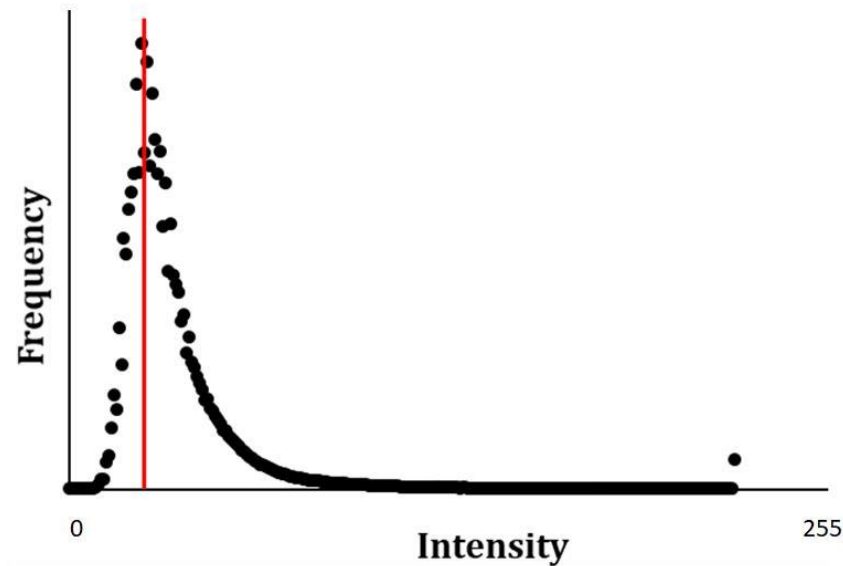


Figure 4-3: RGB peak intensity.

4.3.1.2.2 RGB Intensity Variance

The red intensity was used to determine biochar sample uniformity as preliminary results showed that it provided the greatest difference in mode intensity between biochar samples. The more uniform in colour a sample product is, the narrower the distribution spread of the RGB intensity curve. The RGB intensity was determined using ZEISS Axiocam 105 colour microscope and software. The Axiocam 105 colour software analyzes each individual pixel from the image taken by the microscope and assigns an RGB intensity between 0 to 255, with zero assigned as pure black and 255 assigned as pure white. The frequency of all the pixels were plotted, with the mode RGB intensity displayed as the peak of the curve.

The coefficient of variation is used to analyze the biochars and is defined as follows:

$$\text{Coefficient of Variation} = \frac{\sqrt{\text{Variance}}}{\text{Mean}} \quad (4-2)$$

4.3.1.3 Ash Content

The procedure to determine the ash content complies with ASTM D1762-84: samples of 1 g were placed in a crucible and dried in an oven at 105 °C for 2 hours, then placed in a muffle furnace 750 °C for 4 hours.

4.3.1.4 Skeletal Density

Sample density was measured by volume displacement. Prior to measurements, each volumetric flask was calibrated. Biochar samples were ground in a burr mill, then sieved to 500 µm. 1 g of the biochar powder is placed into a 120 ml volumetric flask along with 20 ml of dispersant (Finish Quantum dishwasher detergent). The flask was mixed until the biochar powder was immersed within the dispersant solution to form a slurry, then filled with de-ionized water to the 120 ml indicator line and weighed. Biochar volume can then be determined based on the volume of the solution displaced, allowing to calculate the density using the following equations:

$$\begin{aligned} \text{Liquid Solution in Volumetric Flask (g)} = \\ (\text{Volumetric flask with BC and liquid solution (g)}) - \text{BC (g)} - \\ \text{Dry volumetric flask (g)} \end{aligned} \quad (4-3)$$

$$\begin{aligned} \text{Biochar Volume} = \text{Volume Displaced (cm}^3\text{)} = \\ \frac{[\text{Calibrated liquid (g)} - \text{Liquid solution in volumetric flask (g)}]}{\rho_{\text{water}}} \end{aligned} \quad (4-4)$$

$$\text{Relative Density} \left(\frac{\text{g}}{\text{cm}^3} \right) = \frac{\text{BC (g)}}{\text{Biochar Volume (cm}^3\text{)}} \quad (4-5)$$

Where the density of water (ρ_{water}) at 25 °C is taken as 0.997 g/cm³.

4.3.1.5 Electrical Conductivity

Leaching of heavy metals and nutrients was studied using a Soxhlet extractor, which continuously washes a sample with fresh recycled solvent, water in this case, over a period of 16 hours. Electrical conductivity was measured using a High Range Hanna Instruments Combo pH/Conductivity/TDS tester. Electrical conductivity measured in mS/cm were corrected based on biochar sample weight and volume of the extraction liquid as follows:

$$\text{Corrected EC} = \frac{EC}{\left(\frac{BC}{V_{\text{extract}}}\right)} \quad (4-6)$$

Where EC is the measured electrical conductivity in mS/cm; BC is the weight of biochar sample in g; and V_{extract} is the volume of the Soxhlet extraction liquid in cm^3 .

Figure 4-4 shows a diagram of a Soxhlet extractor, which can be separated into three sections: a boiling flask, extraction chamber and condenser. The boiling flask is placed in an oil bath of 140 °C and heated to boil the solvent, ensuring only pure solvent evaporates. The vaporized solvent bypasses the extraction chamber and enters the condenser. Cooling water flowing through the condenser then condenses the solvent into the extraction chamber. The extraction chamber houses a cellulose thimble filled with biochar sample that is continuously washed with fresh condensed solvent. This solvent collects in the extraction chamber until a volume of 75 mL is reached, then siphoned through a tube back into the boiling flask to be recycled.

The leaching experiment described above has been adapted from EPA Method 3540C (21) and Chegini (22) used to extract heavy metals and nutrients from solids such as soils, sludges and wastes using a Soxhlet extractor. Deionized water was used to simulate real world conditions of rainfall on agricultural soils.

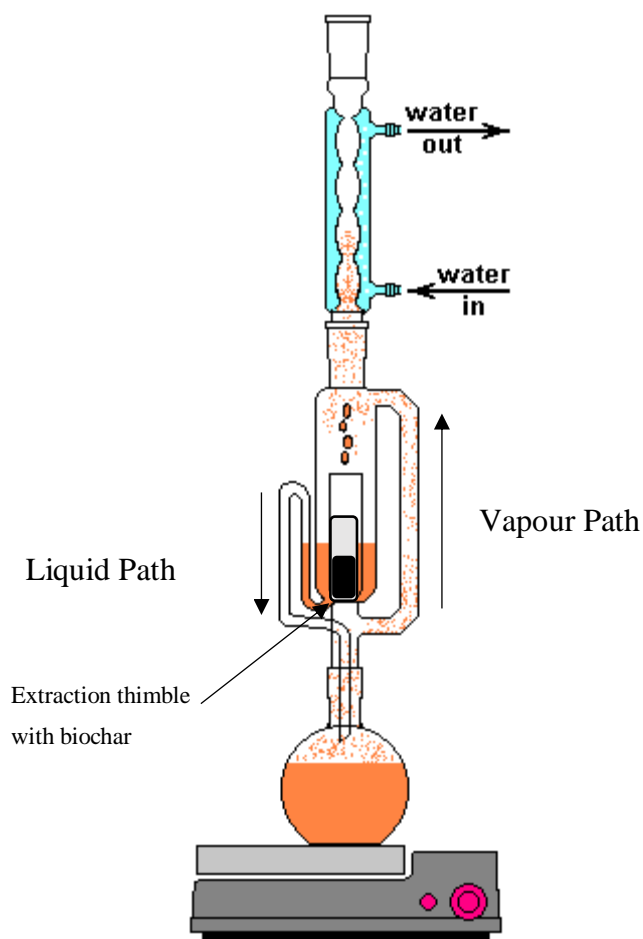


Figure 4-4: Soxhlet extractor (Adapted from Dolinowski(23))

4.3.1.6 Methylene Blue Adsorption

Methylene blue adsorption capacity was used to measure the porosity of biochar. Methylene blue adsorption was chosen over Brunauer-Emmett-Teller (BET) adsorption to characterize porosity because liquid adsorption is more reliable over gas adsorption as biochar interaction with water is more of a concern. The method described was adapted from Raposo et al. (24). All biochars were washed with 95°C deionized water and dried overnight at 105°C to remove impurities and clear pore structures prior to measurements. Based on preliminary studies conducted with activated carbon, an initial methylene blue and deionized water solution of 800 ppm and biochar to methylene blue solution ratio of

1:75 was used for all adsorption experiments. 0.2 g of biochar was combined with 15 mL of methylene blue solution and agitated in a shaker for 48 hrs. Once this stage was complete, 3 mL of the resulting solution was centrifuged at 5000 rpm for 10 min to separate the biochar from the used methylene solution. The spent methylene blue solution was then diluted with deionized water ratio of 1:7.5 into a cuvette and analyzed using a spectrophotometer. The spectrophotometer analyzed the solution at 664 nm, and a calibration curve was used to determine the diluted solutions methylene blue concentration (Equation 4-7).

$$\text{Calibration Curve Concentration} = 4.6724(\text{Abs}) - 0.1465 \quad (4-7)$$

Where Abs = absorbance reading from the spectrophotometer in nm.

4.4 Results and Discussion

Chapter 3 results have shown that the main variable affecting biochar properties are temperature and time for the PSR and RHP, respectively. Therefore, the impact of temperature on PSR char properties and process time on RHP char properties are reported.

Figure 4-5 depicts the biochar yield of both SFD and BFD feedstocks as a function of PSR temperature. As expected, the char yields decrease with increasing pyrolysis temperature and are within the expected yield. The yields (dry basis) for both feedstocks are very similar to one another, except for one of the BFD yields at 450 °C that was much higher than anticipated at 55%. The BFD feedstock was more heterogeneous than the SFD feedstock as, being produced from flower waste, contained soil, small rocks and sand.

In Figure 4-6, the RHP yields of both feedstocks are expressed with respect to processing time. Similar to the PSR (Figure 4-5), overall biochar yield decreases as a function of process time. For both feedstocks, a 2% increase in biochar yield is observed between

processing times of 2 to 3 hrs and is caused from tars condensing on the reactor lid back into the biochar bed.

In contrast to the results shown in Figure 4-5, RHP SFD yields are higher than RHP BFD yields, whereas PSR yields for both feedstocks are approximately the same. SFD yields with the RHP are higher than PSR yields for SFD because its pyrolysis generates large quantities of tar vapours within the PSR. The PSR has a smaller head space and high vapour flowrates which is entraining biochar material in the condensation pipes, leading to an underestimation for the SFD PSR yields. Entrainment of material is not an issue with the RHP as the biochar is not heated as rapidly so the vapour flowrates are lower.

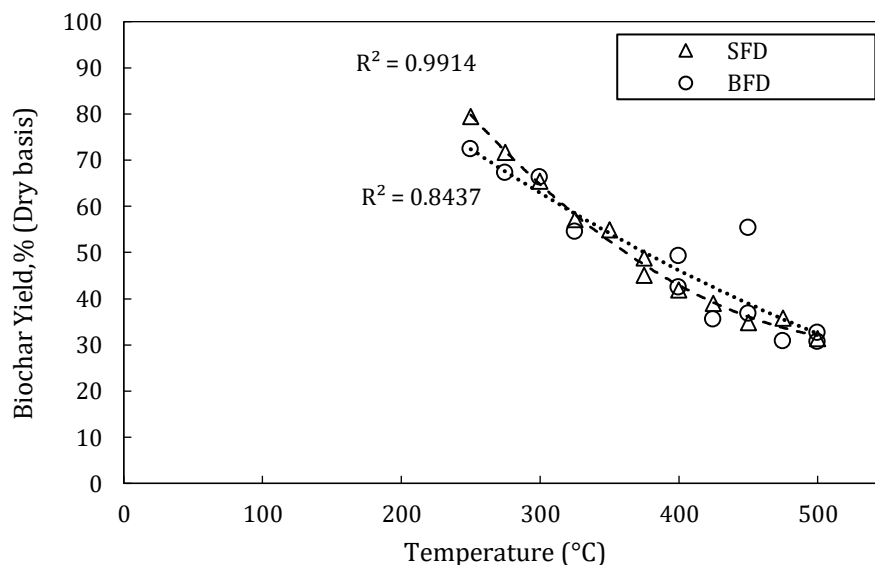


Figure 4-5: PSR biochar yields for SFD and BFD feedstock. Dotted lines represent an empirical curve fit.

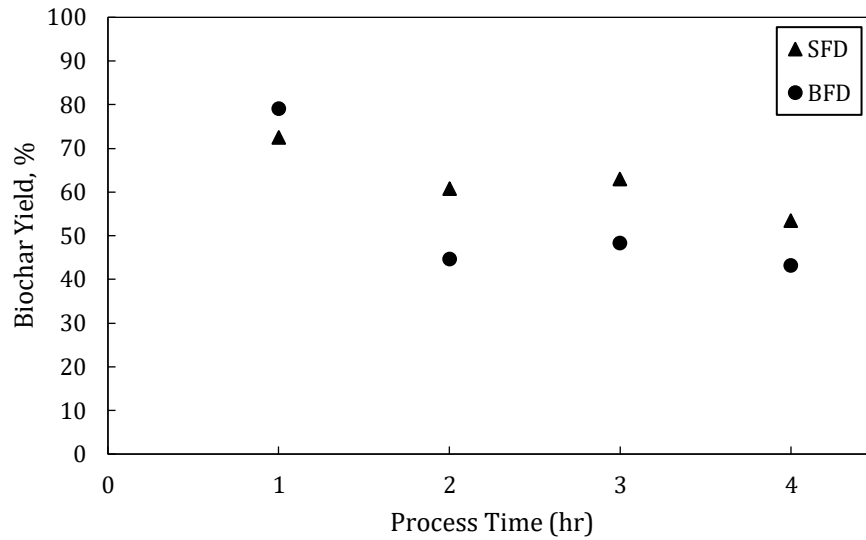


Figure 4-6: RHP biochar yields for SFD and BFD feedstock.

Red mode intensity is used as a tool to track changes in biochar colour with respect to changes in process parameters (temperature or processing time). Figure 4-7 shows the comparison between the red mode intensity of the SFD and BFD derived biochar produced with the PSR. The red mode intensity remains relatively constant for both types of biochar between production temperatures of 250 to 500 °C.

The initial feedstocks are both dark in colour, and therefore does not require high pyrolysis temperatures to become darker. Figure 4-8 depicts the coefficient of variation for the red mean intensity. Both the PSR and RHP derived biochars show a relatively high variability, indicating that there is variability within the feedstock. Figure 4-7

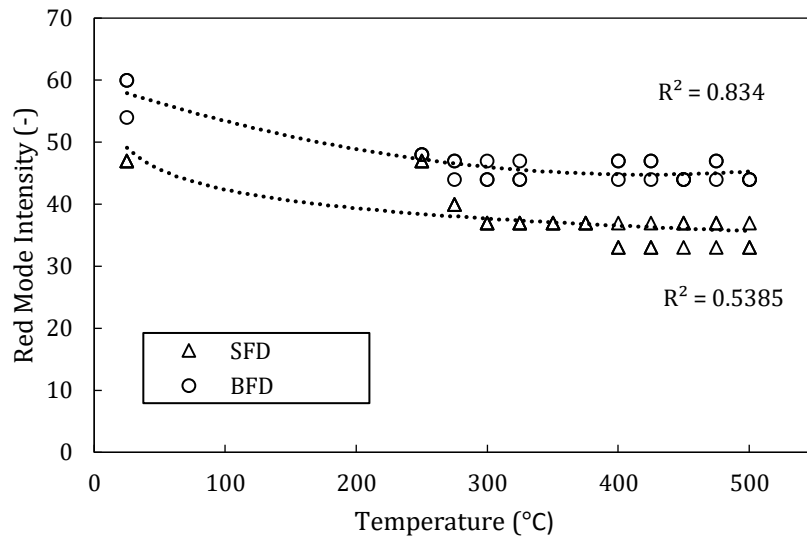


Figure 4-7: Red mode intensity of SFD and BFD derived biochars produced with the PSR between 250 °C to 500 °C. Dotted lines represent an empirical curve fit.

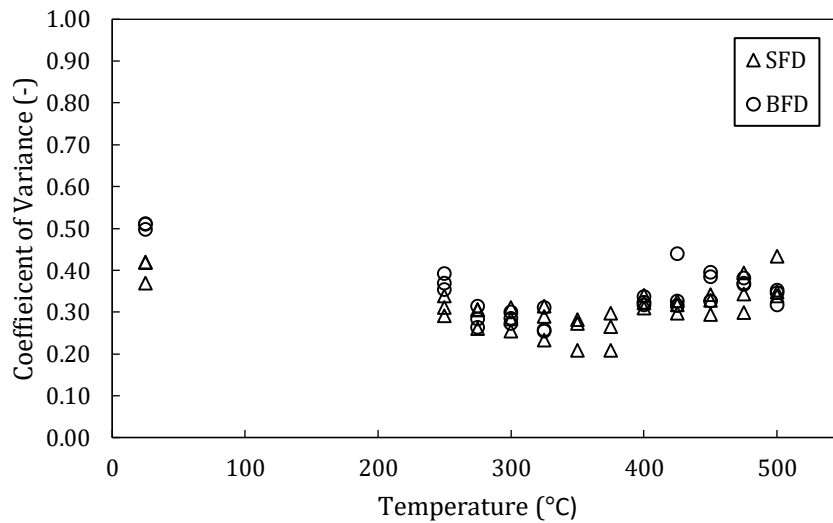


Figure 4-8: Red intensity coefficient of variation of SFD and BFD derived biochars produced with the PSR between 250-500°C.

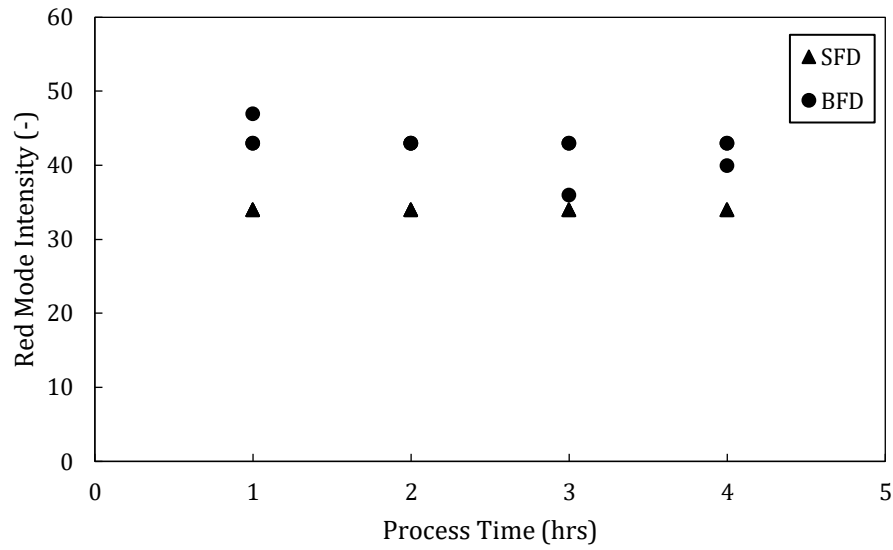


Figure 4-9: Red mode intensity of SFD and BFD derived biochars produced with the RHP between 1 to 4 hrs.

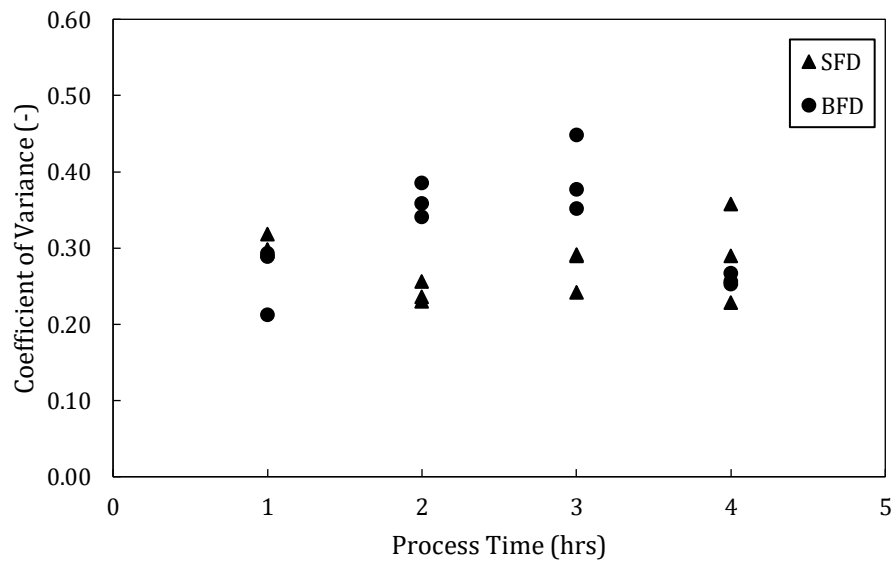


Figure 4-10: Red intensity coefficient of variation of SFD and BFD derived biochars produced with the RHP between 1 to 4 hrs.

Figure 4-11 shows that SFD derived biochars have a much higher ash content than BFD biochars. As SFD feedstock is comprised from food waste, waste materials high in minerals such as bone are likely to be contributing to the high ash content of the resultant biochars. The higher ash content of SFD biochars can be advantageous in terms of soil amendment, as the high mineral content of the feedstock has the potential to provide additional nutrients to soils. However, although SFD biochars may have a higher mineral content, it does not mean that its minerals are easily extracted from the biochar and transferred to soils. The extraction of water-soluble minerals from the biochars is investigated further in this section.

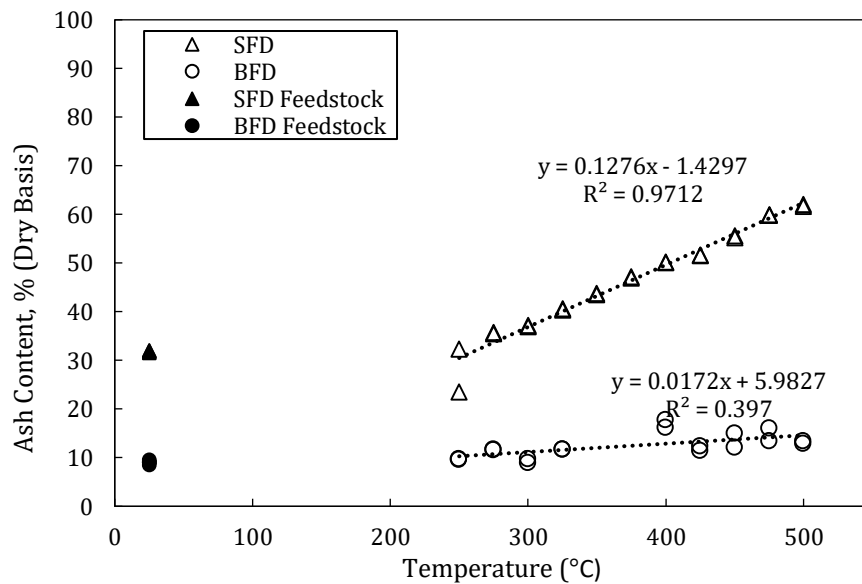


Figure 4-11: Comparison between the ash content of SFD and BFD derived biochars produced with the PSR between 250-500°C. Dotted lines represent an empirical curve fit.

The ash contents of the biochars from the different feedstock digestates are also compared when produced with the RHP. Figure 4-12 agrees with the conclusions made from Figure 4-11, and shows that SFD derived biochars have a higher ash content than BFD derived biochars. In contrast to the results observed for the PSR (Figure 4-11), the ash content of BFD biochars decreased between processing times from 1 to 3 hrs. A decrease in ash content is unexpected, as ash content should increase with pyrolysis temperature/ process time, as the concentration of minerals is increased due to the volatilization of carbon.

However, the ash content between 2 to 3 hrs process time are considerably higher than the ash content range determined in Figure 4-11. For both BFD and SFD biochars, the ash content plateaus between processing times of 3 to 4 hrs, indicating that the RHP process has also stabilized.

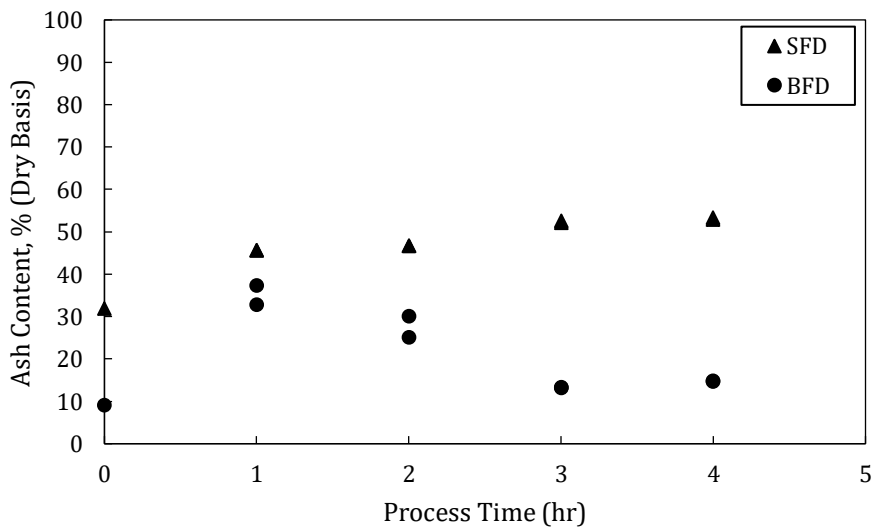
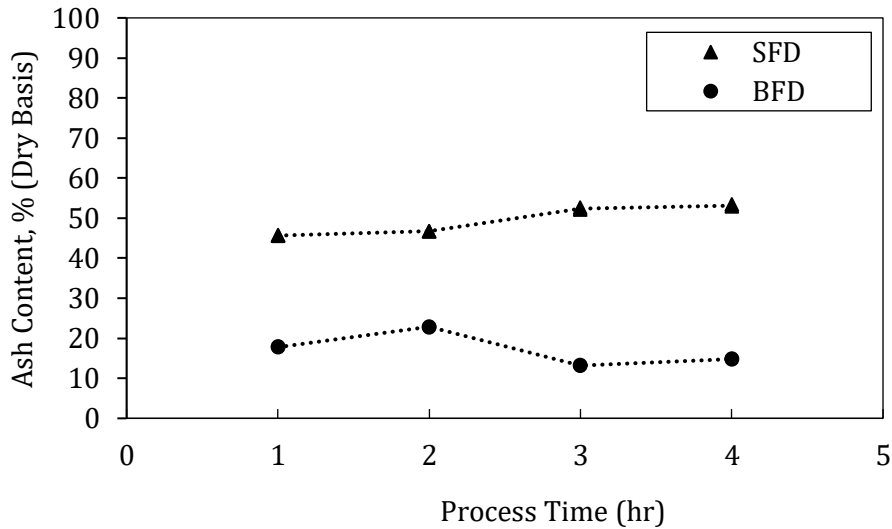


Figure 4-12: Comparison between the ash contents of SFD and BFD RHP derived biochars produced between 1-4 hrs.

Skeletal density of biochar can have an important impact on the physical characteristics of soils when applied as a soil amendment (11,25). Biochar amendment to soils has been shown to reduce the bulk densities of soils and improve soil porosity, which is important for plant root structural support, water and solute movement, and soil aeration. The reduction in soil bulk density is mainly attributed to a mixing or dilution effect, resulting from the low density and high porosity of biochar. Figure 4-13 and Figure 4-14 illustrate that the skeletal density of biochar materials ranges from 1.4 to 2.4 g/cm³. The skeletal density is shown to increase with increasing ash content and temperature or processing time. This is consistent with the trends observed by Brewer et al. (26). With increasing reaction temperature, biochar structure and density approaches that of solid graphite (2.25 g/cm³). The mineral composition present within the biochar structure can contribute to the density, allowing for densities higher than graphite to be reached (12). For both RHP and PSR derived biochars, SFD biochars have a slightly higher skeletal density than BFD biochars. The effects of biochar amendment on the bulk densities of soils needs to be assessed on a site-specific basis, as soil profiles constantly change depending on location. However, as a general rule, studies have observed that the dilution effect is greater when the difference between the density of the biochar and soil is large (11). Therefore, as BFD

biochar has a lower skeletal density, it is likely to have a greater potential to improve soil bulk density compared to biochar from SFD

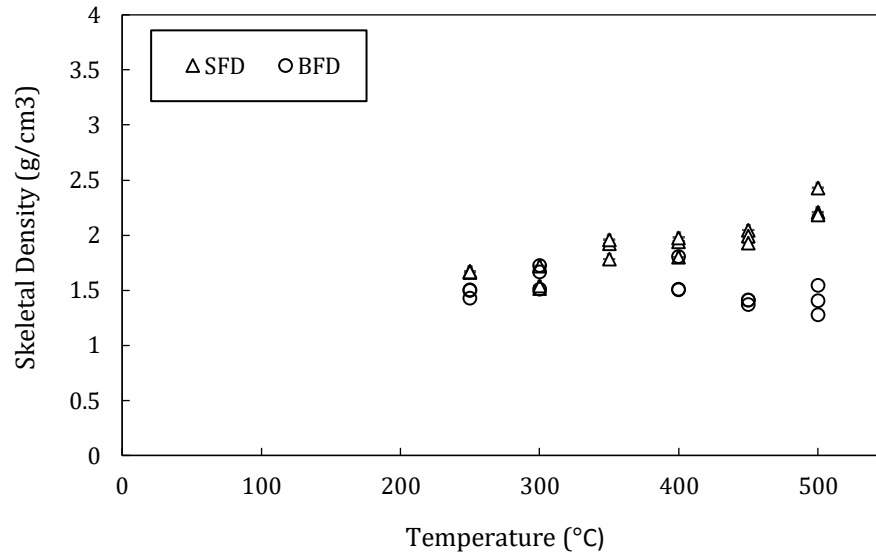


Figure 4-13: Comparison between the skeletal density of SFD and BFD derived biochars produced with the PSR between 250-500°C.

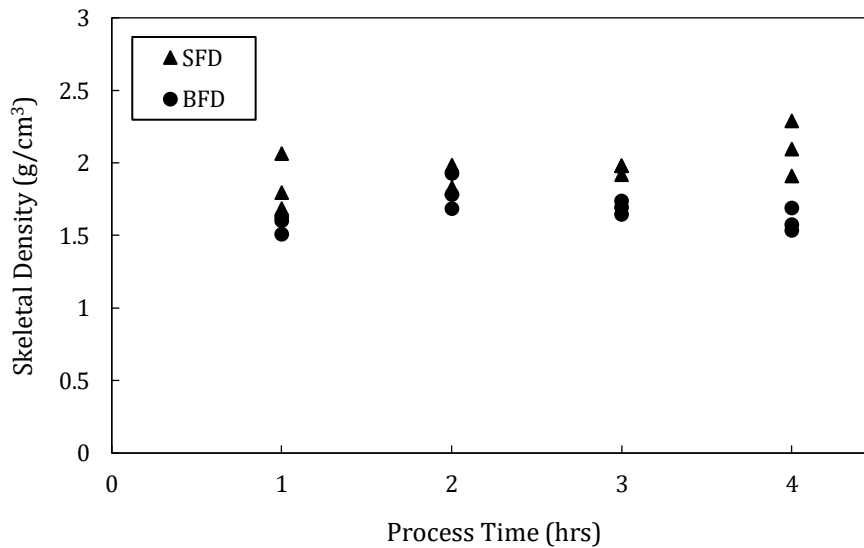


Figure 4-14: Comparison between the skeletal density of SFD and BFD RHP derived biochars produced between 1-4 hrs.

The extraction of water-soluble minerals was investigated to determine which biochar material could be a potential source of additional nutrients for plant uptake. Figure 4-15 and Figure 4-16 show that the electrical conductivity of the Soxhlet extract with respect to the raw feedstock is much higher for BFD derived biochars than SFD biochars. The higher electrical conductivity indicates that BFD biochars release more water-soluble minerals than SFD biochars. The ash content of SFD derived biochars was shown to be approximately 20 to 50% higher than BFD biochars depending on production temperature (Figure 4-11). It was expected that the Soxhlet extracts for SFD biochars would have higher electrical conductivities based on the higher mineral (ash) content of SFD biochars. However, it is likely that the porosity of the biochars plays a role in the release of water-soluble nutrients from the biochar matrix. Typically, biochars with a higher capability of releasing water soluble minerals are better suited for soil amendment applications, as the release of certain minerals provide plants with the nutrients required to increase agronomic growth. However, it is important to identify which minerals are being released (which varies based on feedstock material) in order to pair the biochar with the proper soil profile and generate a positive agronomic response.

Biochar porosity is an important property for soil amendment applications. It has been suggested that biochars with high porosities acts as a soil conditioner. The pore structures support microbial communities that are important for maintaining soil structure by providing shelter from larger microbial predators (27,28). Methylene blue adsorption is often used as a tool to characterize the pore distribution of activated carbons and biochars (29). Figure 4-17 and Figure 4-18 illustrate that BFD biochars have a higher methylene blue adsorption capacity than SFD biochars, suggesting that BFD biochars may be a higher porosity char. The higher porosity of BFD biochars may also explain why the electrical conductivity of the Soxhlet extract was higher in BFD biochars, although the ash (mineral) content is significantly lower than SFD derived biochars, as water may have better access to the nutrients available within the biochar structure. Overall, methylene blue adsorption is observed to decrease with increasing temperature and/or processing time for both feedstocks. As methylene blue adsorption capacity is related to adsorbent pore size and distribution, it is possible that the formation of tars during pyrolysis are plugging the pores which formed during the release of volatile organics, leading to

decreased methylene blue adsorption. Another potential explanation is that the biochar pore structure collapses; however this scenario is less likely given the small changes in skeletal density with increasing temperature/production time (Figure 4-13 and Figure 4-14).

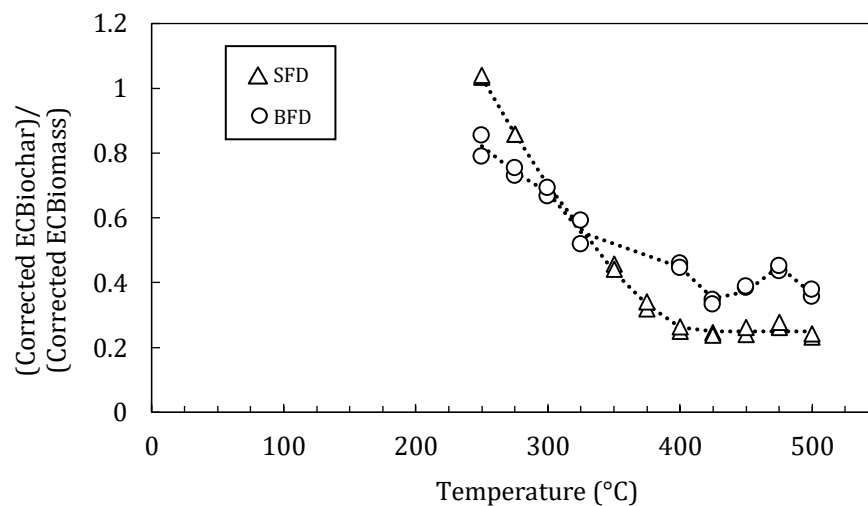


Figure 4-15: Comparison between the electrical conductivity of Soxhlet extract of SFD and BFD derived biochars produced with the PSR between 250-500°C. Dotted lines represent an empirical curve fit.

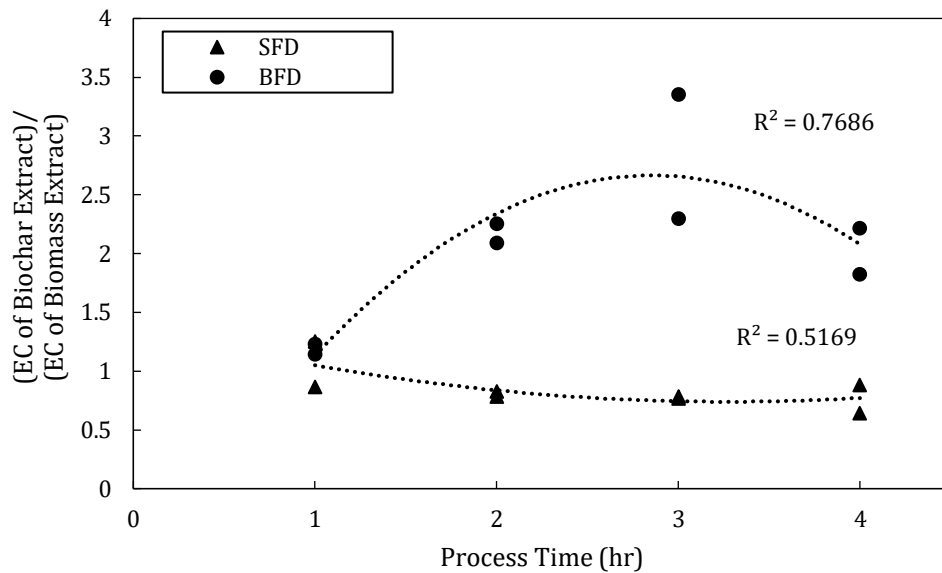


Figure 4-16: Comparison between the electrical conductivity of Soxhlet extract of SFD and BFD RHP derived biochars produced between 1-4 hrs. Dotted lines represent an empirical curve fit.

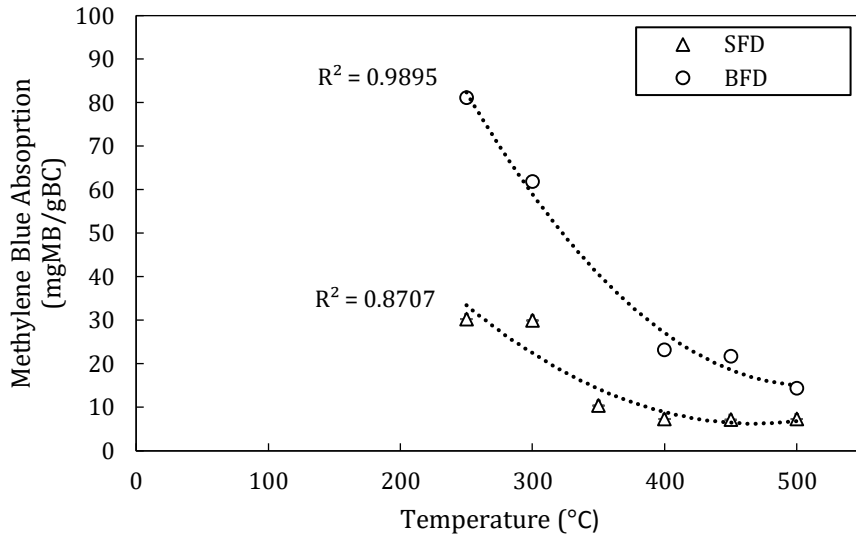


Figure 4-17: Comparison between the methylene blue adsorption of SFD and BFD derived biochars produced with the PSR between 250-500°C. Dotted lines represent an empirical curve fit.

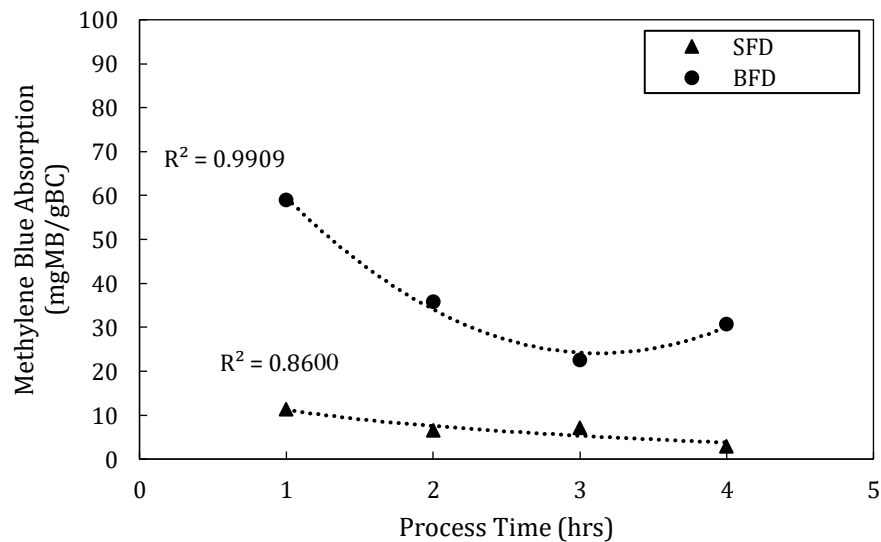


Figure 4-18: Comparison between the methylene blue adsorption of SFD and BFD RHP derived biochars produced between 1-4hrs. Dotted lines represent an empirical curve fit.

Table 4-2 and Table 4-3 summarize the differences between the beneficial soil amendment biochar properties for SFD and BFD chars produced with the PSR. Each of the tables shows the percent increase from SFD to BFD for each of the properties, and it is clear that BFD derived biochars at high and low PSR production temperatures can provide more benefits than SFD derived biochars. BFD chars produced at higher temperatures (500 °C) were also shown to have a greater percent increase from SFD biochar properties than low temperature chars (200 °C).

Table 4-4 summarizes the difference between the average beneficial char properties for SFD and BFD biochars derived from the RHP between 2 to 3 hrs. The results agree with those determined for the PSR and show that BFD biochars produced with the RHP can provide more beneficial soil amendment properties than SFD biochars.

Table 4-2: Biochar properties for PSR chars produced at 250 °C.

	Electrical Conductivity [(mS/cm)/(g/cm ³)]	Methylene Blue Adsorption (mgMB/gBC)	1/Skeletal Density (cm ³ /g)
SFD	1.6	30.3	0.59
BFD	1.5	81.1	0.67
Increase from SFD to BFD (%)	6.7	168	13.6

Table 4-3: Biochar properties for PSR chars produced at 500 °C.

	Electrical Conductivity [(mS/cm)/(g/cm ³)]	Methylene Blue Adsorption (mgMB/gBC)	1/Skeletal Density (cm ³ /g)
SFD	2.4	7.3	0.43
BFD	3.7	14.5	0.71
Increase from SFD to BFD (%)	54.2	98.6	65.1

Table 4-4: Biochar properties for average of RHP chars processed between 2 to 3 hrs.

	Electrical Conductivity [(mS/cm)/(g/cm ³)]	Methylene Blue Adsorption (mgMB/gBC)	1/Skeletal Density (cm ³ /g)
SFD	0.79	6.84	0.52
BFD	2.50	29.2	0.57
Increase from SFD to BFD (%)	216	326	9.6

4.5 Conclusions

In this study, SFD and BFD biochars physical and chemical characteristics are compared to determine their potential as a soil amendment. Both feedstocks were processed using the PSR and RHP.

It was determined that BFD derived chars can potentially provide a better soil amendment than SFD derived biochars based on the differences in biochar properties. BFD derived biochars were found to have lower skeletal density; higher electrical conductivity and methylene blue adsorption capacity than SFD biochars, which are properties that improve soil amendment ability. Biochar addition has been shown to decrease soil bulk density through mixing and dilution effects and is maximized by increasing the difference between biochar and soil densities. The higher Soxhlet extract electrical conductivity and methylene blue adsorption capacity of BFD biochars over SFD biochars provides important insight into the soil amendment capabilities of the materials. Although SFD biochars have a significantly higher ash (mineral) content, BFD biochars were shown to have a higher porosity which allows for better access and release of water-soluble minerals from the biochar structure, which could increase the amount of nutrients released to the soil profile for plant uptake.

4.6 References

1. Giorcelli M, Khan A, Pugno NM, Rosso C, Tagliaferro A. Biochar as a cheap and environmental friendly filler able to improve polymer mechanical properties. *Biomass and Bioenergy* [Internet]. 2019 Jan [cited 2019 May 30];120:219–23. Available from: <https://linkinghub.elsevier.com/retrieve/pii/S0961953418303325>
2. Peterson SC, Chandrasekaran SR, Sharma BK. Birchwood biochar as partial carbon black replacement in styrene-butadiene rubber composites. [cited 2019 May 30]; Available from: <https://journals.sagepub.com/doi/pdf/10.1177/0095244315576241>
3. Qian K, Kumar A, Zhang H, Bellmer D, Huhnke R. Recent advances in utilization of biochar. *Renew Sustain Energy Rev* [Internet]. 2014 [cited 2019 Jun 9];42:1055–64. Available from: <http://dx.doi.org/10.1016/j.rser.2014.10.074>
4. Fiore S, Berruti F, Briens C. Investigation of innovative and conventional pyrolysis of ligneous and herbaceous biomasses for biochar production. *Biomass and Bioenergy* [Internet]. 2018 Dec 1 [cited 2019 May 28];119:381–91. Available from: <https://www.sciencedirect.com/science/article/pii/S0961953418302769?via%3Dihub>
5. Adrados A, De Marco I, López-Uriónabarrenechea A, Solar J, Caballero BM, Gastelu N. Biomass Pyrolysis Solids as Reducing Agents: Comparison with Commercial Reducing Agents. *Mater (Basel, Switzerland)* [Internet]. 2015 Dec 23 [cited 2019 Jun 9];9(1). Available from: <http://www.ncbi.nlm.nih.gov/pubmed/28787805>
6. Li X, Lei B, Lin Z, Huang L, Tan S, Cai X. The utilization of bamboo charcoal enhances wood plastic composites with excellent mechanical and thermal properties. *Mater Des* [Internet]. 2014 [cited 2019 Jun 16];53:419–24. Available from: <http://dx.doi.org/10.1016/j.matdes.2013.07.028>

7. Limwikran T, Kheoruenromne I, Suddhiprakarn A, Prakongkep N, Gilkes RJ. Dissolution of K, Ca, and P from biochar grains in tropical soils. *Geoderma* [Internet]. 2018 [cited 2019 Jun 9];312:139–50. Available from: <http://dx.doi.org/10.1016/j.geoderma.2017.10.022>
8. Lehmann J, Schroth G. TREES, CROPS AND SOIL FERTILITY CONCEPTS AND RESEARCH METHODS [Internet]. CABI Publishing ; 2003 [cited 2019 Jun 9]. 151–165 p. Available from: <http://base.dnsgb.com.ua/files/book/Agriculture/Agricultural-Chemistry/Trees-Crops-and-Soil-Fertility.pdf>
9. Major J, Rondon M, Molina D, Riha SJ, Lehmann J. Nutrient Leaching in a Colombian Savanna Oxisol Amended with Biochar. *J Environ Qual* [Internet]. 2012 [cited 2019 Jun 8];41(4):1076. Available from: <http://www.ncbi.nlm.nih.gov/pubmed/22751049>
10. Liang B, Lehmann J, Solomon D, Kinyangi J, Grossman J, O’neill B, et al. Black Carbon Increases Cation Exchange Capacity in Soils. *Soil Sci Soc Am* [Internet]. 2006 [cited 2019 Jun 8];(70):1719–30. Available from: http://xrm.phys.northwestern.edu/research/pdf_papers/2006/liang_sssaj_2006.pdf
11. Blanco-Canqui H. Biochar and Soil Physical Properties. *Soil Sci Soc Am J*. 2017;81(4):687.
12. Lehmann J, Joseph S. Biochar for Environmental Management [Internet]. 2009 [cited 2019 Jun 9]. Available from: [http://www.css.cornell.edu/faculty/lehmann/publ/First proof 13-01-09.pdf](http://www.css.cornell.edu/faculty/lehmann/publ/First%20proof%2013-01-09.pdf)
13. Biogas Association. Canadian Biogas Study: Benefits to the Economy, Environment and Energy [Internet]. 2013 [cited 2019 Jun 16]. Available from: https://biogasassociation.ca/images/uploads/documents/2014/biogas_study/Canadian_Biogas_Study_Summary.pdf
14. Monlau F, Sambusiti C, Ficara E, Aboulkas A, Barakat A, Carrère H. New

- opportunities for agricultural digestate valorization: current situation and perspectives. *Energy Environ Sci* [Internet]. 2015 Aug 26 [cited 2019 Aug 29];8(9):2600–21. Available from: <http://xlink.rsc.org/?DOI=C5EE01633A>
15. Cross A, Sohi SP. A method for screening the relative long-term stability of biochar. *GCB Bioenergy*. 2013;5(2):215–20.
 16. Yu X, Wu C, Fu Y, Brookes PC, Lu S. Three-dimensional pore structure and carbon distribution of macroaggregates in biochar-amended soil. *Eur J Soil Sci* [Internet]. 2016 Jan [cited 2019 Jun 8];67(1):109–20. Available from: <http://doi.wiley.com/10.1111/ejss.12305>
 17. Zimmerman AR. Abiotic and Microbial Oxidation of Laboratory-Produced Black Carbon (Biochar). *Environ Sci Technol* [Internet]. 2010 Feb 15 [cited 2019 Jun 8];44(4):1295–301. Available from: <https://pubs.acs.org/doi/10.1021/es903140c>
 18. Suman S, Gautam S. Pyrolysis of coconut husk biomass: Analysis of its biochar properties. *Energy Sources, Part A Recover Util Environ Eff* [Internet]. 2017 Apr 18 [cited 2019 Jun 9];39(8):761–7. Available from: <https://www.tandfonline.com/doi/full/10.1080/15567036.2016.1263252>
 19. Sohi SP, Krull E, Lopez-Capel E, Bol R. A Review of Biochar and Its Use and Function in Soil. *Adv Agron* [Internet]. 2010 Jan 1 [cited 2019 Jun 8];105:47–82. Available from: <https://www.sciencedirect.com/science/article/pii/S0065211310050029>
 20. He X, Liu Z, Niu W, Yang L, Zhou T, Qin D, et al. Effects of pyrolysis temperature on the physicochemical properties of gas and biochar obtained from pyrolysis of crop residues. 2018 [cited 2019 Jun 9]; Available from: <https://doi.org/10.1016/j.energy.2017.11.062>
 21. Environmental Protection Agency. EPA Method 3540C: Soxhlet Extraction [Internet]. 1996 [cited 2019 Jun 4]. Available from: <https://www.epa.gov/sites/production/files/2015-12/documents/3540c.pdf>

22. Chegini G, Sanchez Careaga FJ, Pjontek D, Briens C. Impact of Pyrolysis heating characteristics on leachability of biochar minerals. *TCBiomass* [Internet]. 2017; Available from:
<http://www.gastechnology.org/tcbiomass/tcbiomass2017/Ghazaleh-Chegini-Thu-tcbiomass2017-presentation.pdf>
23. Dolinowski T. Soxhlet Extractor. 2011;
24. Raposo F, De La Rubia MA, Borja R. Methylene blue number as useful indicator to evaluate the adsorptive capacity of granular activated carbon in batch mode: Influence of adsorbate/adsorbent mass ratio and particle size. *J Hazard Mater* [Internet]. 2009 Jun 15 [cited 2019 Aug 23];165(1–3):291–9. Available from:
<https://linkinghub.elsevier.com/retrieve/pii/S0304389408014702>
25. Omondi MO, Xia X, Nahayo A, Liu X, Khan Korai P, Pan G. Quantification of biochar effects on soil hydrological properties using meta-analysis of literature data. *Geoderma* [Internet]. 2016 [cited 2019 Jun 9];274:28–34. Available from:
<http://dx.doi.org/10.1016/j.geoderma.2016.03.029>
26. Brewer CE, Chuang VJ, Masiello CA, Gonnermann H, Gao X, Dugan B, et al. New approaches to measuring biochar density and porosity. *Biomass and Bioenergy* [Internet]. 2014 [cited 2019 Jun 24]; Available from:
www.sciencedirect.com<http://www.elsevier.com/locate/biombioe>
27. Laird DA, Fleming P, Davis DD, Horton R, Wang B, Karlen DL. Impact of biochar amendments on the quality of a typical Midwestern agricultural soil. 2010;
28. Burrell LD, Zehetner F, Rampazzo N, Wimmer B, Soja G. Long-term effects of biochar on soil physical properties. 2016 [cited 2019 Jan 10]; Available from:
<http://dx.doi.org/10.1016/j.geoderma.2016.07.019>
29. Barton SS. The adsorption of methylene blue by active carbon. *Carbon N Y* [Internet]. 1987 Jan 1 [cited 2019 Aug 29];25(3):343–50. Available from:
<https://www.sciencedirect.com/science/article/pii/0008622387900054>

5 Conclusions

A new batch reactor called the Rotating Heater Pyrolyzer (RHP) capable of producing several kilograms of biochar was designed and constructed. With the RHP, heat is distributed to the solids via a rotating heating element placed within the reaction vessel. RHP biochars were processed between 1 to 4 hours at a constant induction power input of 3 kW, and it was determined that processing time had an impact on several biochar properties.

RHP biochar properties were compared to biochar produced by a standard batch pyrolysis reactor referred to as the Pyrolytic Shaker Reactor (PSR) to determine if the RHP was capable of producing biochar with comparable properties to ones derived by the PSR at a specific temperature. A number of physical and chemical biochar properties were analyzed for woodchip (WCP), Storm Fisher Digestate (SFD) and Bayview Flowers Digestate (BFD). WCP processed between 2-3 hours in the RHP were found to have an equivalent PSR temperature of approximately 375 to 400 °C. SFD and BFD chars produced at RHP process times of 4 hrs found to have an equivalent PSR temperature of approximately 420 °C and 400 °C, respectively.

SFD and BFD biochars physical and chemical characteristics were compared to determine their potential as a soil amendment. BFD biochars produced in both the RHP and PSR were shown to have characteristics that can improve soil amendment ability when compared to SFD derived chars; including lower skeletal density, higher electrical conductivity in water extracts and higher methylene blue adsorption capacity.

6 Recommendations and Future Work

BFD biochar can provide a better soil amendment compared to SFD biochar. Therefore, future work includes producing kg of BFD biochar using the RHP for further testing as a soil amendment. To properly test soil amendment ability, BFD biochars need to be tested in soil. This could include testing biochar amended soils in greenhouses to see if biomass growth is increased, the potential for pest control, and the potential of leaching hazardous materials such as polyaromatic hydrocarbons (PAHs).

In addition, the effect of the rotating heater stationary time on the resultant biochar properties should be further investigated. Increasing the heaters stationary time likely increases the pyrolysis temperature, as the contact time between the heater plates and reacting particles is increased. Adjusting the heater stationary time may be able to provide better process control over the resultant biochar product required for soil amendment.

Soxhlet and Nespresso extractions were conducted on pure biochar samples, however nutrient and metal extractions may be affected by soil-biochar matrix, Therefore it is recommended that extractions be performed on biochar-amended soils. In addition, temperature may also be another variable influencing nutrient leaching, and it is recommended that the effects of different extraction temperatures be investigated.

The effects of biochar particle size on the electrical conductivity of Nespresso extract should be further studied to provide a more accurate correlation between the Soxhlet and Nespresso extract electrical conductivities. If made more accurate, the Nespresso extraction method would reduce the time required to process samples from 16 hours to 30 s, which would make it suitable for the monitoring of industrial biochar units.

Appendix A: Gast Air Motor Product Specifications

The following is the air motor product specifications used to determine the air consumption, power consumption and torque required to turn the RHP heating element when filled with biomass.

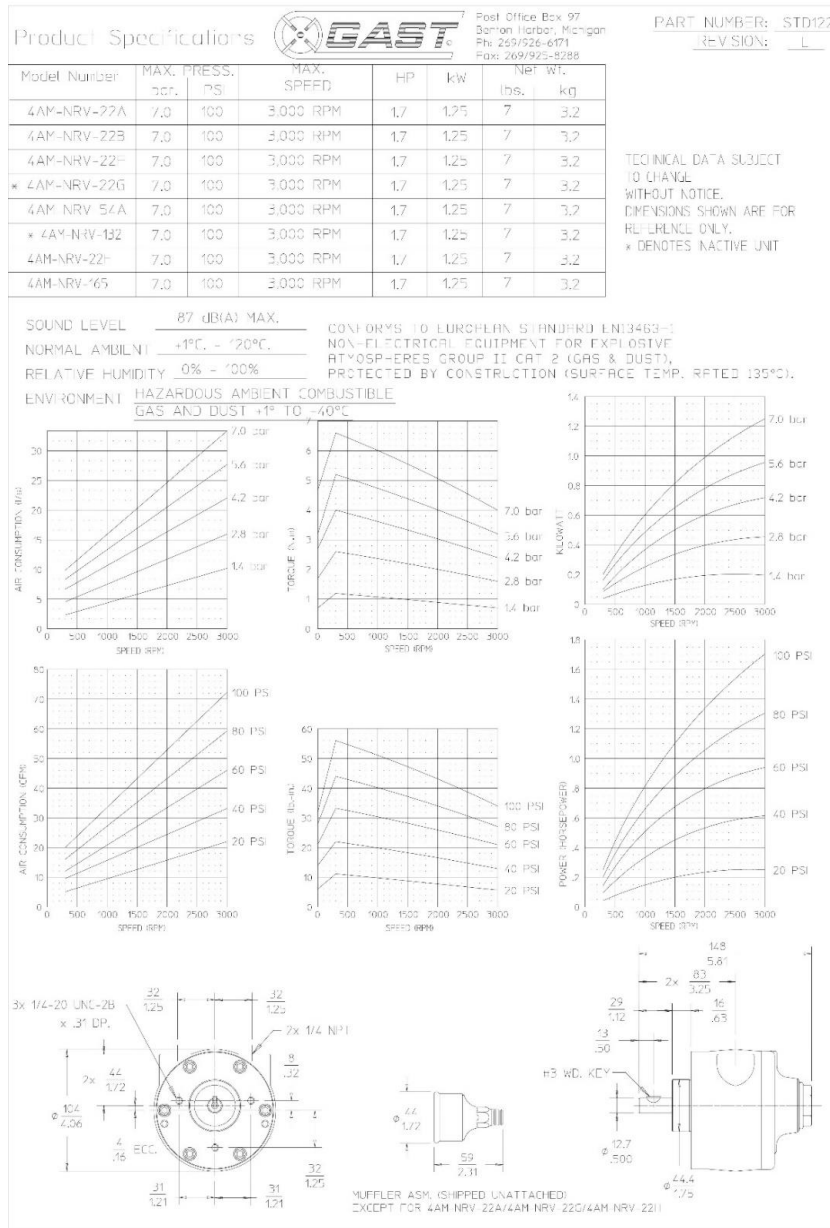


Figure A-1: Gast air motor product specification sheet.

Appendix B: PSR Mixing Images



Figure B-1: Still frames of video taken showing PSR mixing capabilities taken at (a) 0 s; (b) 10 s and (c) 30 s.

Appendix C: Skeletal Density and Ash Content of WCP Biochars

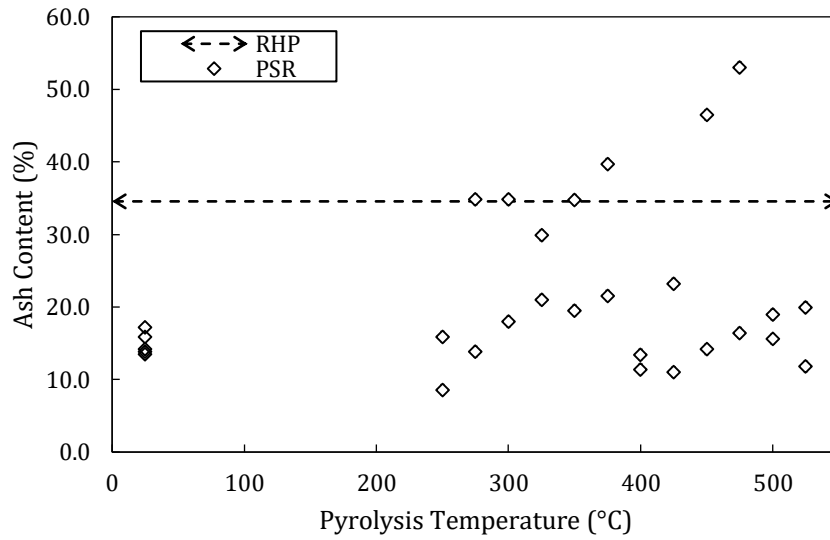


Figure C-1: Effect of pyrolysis temperature on the ash content of PSR WCP derived chars. Point at 25 °C is ash content of raw woodchip biomass.

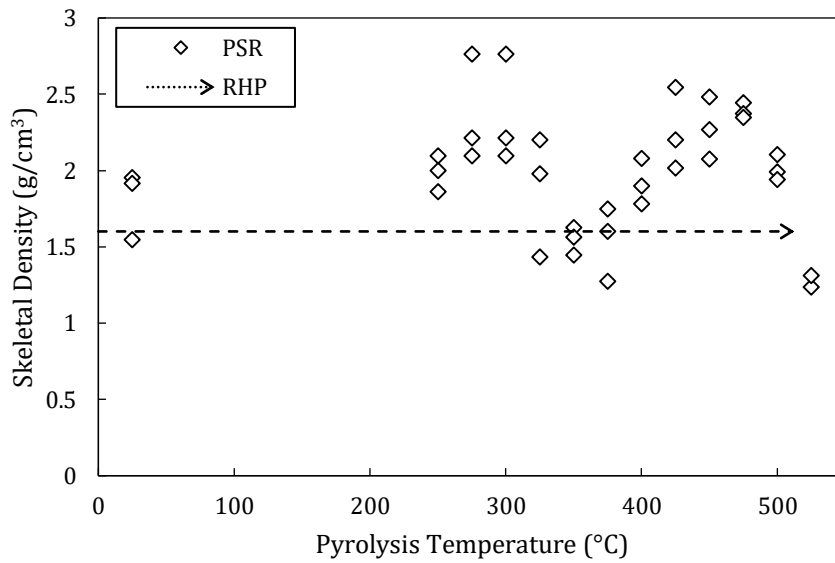


Figure C-2: Skeletal density of PSR WCP derived biochars as a function of pyrolysis temperature.

Appendix D: Nespresso™ Extraction

A new water-soluble nutrient and minerals extraction method referred as ‘nespresso extraction’ was developed to provide a quick and simple method to characterize biochar salinity based on the electrical conductivity (EC) of the liquid extract. As previously described in 3.3.1.5 this extraction method utilizes a nespresso coffee maker, and mimics the mechanism used in Soxhlet extractors with a minimized number of cycles. Figure D-1 shows a strong positive linear correlation ($R^2 = 0.9093$) between the electrical conductivity of nespresso extraction liquids and Soxhlet extraction liquids, indicating that nespresso extractions can provide reliable electrical conductivity measurement.

The effect of pyrolysis temperature for PSR derived chars and process time for RHP chars on electrical conductivity relative to raw woodchip biomass EC was investigated. In Figure 3-5 the electrical conductivity of Soxhlet extracted liquids was observed to increase linearly with pyrolysis temperature. The estimated Soxhlet electrical conductivity calculated from the relationship derived in Figure 3-5 is also displayed. These results are in agreement with Singh et al. (2010) and Kloss et al. (2012). Soxhlet extractions had higher EC than nespresso extractions. This was expected due to the effect of dilution on electrical conductivity for Nespresso extractions. Differences in particulate size may be contributing to the major differences between Soxhlet and nespresso estimated Soxhlet electrical conductivities. Metals and nutrients have a higher diffusion rate in Soxhlet extracts due to longer exposure times and are therefore more tolerable to larger variations in particulate size. However, the residence time between the extraction liquid and biochar for the nespresso extractions is much shorter. Smaller particulate sizes provide larger surface area for the extraction liquid to contact active sites and extract metals and nutrients. By tightly controlling the size of biochar particulate size tested in the nespresso extractor, the accuracy of the nespresso extractor can be optimized.

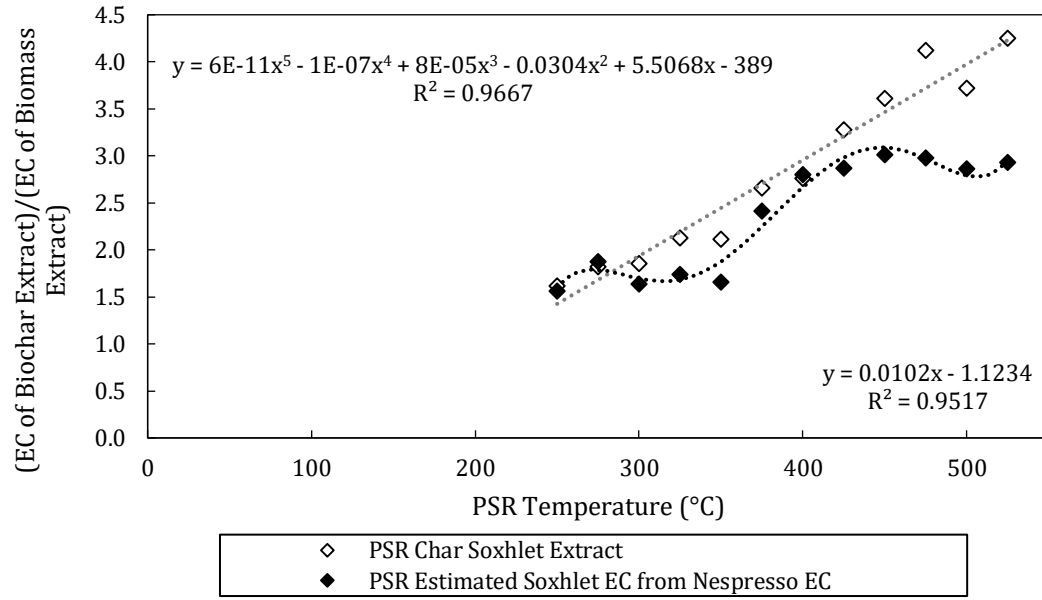


Figure D-1: Effect of temperature on EC of Soxhlet extracted liquids with reference to raw woodchip feedstock EC. The estimated Soxhlet EC from Nespresso EC using the correlation determined in Figure 3-5.

Appendix E: Equivalent PSR Temperatures for PSR Digestate Derived Biochars

The same analysis procedure used to determine the equivalent PSR temperature of woodchip RHP derived char in Chapter 3 was applied to SFD and BFD chars produced with the RHP.

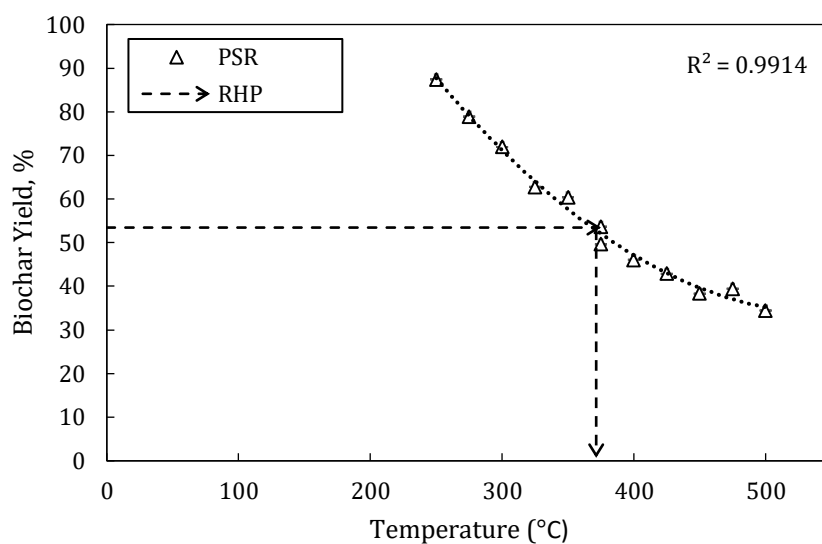


Figure E-1: Effect of temperature on SFD PSR biochar yield. The corresponding pyrolysis temperature of the RHP char yield processed for 4 hrs is also shown. Duplicate runs are shown.

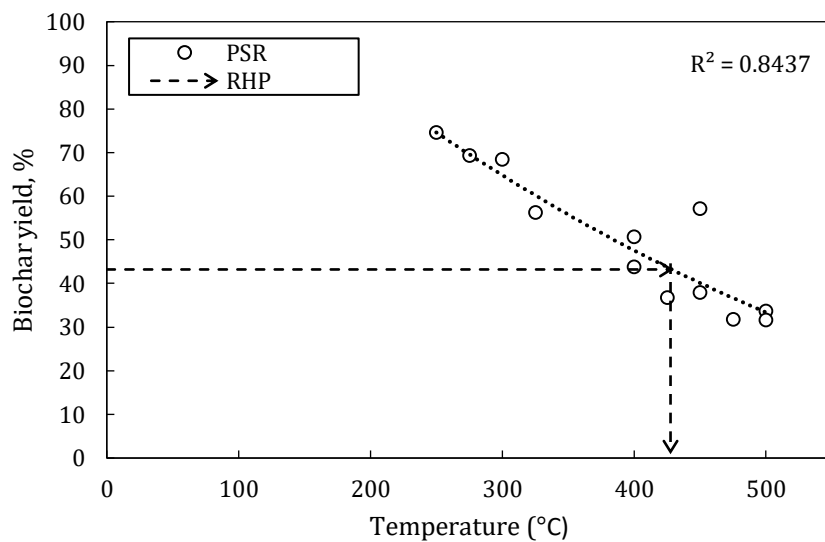


Figure E-2: Effect of temperature on BFD PSR biochar yield. The corresponding pyrolysis temperature of the RHP char yield processed for 4 hrs is also shown. Duplicate runs are shown.

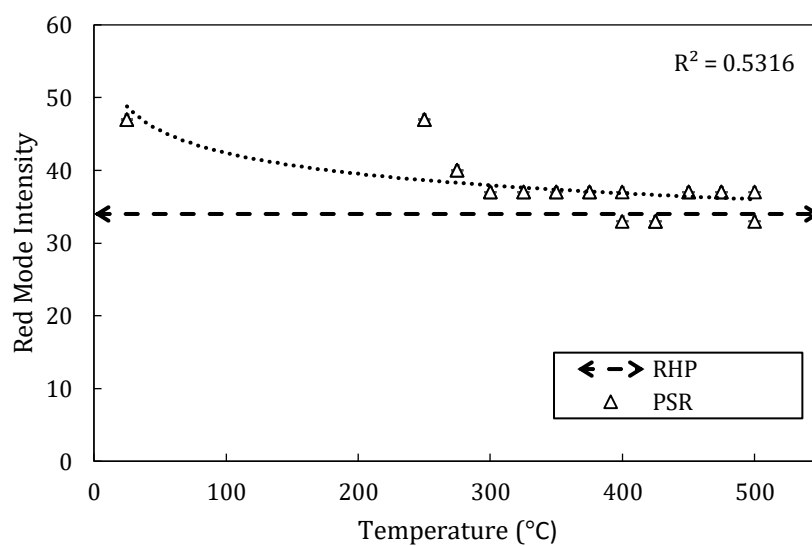


Figure E-3: Effect of pyrolysis temperature on the mode red intensity of PSR SFD derived biochars. Dashed line corresponds to the red mode intensity of RHP SFD char processed at 4 hrs.

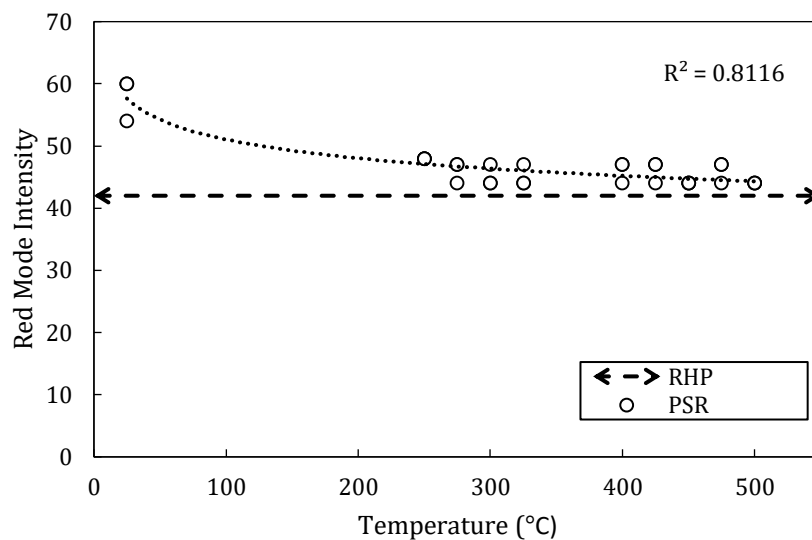


Figure E-4: Effect of pyrolysis temperature on the mode red intensity of PSR BFD derived biochars. Dashed line corresponds to the red mode intensity of RHP char processed at 4 hrs.

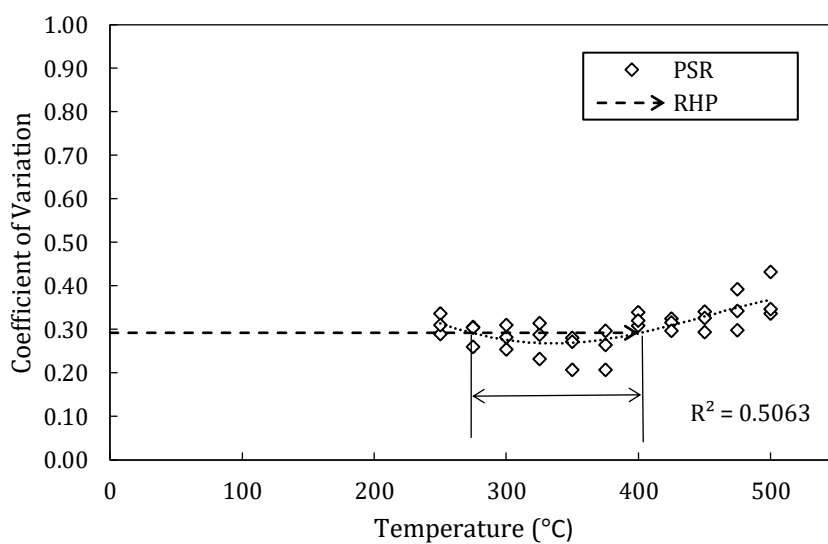


Figure E-5: Effect of temperature on the red intensity coefficient of variance on PSR SFD derived chars. Dashed line represents RHP SFD char processed at 4 hrs.

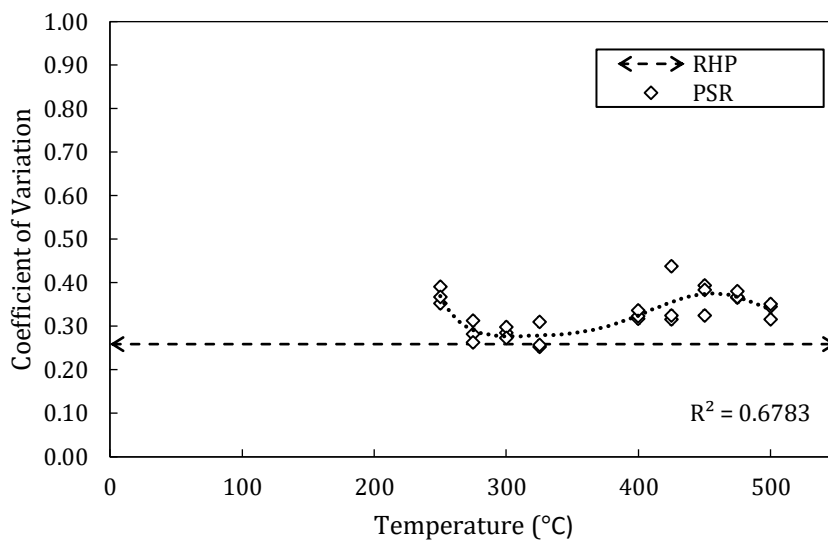


Figure E-6: Effect of temperature on the red intensity coefficient of variance on PSR BFD derived chars. Dashed line represents RHP BFD char processed at 4 hrs.

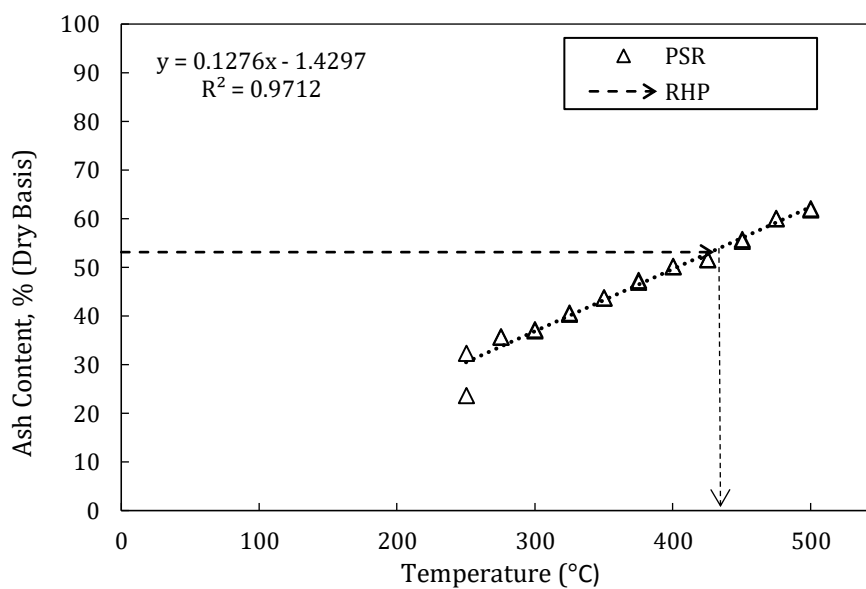


Figure E-7: Effect of pyrolysis temperature on the ash content of PSR SFD derived chars. Dashed line represents RHP SFD char processed at 4 hrs.

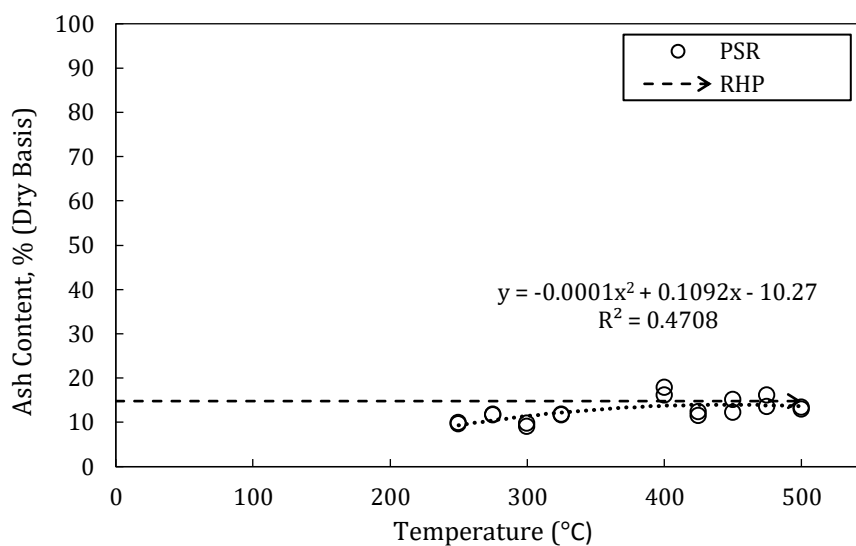


Figure E-8: Effect of pyrolysis temperature on the ash content of PSR BFD derived chars. Dashed line represents RHP BFD char processed at 4 hrs.

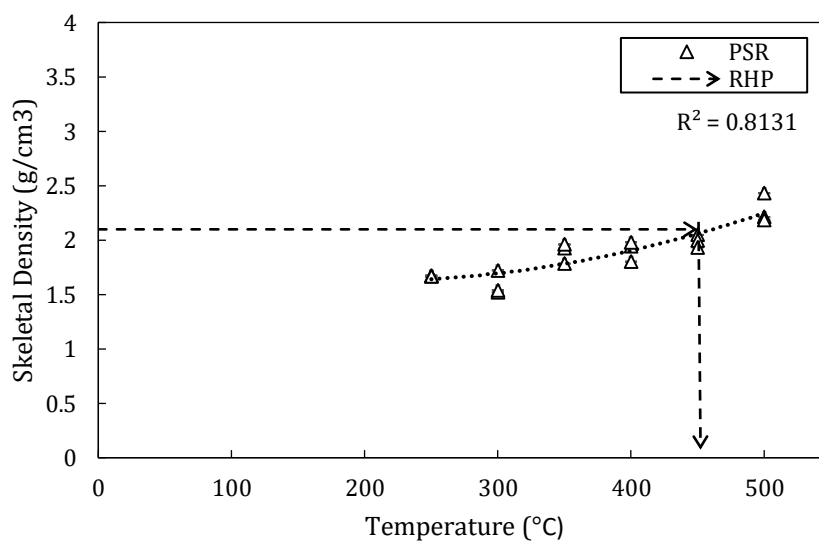


Figure E-9: Skeletal density of PSR SFD derived biochars as a function of pyrolysis temperature. Dashed line represents RHP SFD char processed at 4 hrs.

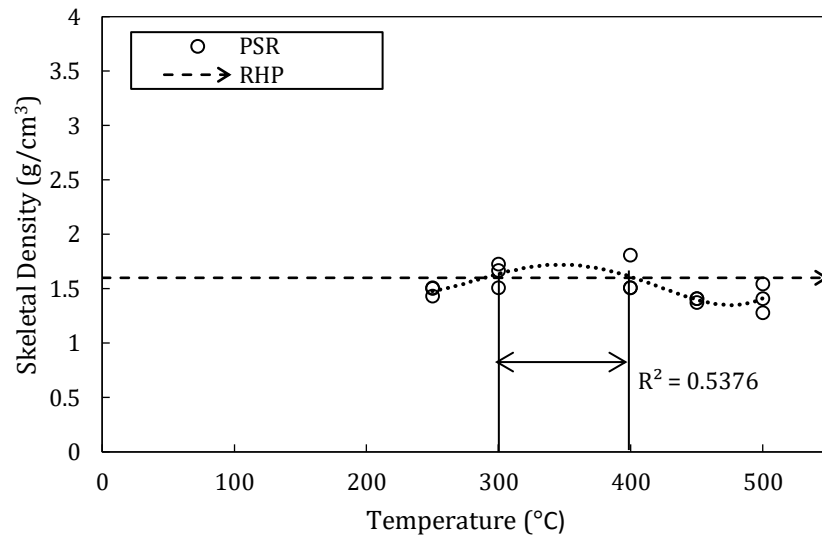


Figure E-10: Skeletal density of PSR BFD derived biochars as a function of pyrolysis temperature. Dashed line represents RHP BFD char processed at 4 hrs.

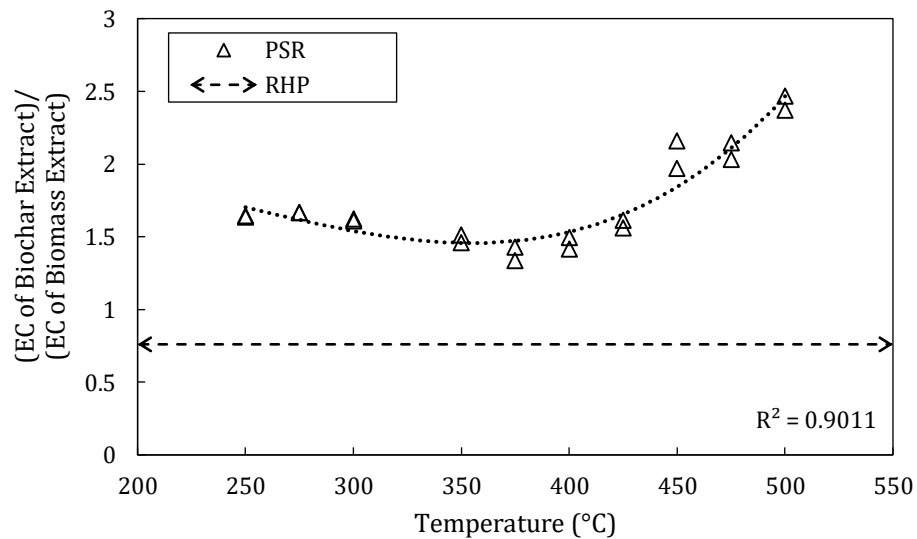


Figure E-11: Effect of temperature on PSR SFD electrical conductivity of Soxhlet extracted liquids with reference to raw SFD feedstock EC. EC = Electrical conductivity. Dashed line represents RHP SFD char processed at 4 hrs.

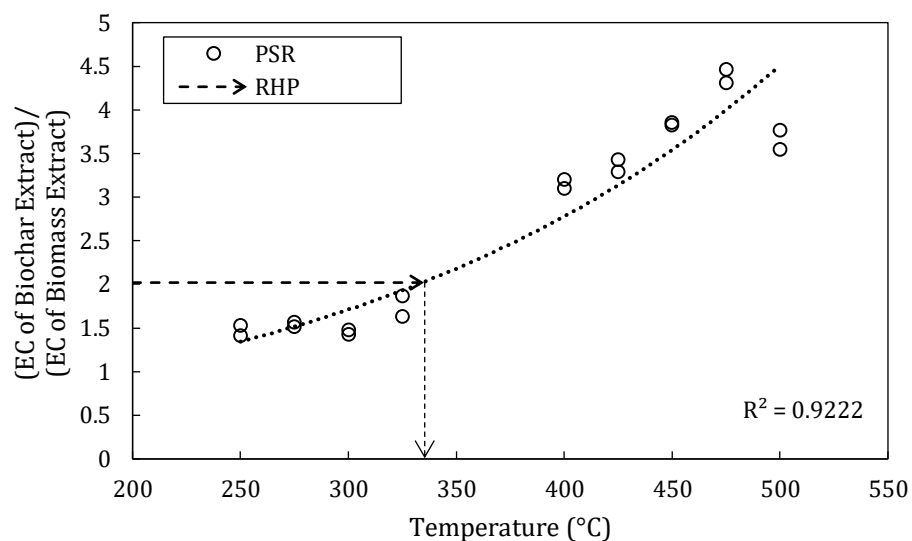


Figure E-12: Effect of temperature on PSR BFD EC of Soxhlet extracted liquids with reference to raw BFD feedstock EC. EC = Electrical conductivity. Dashed line represents RHP BFD char processed at 4 hrs.

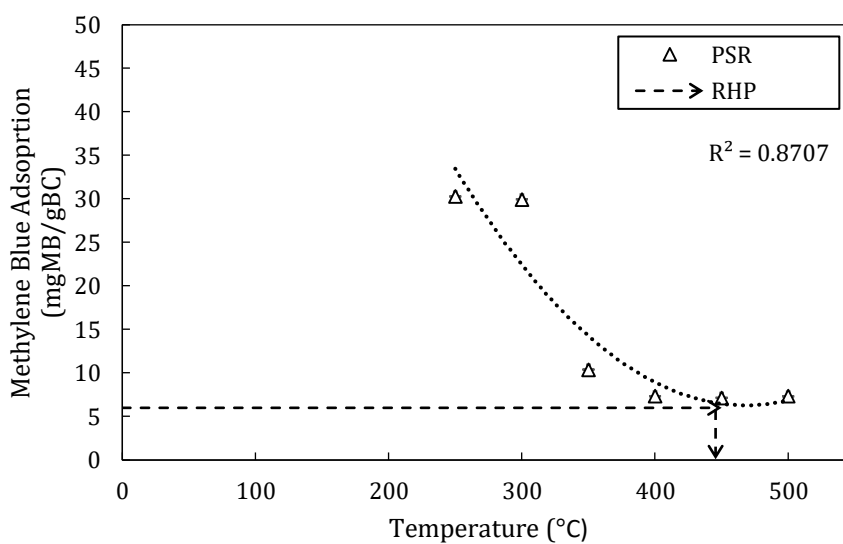


Figure E-13: Effect of temperature on PSR SFD biochar methylene blue adsorption capacity. Dashed line represents RHP SFD char processed at 4 hrs.

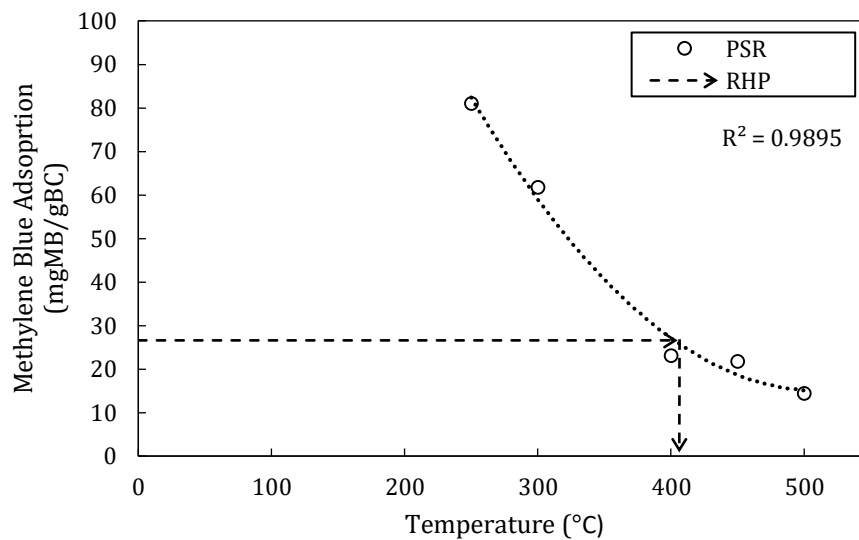


Figure E-14: Effect of temperature on PSR BFD biochar methylene blue adsorption capacity. Dashed line represents RHP BFD char processed at 4 hrs.

Curriculum Vitae

Ariel Porat

Post-secondary Education and Degrees:

Master of Engineering Science **2017 - 2019**
Chemical and Biochemical Engineering
Western University, London, Ontario, Canada

Bachelor of Engineering Science **2013 - 2017**
Chemical and Biochemical Engineering
Western University, London, Ontario, Canada

Honours and Awards:

Faculty of Engineering Dean's Award **May 2017 - August 2017**
Western University, London, Ontario, Canada

Dean's Honour List **2016 - 2017**
Western University, London, Ontario, Canada

Global Opportunities Award **2016**
Western University, London, Ontario, Canada

Related Work Experience:

Teaching Assistant, Chemical and Biochemical Engineering **2017 - 2019**
Western University, London, Ontario, Canada

Undergraduate Research Assistant, Chemical and Biochemical Engineering **2017**
Western University, London, Ontario, Canada

Summer Engineering COOP Student **2014 - 2015**
Litens Automotive Group Ltd, Concord, Ontario, Canada